UNIVERSITY OF NEW MEXICO
ALBUQUERQUE

ENGINEERING EXPERIMENT STATION

Technical Report EE-69

A SYSTEM FOR RECORDING ELECTROMAGNETIC
ATMOSPHERIC NOISE IN 3-50 cps REGION

by

James F. White

January 1962

Engineering Experiment Station
University of New Mexico
Albuquerque, New Mexico

A System for Recording Electromagnetic Atmospheric Noise in 3-50 cps Region

by

James F. White*

*E.E. Department
University of New Mexico
Albuquerque, New Mexico

CONTENTS

LIST OF FIGURES

LIST OF FIGURES (Con't)

LIST OF FIGURES (Con't)

vi

1. Introduction

A. Historical Background

The electromagnetic noise spectrum extends from below 1 cps to above 3,000 mcs. Within this spectrum many phenomena of atmospheric noise have been observed. Those atmospherics which occur in the audio frequency region of the spectrum have been given not only descriptive but also subjective names by many different investigators. As a result, it is often difficult to determine from the literature what aspect of the noise phenomenon is being considered. In addition, references to low frequencies involved in certain experiments are vague. A brief history of atmospherics research is presented here in order to explain the terminology, to show the frequencies involved, and to give some indication of the many aspects of atmospheric noise.

Throughout this paper, VLF (Very Low Frequency) refers to the 3-30 kc region as defined at the Atlantic City Radio Convention 1947 [Tepley 1959]. The 1-3,000 cps range is called the ELF (Extremely Low Frequency) range [Wait 1960a, Wait and Carter 1960, Wait, 1960b] . The term "atmospherics" includes all atmospheric noises and, on the basis of the source of the noise, is subdivided into three parts, viz., whistlers, VLF emissions, and "sferics" [Helliwell, 1958] .

Whistlers occur in the 1-30 kc region of the spectrum and consist of long descending tones with durations that vary from 2 to 3 seconds. They were first observed by Barkhausen in 1919. It is believed that they are due to the dispersion of lightning energy through the ionosphere guided along the earth's magnetic

1

flux lines [Helliwell, 1958] . Helliwell and Morgan [1959]
mention several types of whistlers--pure tone, swishy, multiple,
short, long, echo, and nose. Helliwell, et al. [1956] observed
that the whistler was not a homogeneous band of noise as
previously observed, but was a rapid succession of discrete
traces or pure tones. Each trace appeared at approximately
1500 cps and separated into two branches--one decreasing in
frequency as usual, but the other increasing in frequency
contrary to Eckersley's dispersion law. Helliwell calls this
the "nose whistler" due to the characteristic shape of the two
branches arising from the initial "nose" frequency. This
disclosure was largely due to better frequency resolution
provided by the spectrograph used in the analysis [Gruentz,
1951, Potter, 1945, Grierson, 1957] .

Another type of atmospheric is "VLF emissions"--a name
first proposed by Gallet [1959] . These emissions occur in
the same frequency range as whistlers and are thought to be
generated in the exosphere [Helliwell, 1958] . Crary and
Helliwell [1961] developed equations for the duct propagation
of both whistlers and VLF emissions.

Finally, the last category of atmospherics is called
"sferics." They are due to lightning sources and are propagat-
ed in the earth-ionosphere cavity by ground wave or by
reflections. These sferics include tweeks, warbling, chirping,
risers, hooks, hiss, and chorus. The name "dawn chorus" was
introduced by Storey because it sounds like the warbling of
birds at dawn. This chorus is a combination of short

(0.1 - 0.2 second) rising whistlers and warbling tones the occurrence of which increases near the auroral zone. Although the chorus has been known for many years, no systematic study has been made [Gallet and Helliwell, 1957]. Tweeks are musical sounds produced by long pulse trains as a result of the number of reflection paths between the ionosphere and earth. According to Helliwell [1958], they may be quite long (50-100 milli-seconds) and are often mistaken for whistlers. Watts [1957b] concludes from his work that this is not associated with indivi-dual sferics or whistlers. His analysis shows that the greatest amplitude is centered around 3 kcs [Watts, 1957a]. Martin et al. [1960] have indicated that hiss is broadly centered around 8 kcs. Although chorus, hiss, and risers are heard during magnetic storms, their origin is unknown [Helliwell, 1958].

Tepley [1961b] refers to "hm" emissions--hydromagnetic emissions. These emissions occur in the 0.5 to 5 cps region and are single frequency oscillations which may vary slowly with time.

At the extreme low frequencies there exist small fluctua-tions in the geomagnetic field which are called geomagnetic micropulsations [Boothe, et al., 1960]. These pulsations have been known since 1861. They have periods of several seconds to several minutes and, according to Campbell [1959], occur in two groups with periods of 1-3 minutes and 5-30 seconds and have flux densities approximating $1/3 \gamma$ with recordings as high as 40γ ($\gamma = 10^{-5}$ gauss $= 10^{-9}$ webers/m^2). Duffus, et al. [1957] conclude from their observations that these

micro-pulsations do not occur simultaneously everywhere as is "occasionally stated in the literature."

Earth currents, telluric, or magneto-telluric fields pertain, of course, to the E and H fields of the earth. These currents were discovered, according to Hopkins [1960] , in ground return circuits of telegraph lines where potentials are sufficient to energize the system without batteries. These phenomena, of course, are also present in underwater communications cables. Although diurnal and seasonal variations have been investigated, variations of shorter periods--frequency range from .005 cps to 1 cps--have only recently been studied [Smith, et al., 1960] .

Long delay echoes with a delay from 2 to 20 seconds were first observed by Van der Pol and Störmer in 1928. Budden has investigated this phenomenon with no success. Apparently there is no explanation for these long delay echoes. However, Storey, who has done theoretical work on whistler traces [Storey, 1957] , believes that the long delay echo is not produced by whistler mode type propagation.

In general, most investigators attribute low frequency noise to thunder-storm activity [Gustafsson, et al., 1960] . However, Gallet and Helliwell, [1959] believe that a portion of this noise originates in the ionosphere. Pierce [1960b] is considering the work of Large [1957] , Large and Wormell [1958] , Aarons [1956] , and Willis [1948] concluded that above 20 cps the electric and magnetic fields are electro-magnetic and due to sferics while below 20 cps the E and H fields are due to different sources, i.e., the E field is due

to moving space charges and the H field to ionosphere and earth currents. Campbell [1959] states that the interval in which the dominant signals change from those due to slow tail sferics to geomagnetic pulsations is in the 0.2 to 2.0 cps range. This agrees with Hopkins [1960] who has noticed that micropulsations occur below 0.2 cps and that signals due to sferics are above 2 cps. He further noted that there is very little energy in the transition band at 1 cps. Duffus, et al. [1957] have conducted experiments in this area of the spectrum between pulsations and atmospherics. Holzer and Deal [1956] also have investigated this spectral region.

According to Gustafsson, et al. [1960], the existence of natural electromagnetic radiation in the audio frequency range was first discussed by Menzel and Salisbury [1948]. Aarons and Henissart [1953] reported correlation between low frequency magnetic fluctuations and geomagnetic disturbances and solar phenomenon. In 1960, Aarons, et al. [1960] observed two bands of noise which correlated with geomagnetic disturbances, viz., 600-950 cps centered at 750 cps (the gyro frequency of protons at 100 km) and 1.8 to 4.5 kcs. They were considering the possible source of low frequency radiation to be emissions due to protons revolving around geomagnetic field lines at the gyro frequency. However, Gustafsson, et al. [1960] in their experimentation found no correlation between low-frequency noise and magnetic activity or between 20 to 200 cps range and solar noise at 200 mc during SID (Sudden Ionosphere Disturbance). A year later, Pierce [1961] observed that SID had no effect in the 10 to 20 kc range but that attenuation increased below 10 kcs and decreased above 20 kcs.

In addition to observations mentioned above, considerable interest has been shown in sferic waveforms. For the purpose of discussion, a typical waveform is shown in Figure 1.1.
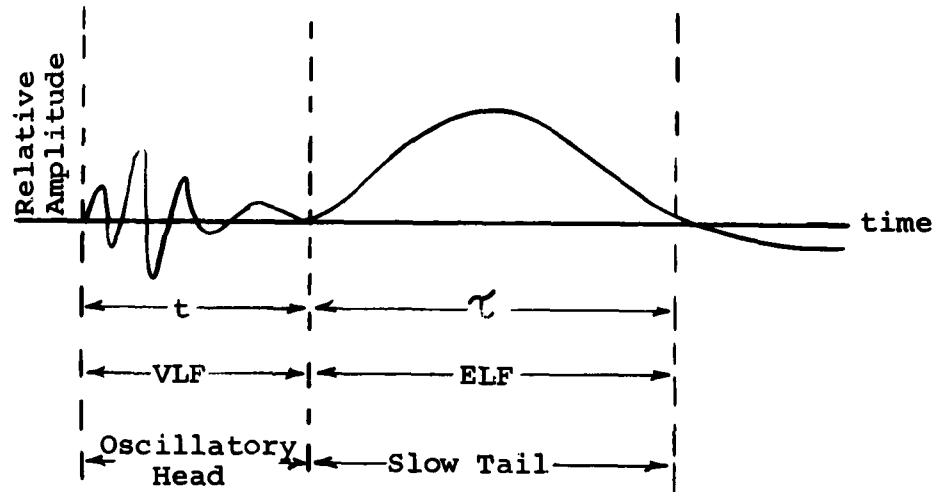
Figure 1.1 A typical atmospheric waveform

These waveforms are usually amplified with wide-band receivers and displayed on an oscilloscope for photographic purposes. Wide-band equipment is necessary if both the VLF and ELF portions of the waveform are to be observed.

Watson-Watt, et al., [1937] observed the presence of the slow tail and also the increased separation of the head and tail with increase in propagation distance. They used the time duration "t" and "$\frac{\tau}{2}$" as parameters in what was apparently the first detailed study of the slow tail. Hepburn and Pierce [1953] also investigated the slow tails and measured "$\frac{\tau}{4}$".

Appleton and Chapman [1937] noticed that all these waveforms had characteristic patterns and that frequencies around 2 kcs

were either originally missing or highly attenuated. In order to determine the cause of this apparent absorption at 2 kcs, Chapman and Edwards [1950] simultaneously recorded waveforms and frequency spectrum. Subsequent observations by Chapman and Matthews [1953] , Chapman and Jolley [1954] , and Chapman and Macario [1956] showed that there was in fact an absorption at 2 kcs. This effect contradicted the Austin-Cohen law [1911] which says that attenuation decreases with frequency. Actually this law was based on observations of VLF propagation above 12 kcs. In 1957, Wait [1957] theoretically established this absorption band at 1 to 3 kcs.

The attenuation coefficient "α" in the ELF region is quite low. Chapman and Macario [1956] from their amplitude spectra measurements, found "α" to be 1 db/1000 km at 100 cps. Tepley [1959] has also experimentally determined "α" and dispersion in the ELF region. In addition to these studies of "α," substantial work has been done on the waveform patterns themselves. Chapman and Pierce [1957] observed the different waveforms as a function of geographical location where distance and lower ionosphere conditions were considered the same. In addition, Hepburn [1958] classified waveforms according to source, distance, and geographical effects. See also Hepburn [1957a] and [1957b] .

Hepburn and Pierce [1953] established experimentally an empirical law for "t" and "$\frac{T}{4}$" as a function of distance for both night and day. They also worked out values of ionosphere height and conductivity using Hales [1948] theory These figures were later revised by Hepburn [1957b] . Liebermann's

[1956a] experimental results for slow tail propagation fit his theory [Liebermann, 1956b] for values of ionosphere heights and conductivity which did not agree with those of Hepburn and Pierce [1953] or Hepburn [1957] . Pierce [1960b] states that these different results have never been resolved. However, Wait [1960b] indicates that the different results are reconcilable if it is remembered that Hales' [1948] theory is only good for narrow band type of signals, i.e., quasi-monochromatic.

In addition to the observation of "t" and "$\frac{\tau}{2}$," the polarity of the slow tails has also been of interest. Liebermann [1956a] was apparently the first to observe two types of slow tail pulses. The normal tail is shown in Figure 1.1. The "anamolous" tail is initially positive-going but completes a full cycle in the period "τ" before tapering off. Whitson [1960] reported an apparent phase reversal of ELF waveform-- positive-going at St. Johns, Newfoundland and negative-going at Thule, Greenland. He states that further investigation is necessary before such a reversal can be considered a reality. Taylor [1961] noted that the positive-going tails had more well defined relationship between such parameters as radiated energy, peak field strength, $\frac{\tau}{2}$, and frequency of the spectral peak than the negative-going tails. Tepley [1961a] , who also considered the polarity of slow tails, believes that the negative polarity is due to intra-cloud discharge, not to propagation effects, and that the positive polarity tail is due to regular cloud-to-ground discharge.

Experimental evidence of propagation as a function of direction has been obtained. Lutkins [1939] was the first to

observe that waveforms from the west contained more oscillations and were smoother than those from the east. Crombie [1958] found that VLF signals were attenuated less in West-to-East propagation. Barber and Crombie [1959] showed that ionosphere reflection depends on the direction of propagation. This, of course, supports the experimental evidence.

Other aspects of atmospheric noise such as the electro-static field and lightning itself have been observed and studied. Watt [1960] finds that in fair weather the electrostatic field is approximately 100 v/m and in foul weather as high as 4,000 v/m. During fair weather, the static E field fluctuations are around 1 v/m [Pierce 1955] . The duration of field changes due to lightning is as long as one second [Pierce 1960b] . Lutkin [1939] has measured fields up to 600 v/m at a distance of 5 km from a storm. Wilson [1920] found that the field changes due to a nearby thunderstorms were usually positive. Lightning has been found to occur on the average of 100 strokes/sec over the earth [Liebermann 1956a] . This average over the earth's surface also agrees with Davis [1961] .

B. The Status of ELF Noise Data

Regardless of the numerous investigations of atmospheric noise, the experimental data in the ELF region is rather limited [Wait and Carter, 1960; Wait, 1960d; Watt, 1960] . The experimentation that has been done in this region has been "incidental to the reception of higher frequencies" [Liebermann 1956a] , in connection with recording of slow tails [Wait, 1960b; 1960e] , and in geomagnetic work at frequencies below 0.1 cps

[Goldberg, 1956] . Duffus, et al. [1958] refer to their experiment in 1957 as being conducted in the "somewhat neglected frequency range 0.1 to 30 cps." The meagerness of noise information in the ELF region is indicated by the fact that the International Radio Consultative Committee Compilations extend down to only 10 kcs.

This lack of ELF noise data is a hindrance to experimenters in developing receiving equipment and to theoretical investigators in analyzing their work. In discussing his system for sferic observations, Whitson [1960] mentions that it was made flexible because the nature and magnitude of sferics in the arctic were unknown. Pierce [1960a] maintains that further theoretical work in ELF propagation is "academic" as long as experimental observations remain "so scanty."

In contrast to the experimental work in the ELF region, considerable attention has been given to theoretical work by Schumann [1952a, 1954a, 1954b] , Wait [1956] , and Liebermann [1957] . One aspect of these studies has been the development of the mode theory in which the earth and ionosphere are considered as a resonant cavity. The resonant frequencies of this cavity were apparently first suggested by Schumann [1952b] . The first three Schumann mode frequencies--10.6, 18.3, and 25.9 cps--were also determined by Wait [1960a] .

In spite of the theoretical work on the mode frequencies, there has been practically no effort made toward securing experimental evidence of their reality. At the time of this literature survey, Balser and Wagner [1960] reported their unsuccessful experiment to observe these resonant frequencies

They concluded that further experimentation was necessary at frequencies nearer to the fundamental 10.6 cps.*

C. The Need for ELF Noise Investigation

The absence of information in the ELF region does not of itself constitute a need for further physical research. However, as pointed out in the previous section, this situation has hampered theoretical work and has had a bearing on experimentation. Many researchers in atmospheric noise have expressed the need for further investigations in the lower VLF and the ELF regions of the spectrum.

In 1957, Watt and Maxwell [1957] emphasized the importance of knowing not only the character of atmospheric noise but also the level when determining system performance. They show that the limiting noise factor in VLF communications is atmospheric noise rather than man-made or thermal noise and conclude that the "need for a detailed investigation of the statistical character of atmospheric noise is readily apparent." Anderson [1961] demonstrated that natural noise is also the basic limitation in the 1 to 1,000 cps region and pointed out that system attenuation figures in this region must be related to expected noise power to have "practical significance." Evaluating the expected noise power proved to be a problem since the noise data (1 to 1,000 cps range) published in the literature had a wide range of values and was difficult to interpret.

---

*In 1961, after the investigation discussed in this paper was in progress, Fitchen, et al. [1961] reported evidence of resonance at 9 cps while, according to Raemer [1961] , Balser and Wagner (in a subsequent experiment) reported 8 cps as did Maple [1961] .

In addition to the importance of noise data in the analysis of communication system performance, other manifestations of atmospheric noise are considered important. For example, more detailed results are urgently needed on ELF propagation [Pierce, 1960a] . More measurements are required to accurately fix the source of the noise and to determine the dependence or independence of the propagation path upon geomagnetic or geographical effects [Wait, 1960b].

Perhaps the main motivation for further research in the ELF and the lower VLF region arises from the implications even at the present state of knowledge. The extremely low attenuation in this region of the spectrum implies world-wide communication systems. The fact that these frequencies penetrate the ionosphere because of magneto-ionic phenomena further implies space communications [Wait, 1960c]. Other less spectacular, but nevertheless important, possibilities have also been considered. The correlation between atmospherics and the atmosphere potential gradient at sea suggest a means of measuring world-wide thunderstorm activity [Holzer and Deal, 1956]. In addition, the ELF radiated from lightning can serve as a thunderstorm location system [Wait, 1960b].

D.   The Noise Data

The conclusions reached as a result of this literature review are (1) that very little data has been obtained in the ELF region and (2) that a need for further data exists. This investigation was undertaken to contribute to the fulfillment

of this need by seeking evidence of the Schumann frequencies and by securing noise amplitude data in the 0 to 50 cps region.

The noise data were recorded for approximately 30 minutes and are considered representative of the noise activity for the hour during which they were taken. During the data processing, the output of each of 10 filters is rectified and integrated. This output is expressed in field strength units. Thus the data are available for plotting purposes in units of field strength for each frequency for each hour recorded. Sample plots of the data are given in Chapter 6.

E. Instrumentation

Although information in the literature concerning instrumentation is lacking in detail, the overall systems are generally given or are discernible. This is the case since the instrumentation approach is determined largely by the particular aspect of the noise phenomenon that is being investigated. In the study of waveform patterns, for example, the display on an oscilloscope is photographed. Information on attenuation as a function of frequency and distance can be obtained by a simultaneous oscilloscope display of the sferic waveform and its spectrum. In whistler experimental work, the spectrograph is the main research instrument.

Amplitude versus frequency information is often provided by a sweeping or scanning filter and a pen recorder arrangement. This method provides a permanent but not a readily reproducible record of the data. It has only been comparatively recently that data has been recorded and stored on magnetic tape. This

means of recording data has the distinct advantage that the
data can be repeatedly processed. In addition, the magnetic
tape can be played back at speeds which are many times the
recording speed. This method eases the filtering requirements
and saves processing time. The recording of the data on
magnetic tape implies that the frequency range of the data is
within the response of the recorder.

The frequency range of interest in this investigation was
below the lower limit of the response of the available tape
recorder. The system discussed in this paper was devised to
make the recorder compatible with the data. This system is quite
different than those discussed in the literature. Essentially
the noise data is frequency translated to within the frequency
range of the recorder during the record mode and restored to
its original position in the spectrum during the play-back mode.
A synchronizing signal ensures proper demodulation during
play-back independent of tape speed. This signal also is a
means of monitoring frequency variations due to speed changes.
In this manner, excursions outside of the filter bandwidths
are observed. Lastly, this synchronizing signal is available
as a control signal for a servo system to automatically control
motor speed during play-back if necessary.

2. The Overall System

Several design criteria are incorporated in the system. These criteria are due to environmental conditions and to the desire for flexibility. Inasmuch as the natural electromagnetic noise is the desired data, man-made noise and interference are eliminated by recording in remote locations free of such artificial noise sources. The data-taking system itself is battery-operated to eliminate power transforming equipment and its associated noise and to facilitate transporting the equipment to these remote sites. All components of the system function properly at temperatures up to approximately 40°C. This upper temperature limit allows data-taking during the summer months and in relatively warm weather.

In order to incorporate the greatest possible flexibility in the system, the data is recorded on magnetic tape. Thus the data is permanently preserved in a form that can be repeatedly recovered. This permits processing the same information by more than one method.

In the development of any data-collecting system it is essential that the design be compatible with a feasible data-processing system. In the final analysis the main concern is whether or not the data can be recovered in an economical manner. Perhaps one of the most direct methods of data recovery is by filtering. This is particularly so in this case since the relative activity at different frequencies in the 0 to 50 cps range is desired. This display of data can be directly compared with the Schumann mode frequencies.

Considering the various types of filters, the Wien-Bridge and Twin-T were selected largely on the basis of economy, i.e., being composed of resistance and capacitance. The Wien-Bridge was rejected since there is no common ground for the input and output.

A complete discussion of the Twin-T filter is given in Appendix A. Figure A9 in Appendix A shows that the resistance and capacitance required for frequencies in the 0 to 50 cps range have values that are readily available.

The ability to filter a particular frequency was experimentally verified. Equivalent circuit Q's on the order of 25 were readily attained. The selective amplifier used permitted adjusting the "Q" to any desired value less than maximum (25).

This paper is concerned with the data-collecting system. However, the basic idea involved is inherently related to the method of modulating and demodulating during data-collecting and data-processing. Consequently, the basic idea is briefly described here before proceeding with a detailed discussion of the data-collecting system.

A block diagram of the data-collecting system is shown in Figure 2.1. The data-signal, as shown in this figure, is fed through a switch and is interrupted or "chopped" at a rate determined by the oscillator. The multivibrator is synchronized by the oscillator and drives the switch. The data is recorded on the data-track of the tape as sidebands about the switching frequency. Simultaneously, the oscillator signal is recorded on the synchronizing (sync) track of the duo-track tape of the magnetic tape recorder.
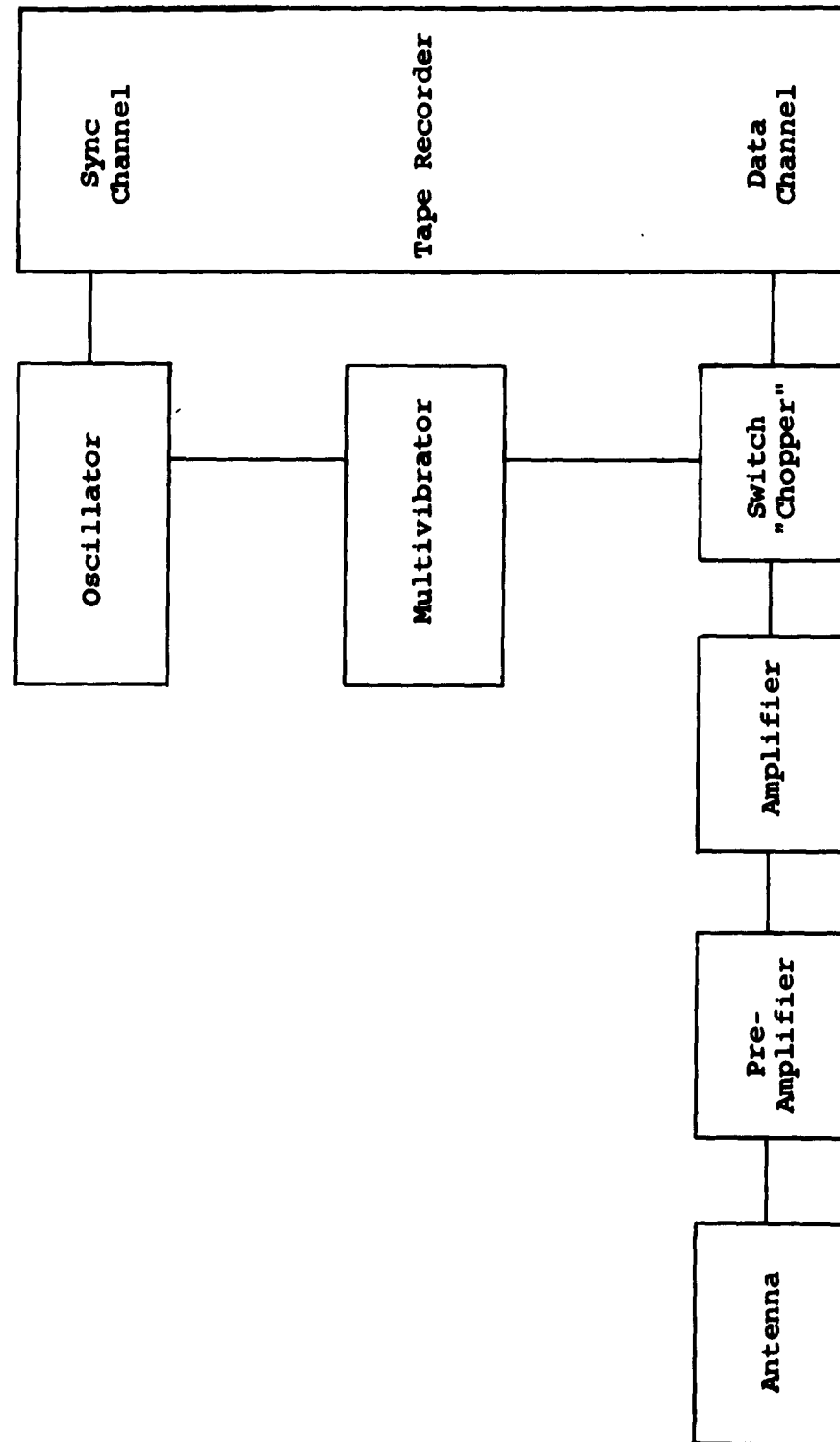
Figure 2.1 Block diagram of data-collecting system

During data-processing (Figure 2.2), the output of the data-track is fed through the switch and interrupted or "chopped" at a rate determined by the signal from the sync-track. The low-pass filter removes the fundamental and harmonics of the switching frequency and passes the original data spectrum.

Thus in this system the sync signal and the data carrier are always of the same frequency and phase regardless of speed variations of the tape recorder during recording or playback. Since the sync signal is actually the demodulating frequency and the data carrier frequency is the original modulating frequency, the modulating and demodulating frequencies are always of the same frequency and phase. It is analytically shown in Appendix C that such similarity in frequency and in phase of both the modulating and demodulating carriers is a necessary requirement for this type of demodulation.
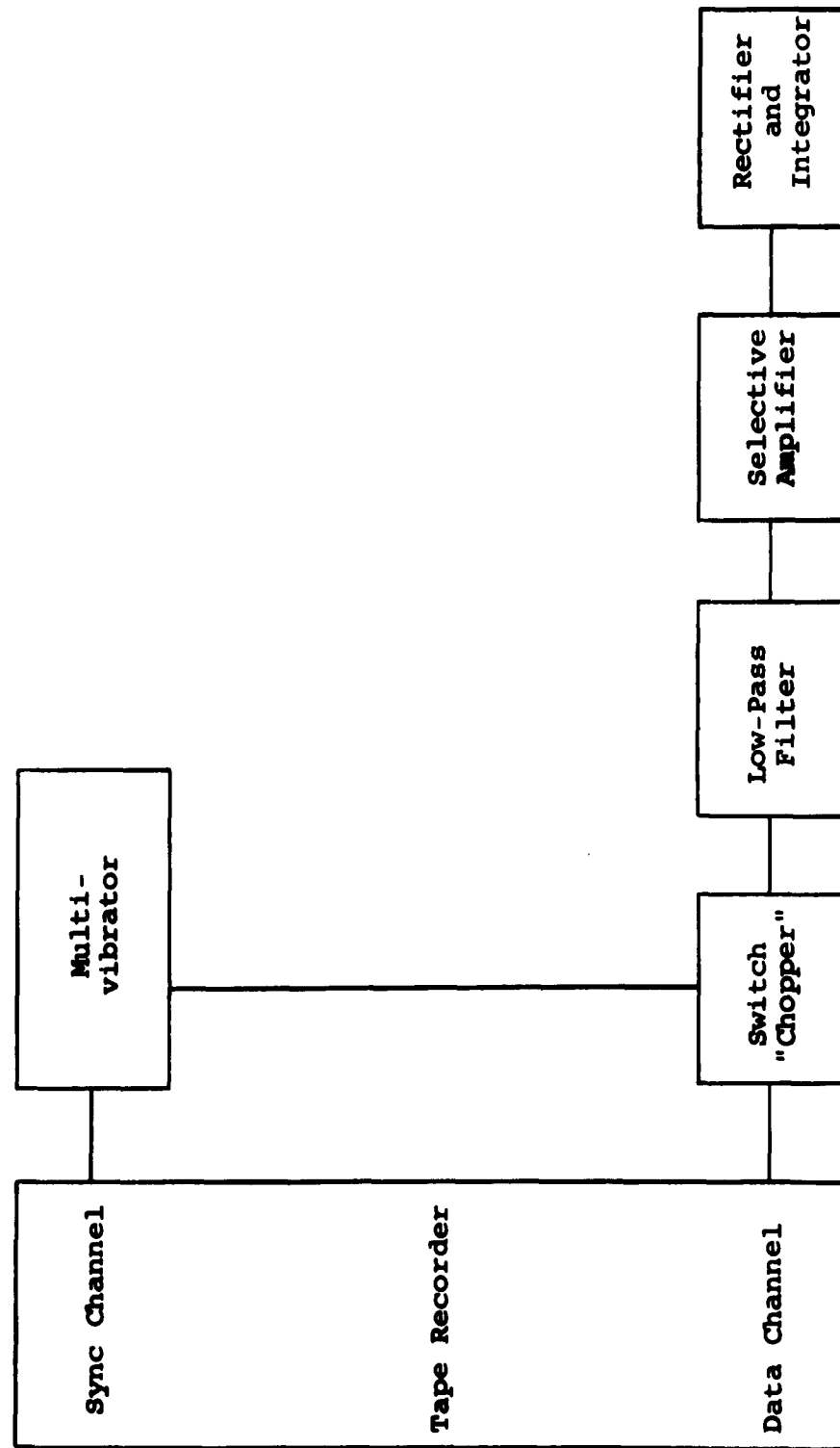
Figure 2.2 Block diagram of data-processing system

3. Individual Units of the System

A. Tape Recorder

The initial requirement, portability, can be met in either of two ways--using an a-c operated recorder with a battery-powered converter or a battery-operated recorder. The converter arrangement was rejected because the possibility of noise-free operation is not guaranteed with either mechanical or solid-state type converters.

The decision to use a battery-operated tape recorder necessitated an investigation into the effect of speed character-istics upon reproduction. This is particularly so for a battery-operated tape recorder since speed specifications while usually not available are generally less stringent than a-c operated machines. It is shown in Appendix B that the percent-age frequency change is proportional to the percentage speed variation. Since filtering during the data-processing is to be accomplished with circuit Q's up to 40, the maximum speed variation must be within approximately 0.6%.

A survey of available recorders showed that the frequency response was approximately 150 to 5,000 cps at the slow tape speeds. Obviously some means of frequency translation is necessary to place the data in the response region of the recorder. In addition, the method of accomplishing this trans-lation must be compatible with speed variations inherent in the recorder and with the demodulation system.

Frequency translation immediately suggests a switching technique. A complete discussion of both single-ended and

bi-polar switching as a modulation method is presented in
Appendix C. The conclusion reached in this discussion is that
single-ended switching is much simpler and more economical.

To ensure that this switching-type modulation system would
be compatible with a similar demodulation system, an inquiry
into the demodulation process was made as shown in Appendix C.
This inquiry shows that demodulation by switching can be
accomplished provided the modulating and demodulating carriers
are of the same frequency and phase.

In view of the frequency and phase requirements, demodula-
tion by envelope detection was considered. However, the
switching method offered several advantages in spite of the
necessity for incorporating a synchronizing track along with
the data track on the recording tape. The synchronizing signal
and modulated carrier arising from the same frequency source
and simultaneously recorded and played back, always fulfill
the frequency and phase requirements simply because they are
both simultaneously subjected to the same tape speed variations.
In addition, the synchronizing signal provides a means for
monitoring circuit operation during data-processing since the
data undergoes the same percentage variation in frequency as the
synchronizing signal due to speed variations.

The Steelman Model 2-7111 portable tape recorder was
selected largely on the basis of economy. This is a two-
speed (1 7/8 and 3 3/4 ips), two-track record and playback
machine. It is completely transistorized and battery-operated.
Since mid-frequency response occurs at 1000 cps at the slow
speed, this frequency was selected for switching. At the slow

speed approximately 32 minutes of recording time is obtained
by using 300 ft. of 1/2 mil tape a 1/4 inch wide.

Several modifications were necessary to adapt the tape
recorder to the system. The extent of these modifications can
be seen in Figures 3.1 and 3.4 which are block diagrams before
and after the modifications were made. The first consideration
in adapting the recorder to the system was the feasibility of
using the erase head as a recording head for the 1 kc synchroniz-
ing signal (sync signal). Using this method gave excessive
inter-channel modulation regardless of the head position. This
was due apparently to the large air-gap in the erase head core.
Replacing the erase head with a regular recording head and
leaving the bias oscillator disabled gave satisfactory results.
In fact, tests indicated that inter-channel modulation was
approximately -40db.

Results of these tests further showed that the impedance
to the sync head was 6 k-ohms and that it required approximately
1.0 volts for satisfactory level of recording. However, in
the play-back mode, the output of this head was approximately
4 mv. To reduce the amplitude requirement for the oscillator
in the data-collecting system, this 250/1 voltage ratio is made
up during data processing by an additional amplifier. The
phone jack which normally shunts the speaker was connected
directly to the sync head to serve as "sync in" and "sync out"
terminals in the record and play-back modes, respectively.

The effects of disabling the bias oscillator were investi-
gated. The purpose of this oscillator is to remove any residual
magnetism on the magnetic tape which causes noise and
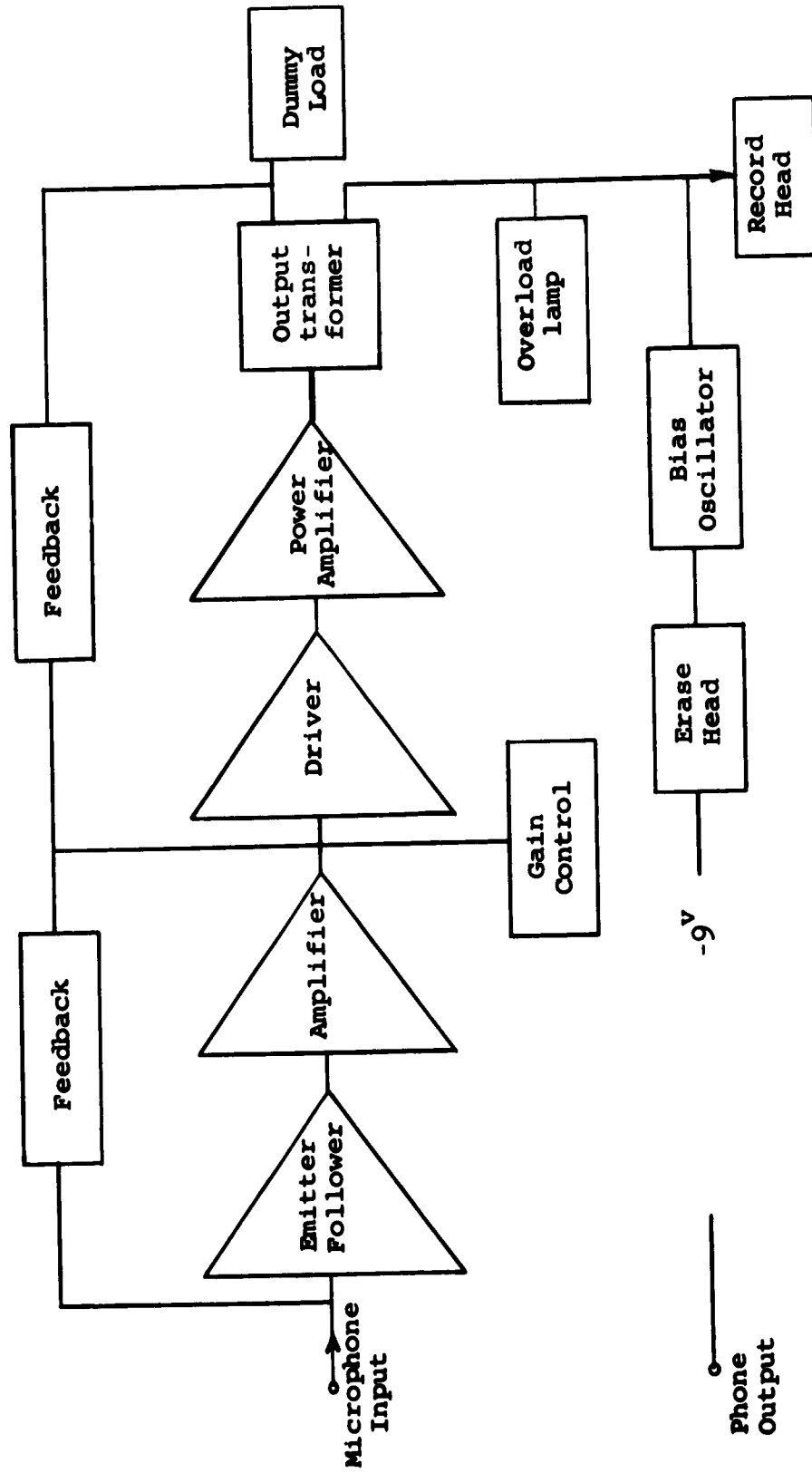
Figure 3.1 Block diagram of tape recorder in record mode before modification
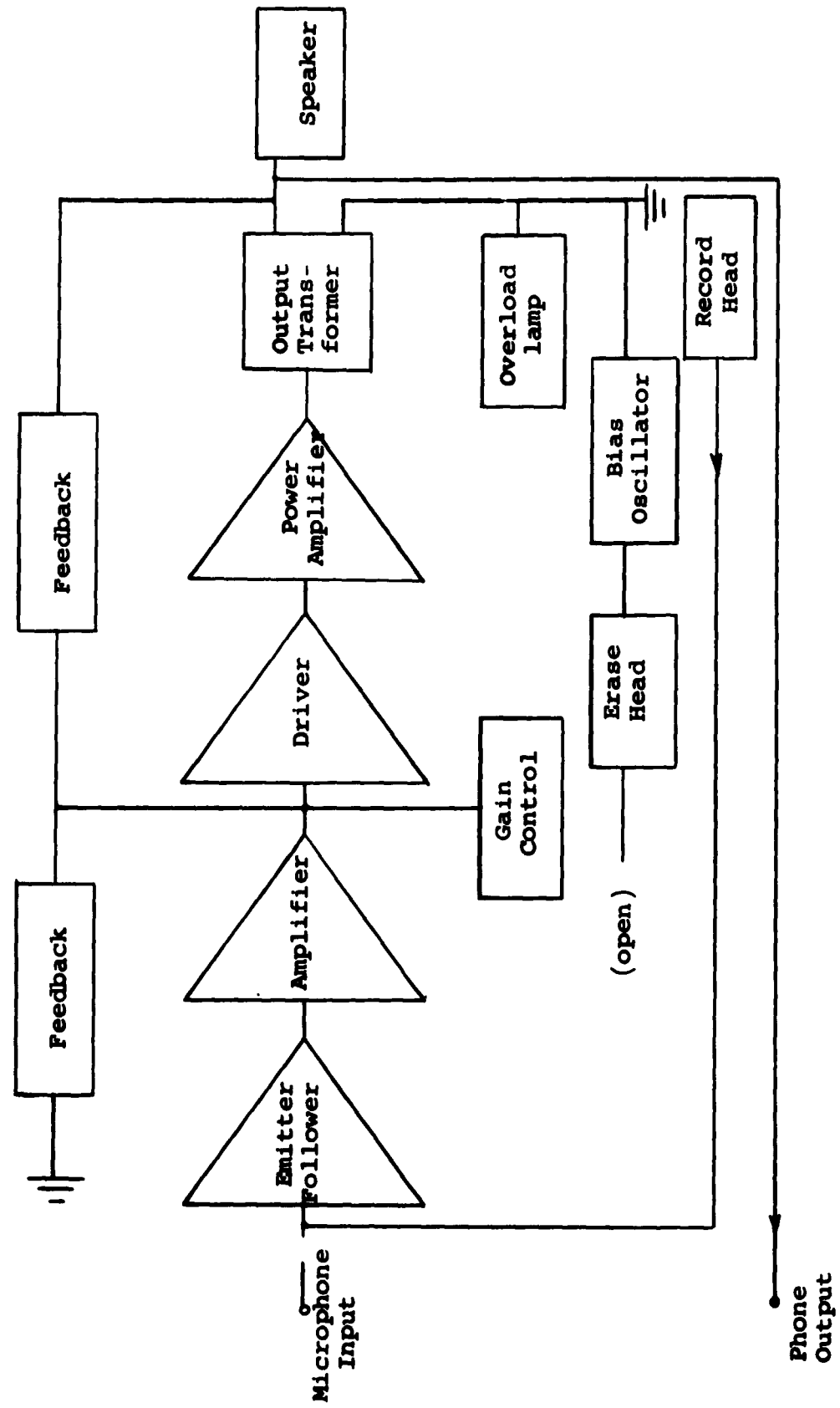
Figure 3.2 Block diagram of tape recorder in playback mode before modification
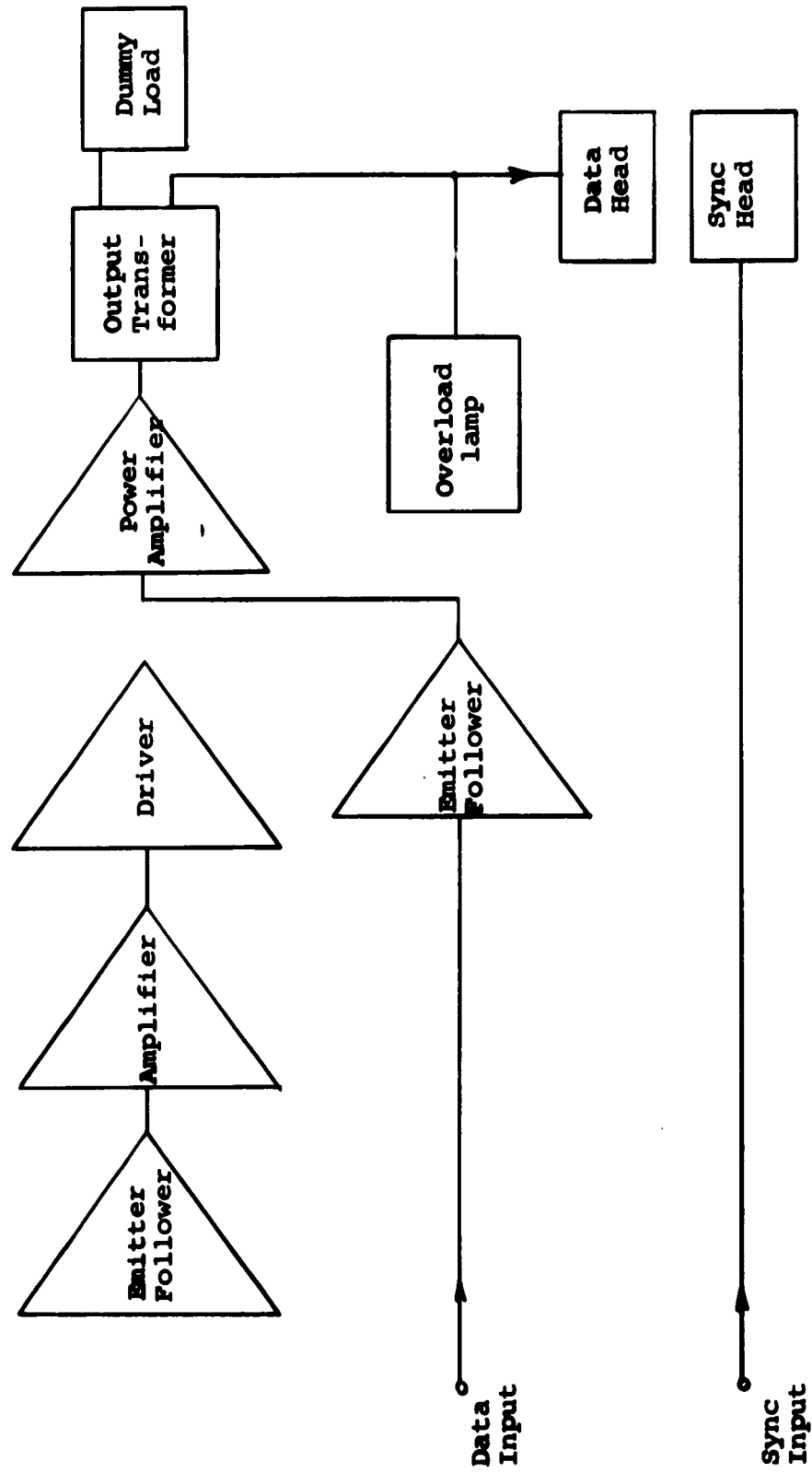
Figure 3.3 Block diagram of tape recorder in record mode after modification
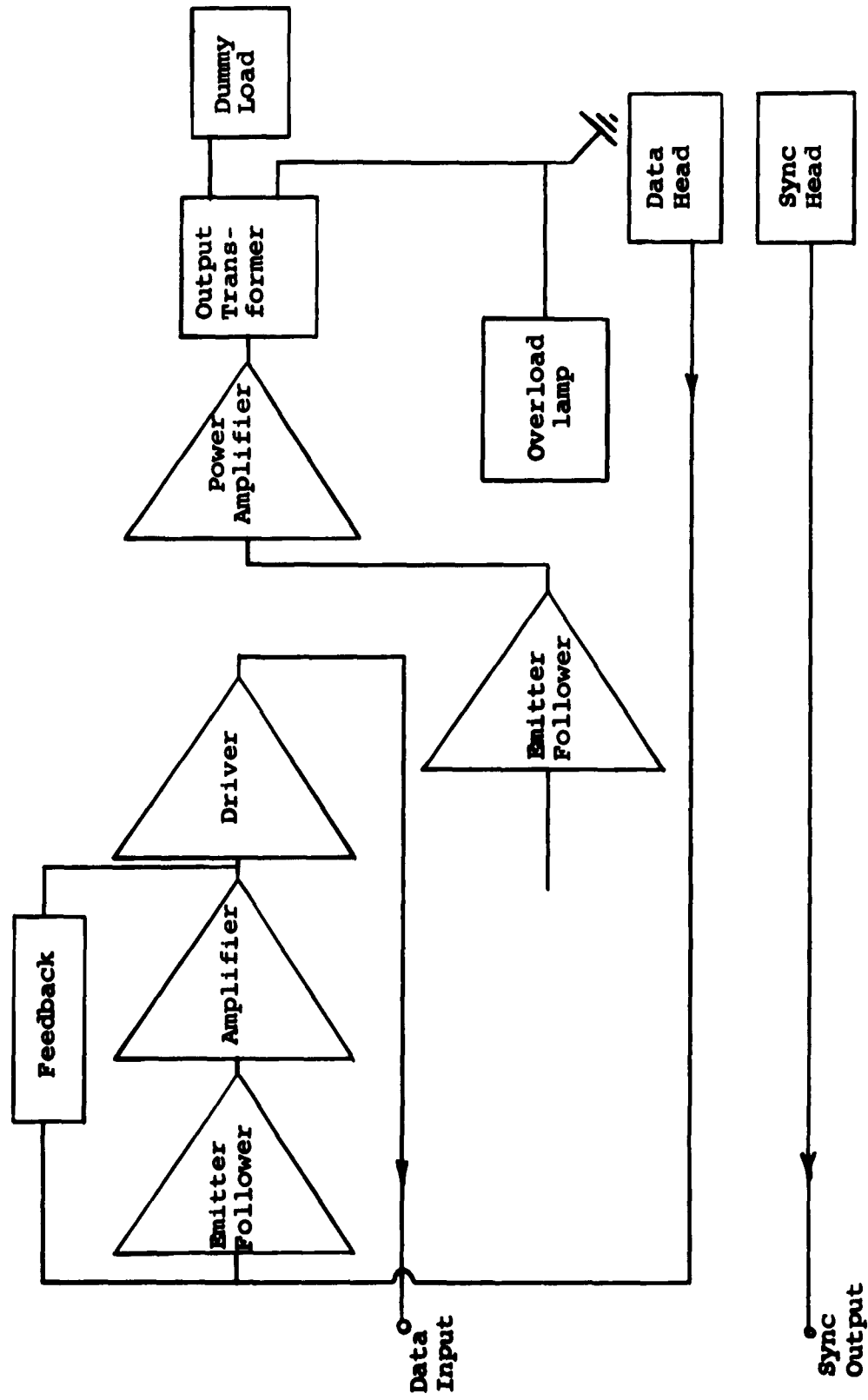
Figure 3.4 Block diagram of tape recorder in playback mode after modification

nonlinearities. Tests indicate that the linearity character-
istics on record and play-back are satisfactorily preserved
when the tape is de-magnetized prior to recording. Thus, as a
matter of procedure all tapes are bulk-erased before recording.

The output of the switch when fed into the low-level input
terminals of the recorder overloaded its amplifier. This
amplifier consisted of an input emitter follower, common
emitter voltage amplifier, and a common emitter driver feeding
a pushpull power amplifier. The input impedance of this power
amplifier is 2700 ohms. A 2.5 volt (peak-to-peak) signal at the
input of this amplifier gives a 13 volt (peak-to-peak) signal
at the collector side of the output transformer and causes the
"overload lamp" to just come on. The overload lamp is in shunt
with the regular record head (hence to be referred to as the
data head) and is connected to a secondary of the power amplifier
output transformer. Tests indicate that this overload lamp
gives an accurate indication of overloading in the power
amplifier.

The output of the switch was in excess of 1.25 volts
(peak) with an impedance of 56 k-ohms. This indicated that
impedance matching between the switch and power amplifier was
necessary. To this end several modifications were made.

The speaker was removed and the speaker dummy-load was
connected at the function switch so that it remained in the
circuit in both the record and play-back mode instead of the
record mode only. This change insured that the reflected
impedance as seen by the power amplifier remained the same in
both modes as before.

An emitter follower installed in the place vacated by the speaker served as an impedance matching device between the switch and the power amplifier. Actually the emitter follower loaded the switch such that the overload lamp just came on when the switch was saturated, i.e., the modulation on the switch was maximum. Thus monitoring the overload lamp was as effective as monitoring the switch itself. With this modification the first three stages were not used in the record mode. Therefore the function switch on the recorder was rewired so that in the record mode (1) the microphone jack (hence referred to as the data input jack) was connected to the emitter follower and power amplifier, and (2) the battery power was removed from the first three stages.

Connecting the switch to the power amplifier through the emitter follower worked satisfactorily. However, in the play-back mode, a 12 kc oscillation was present in the output even when no tape was being run.

In the original circuitry there were two feedback circuits--(1) the main feedback circuit around the power amplifier and the third stage, and (2) the microphone compensating feedback circuit around the first and second stages during record and from the second stage to ground during play-back. Opening the main feedback circuit reduced the magnitude of the oscillation somewhat. The instability was caused by the feedback from the second stage to ground. The function switch was modified to put this feedback circuit around the first two stages during the playback mode and open the circuit in the record mode. This modification did not effect the response in the region of interest--1000 $\pm$ 50 cps.

The speed of the tape recorder motor is set by an electro-mechanical governor. The supply voltage indicator lamp is energized by transformer coupled pulses due to the governor contacts. Thus, the operation of the governor can be monitored. This lamp extinguishes when the battery voltage drops to approximately 50% of its normal value.

B. Oscillator

Theoretically there are no criteria for choosing a type of oscillator for this application other than that it produces a sinusoidal output and is stable. However, for practical reasons, there are a few requirements that the oscillator must satisfy.

The oscillator must function properly at temperatures up to $40^{\circ}C$. This upper temperature limit was mentioned previously as being applicable to the whole system.

The supply voltage required must be of such value that the physical size and configuration of available batteries is suitable for portability. In addition, the current drain must be minimal for reasonably long battery life.

The output of the oscillator must be of sufficient amplitude to synchronize a multivibrator. This amplitude should not be a critical function of battery voltage. In addition, the waveform should be relatively undistorted.

The output impedance should be sufficiently low to preclude loading by the multivibrator, tape recorder synchronizing channel, and the oscillator test point. This test point is to be incorporated so that the output of the oscillator can be monitored continuously or at the discretion of the operator.

The oscillator frequency should be such that it falls within the flat response region of the tape recorder. This frequency must also be such that reasonably small components can be used for convenient packaging and construction.

The frequency stability should be within .025 per unit bandwidth for the range of tolerance of battery voltage

which will produce sufficient output to synchronize the multivibrator. Provisions for frequency adjustment should be incorporated.

A Colpitts transistor oscillator shown in Figure 3.5 was finally selected since it was in harmony with the specifications. As mentioned before, the frequency of 1000 cps was chosen on the basis of the tape recorder response. At this frequency the physical size of the elements is still suitable for packaging. The battery, to supply approximately 9 ma at 22.5 volts for a reasonable length of time, can also be physically accomodated in a small portable system.

The output voltage varies from 1.0 to 1.5 volts (peak) for a corresponding change in battery voltage from 19.5 to 22.5 volts. The output impedance is approximately 170 ohms. These output characteristics permit driving the sync head directly. This output voltage range is also adequate to synchronize the multivibrator throughout the adjustable frequency range of the oscillator--960 to 1300 cps.

The variation of frequency versus battery voltage with temperature as a parameter, presented in Figure 3.6, is within 1.8% over a 19.5 to 22.5 voltage range. The upper temperature limit satisfies the temperature specification for the system.
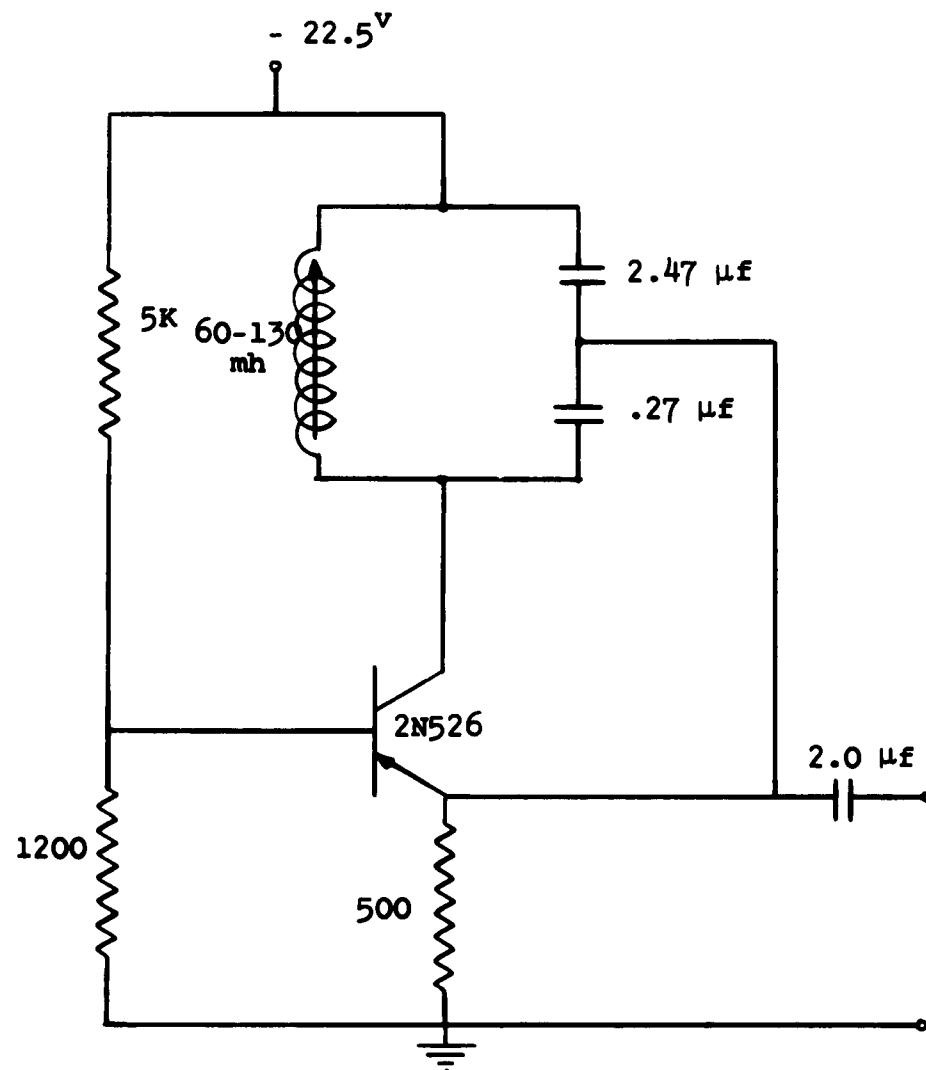
Figure 3.5 Schematic diagram of the oscillator
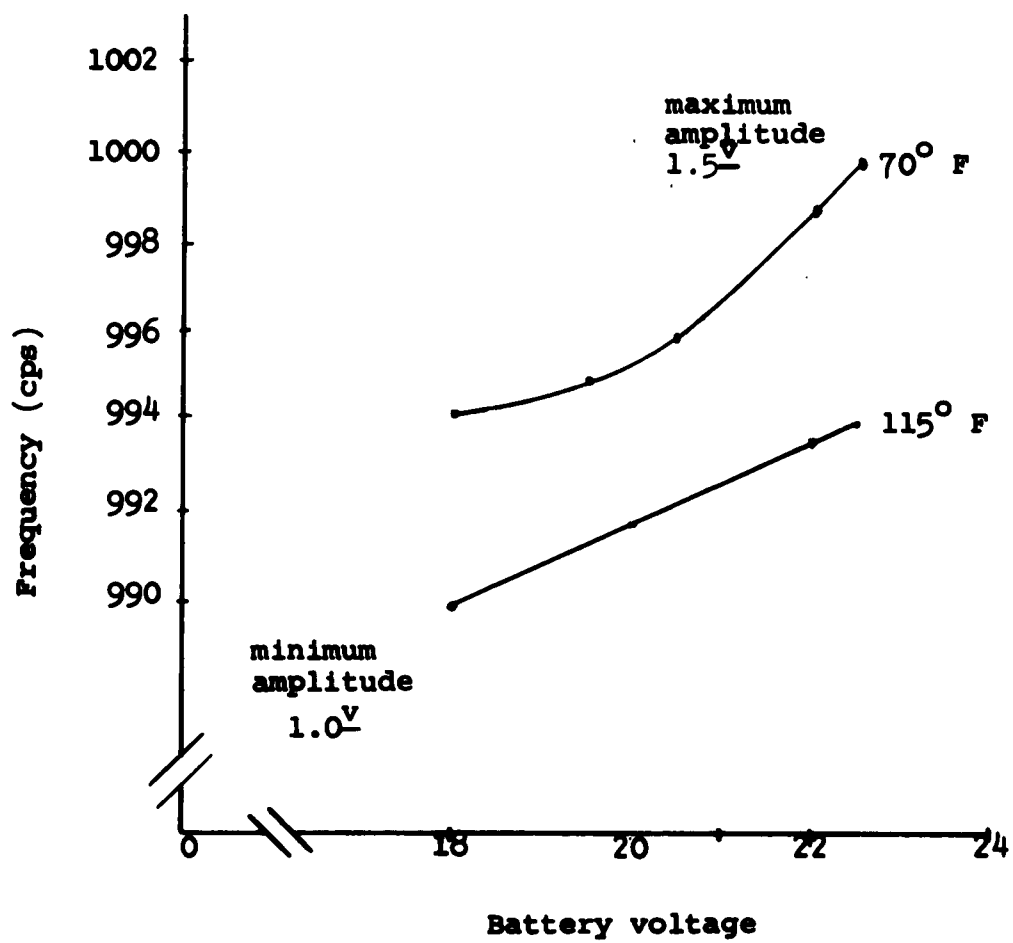
Figure 3.6 Oscillator frequency versus battery voltage
for variations in temperature

C. Multivibrator

The function of the multivibrator is to drive the switch at a rate determined by the oscillator. The output waveform should be symmetrical and have sufficient amplitude over a reasonable battery voltage range to drive the switch properly. Here as throughout the system the physical sizes of batteries and parts are a consideration.

The circuit which was finally developed is shown in Figure 3.7. The output waveform is symmetrical and at least 4 volts (peak-to-peak) for a supply voltage range of 7 to 9 volts. This signal is adequate to drive the switch.

The multivibrator is free-running at approximately 1000 cps with no sync input. With maximum battery voltage (9 volts) on the multivibrator, the output of the oscillator (1.0 to 1.5 volts) is sufficient for synchronizing the multivibrator over the frequency range 960 to 1300 cps. In addition, the sync input impedance is approximately 1200 ohms which results in negligible loading of the oscillator.
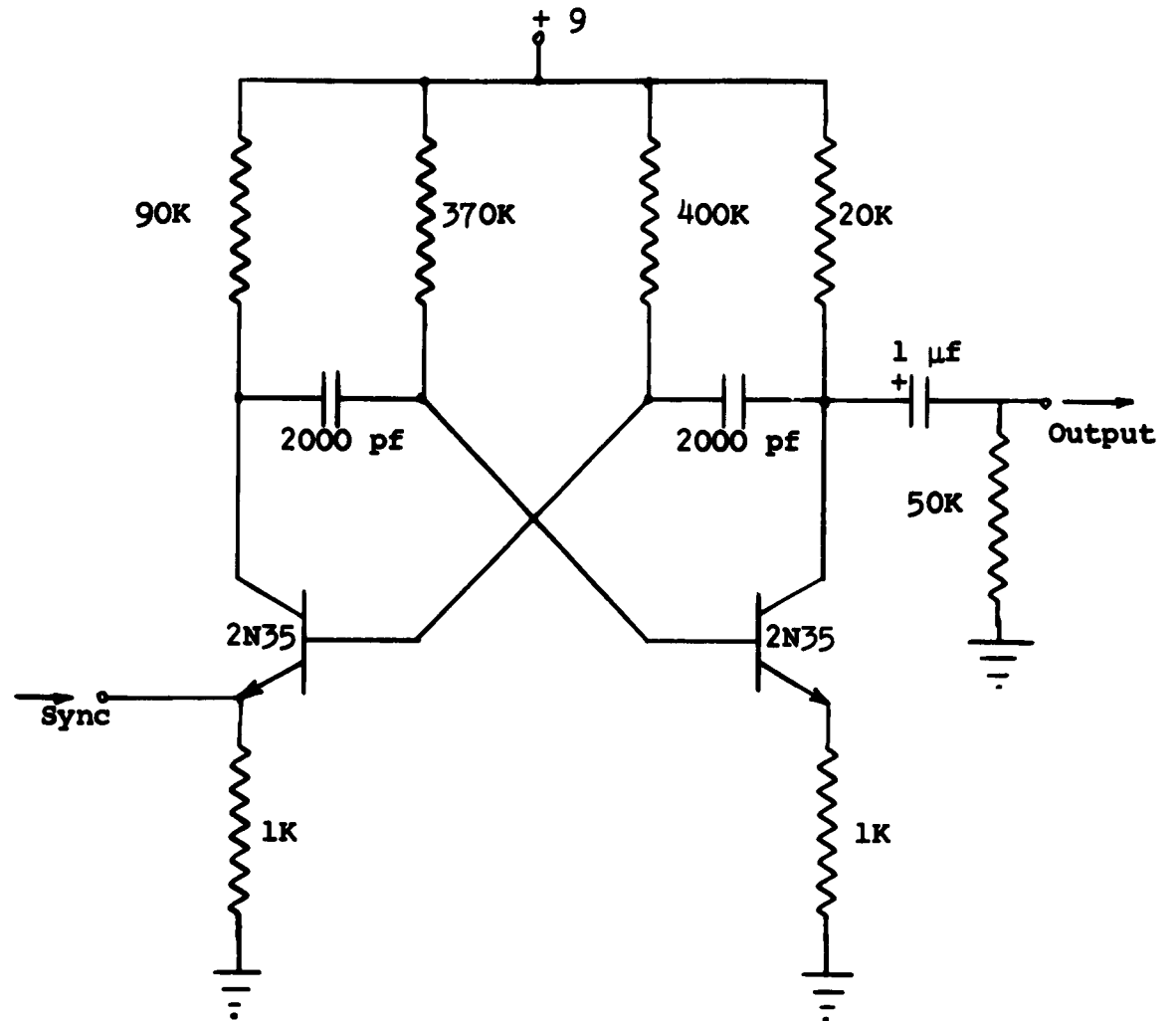
Figure 3.7 Schematic diagram of the multivibrator

D. Switch

The function of the switch is to interrupt or "chop" the data at the oscillator frequency. As mentioned before, this switching can be accomplished by either of two basic methods-- single-ended and bi-polar. The single-ended method was selected primarily bacause of simplicity. A complete analytical discussion of the switching technique is given in Appendix C.

The final circuit design is shown in Figure 3.8. As mentioned previously in the Tape Recorder section (3A), an emitter follower was installed in the tape recorder as a matching device between the power amplifier of the recorder and the switch. To prevent overdriving this power amplifier, the "match" was such that saturation of the switch caused the over-load lamp to come on. This indication serves as a means of monitoring and setting the amplifier gain.

With the tape recorder connected, the switch has a 0.5 volt (peak-to-peak) output in the emitter circuit. This means, of course, that data-signals of 1.0 volts (peak-to-peak) can be satisfactorily chopped without saturating the switch. These waveforms are shown in Figure 3.9.

The switch requires a 4.0 volt square wave at the base for proper operation. This was really a specification applied to and fulfilled by the multivibrator. The input impedance for the data circuit is approximately 50 k-ohms. This impedance does not load the amplifier. That there should be no such loading was actually a design requirement on the switch because the type of amplifier had already been selected.
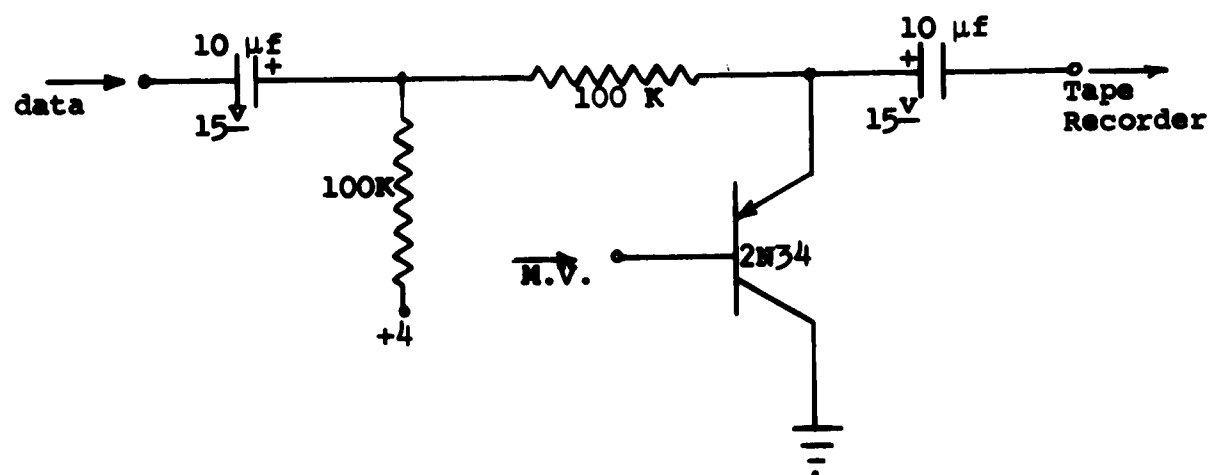
Figure 3.8   Schematic of the switch, "chopper"

Switch output with no data

(a)

Switch output with arbitrary data

(b)
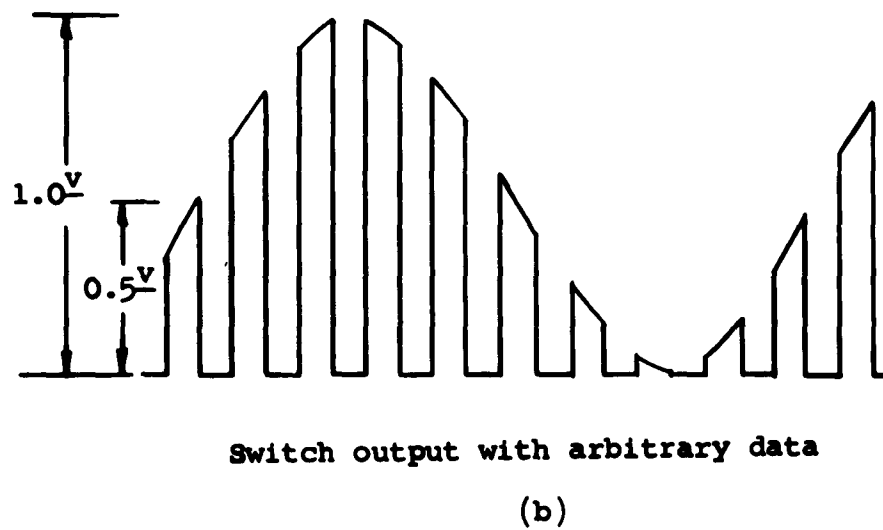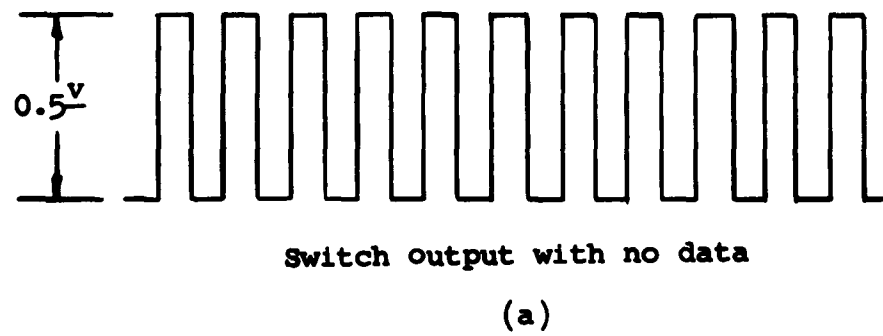
Figure 3.9   Diagram of the switch output waveforms

E. Amplifier

The requirements stipulated for the amplifier were based on the assumption that very low signal strengths would be encountered. This assumption also necessitated a low noise figure requirement.

The circuit in Figure 3.10 was finally selected largely on the basis of low noise figure. Direct coupling throughout the circuit affords economy of parts and space. The overall gain is approximately 1000 over the range of 3 cps to 30 kcs. Thus, with the selection of this amplifier, the specifications for the system were altered from 0 to 50 cps to 3 to 50 cps. Mercury batteries are used because of their low-noise and constant terminal voltage characteristic. The low drain on these batteries makes possible about 1500 hours of service.

The circuit has good stability over a large temperature range. In fact, satisfactory performance can be secured at temperatures around 45°C. The stability is also good for large variations in transistor characteristics. This facilitates interchangeability.

Due to feedback the input impedance is essentially the impedance of the input capacitor and series resistor. Thus, with the gain in the X1000 position, the input impedance is essentially 470 ohms. With a low impedance source (much lower than 470 ohms), the input current is a function of the input series resistance. This fact is evident since the input resistance differs by a factor of ten and the gain differs by the same factor. The 4.7 k-ohm input resistance was permanently removed since only the gain X1000 is of interest.
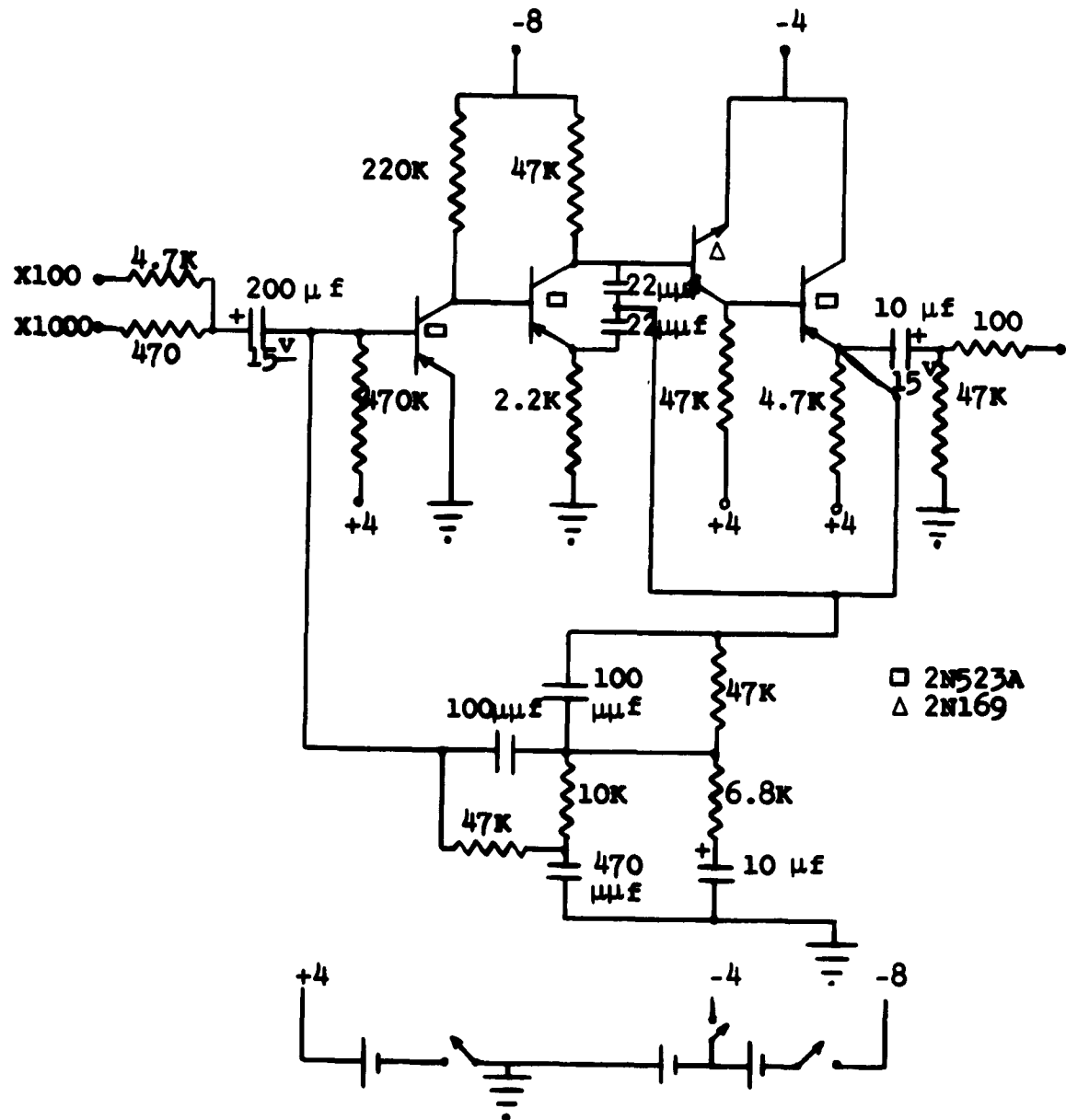
Figure 3.10 Schematic diagram of the amplifier

The no-load maximum undistorted output with a 1 kc test signal was 3.1 volts (peak) for a 3.45 mv (peak) input from a low impedance source. This is a gain of approximately 900 in the X1000 position. Clipping occurs for loads less than 7 k-ohms.

The measured output impedance was approximately 1800 ohms. Under no-load conditions the output has an inherent load--the 10 uf capacitor and 47 k-ohm resistor. This "no-load" condition can be incorporated in the switch. The input impedance of the switch was designed with this in mind. In the final system, the switch, Figure 3.8, is connected directly to the emitter of the last stage in the amplifier. With this connection the gain of the amplifier in the X1000 position is approximately 970. The gain variation from 5 to 1000 cps is about 0.5 db.

The basic feedback circuit is from the output to the input of the amplifier. This feedback circuit consists of a lead-lag circuit connected to the amplifier output in series with a bridge-T circuit connected to the amplifier input. The necessary magnitude of the feedback voltage is controlled primarily by the lead-lag circuit. This circuit also provides the necessary phase-lag at the lower frequencies. However, the phase-lead that is introduced is excessive in the 10 to 50 kcs region.

The bridge-T network while having very little effect on the magnitude of the feedback voltage introduces a phase-lag that increases with frequency to 34 kcs. Beyond 34 kcs, this phase-lag changes quickly to a phase-lead that increases with frequency. The net effect of the lead-lag and bridge-T circuits

is that in the 26 to 52 kcs region the phase-lead increases rapidly and is excessive. This excessive phase-lead causes instability at the higher frequencies.

A second feedback circuit is connected from the output of the amplifier to the second stage. The output voltage of the amplifier is injected into the emitter and collector of this second stage through 22 uuf capacitors. Due to the small capacitance, this feedback circuit is effective only at the higher frequencies above approximately 26 kcs. The additional phase-lag introduced by this feedback circuit reduces the overall phase-lead at the higher frequencies and provides high frequency stability.

The low noise figure of from 2.4 to 5 db is the culmination of several factors. Perhaps the foremost of these factors is that the germanium transistors have an inherently low noise characteristic. To further reduce the noise, the first stage is operated at very low collector voltage and current. And finally, the mercury batteries themselves possess a low noise performance rating.

F. Pre-Amplifier

The most stringent requirement for the pre-amplifier is a
high impedance input. This came about because the antenna had
at this point already been determined. The antenna impedance as
a function of frequency is shown in Figure D3 of Appendix D.
To prevent loading the antenna and to secure a reasonable signal-
to-noise ratio at the input, a high impedance device is necessary.

The usual type of transistor is immediately eliminated from
consideration in the pre-amplifier because of the high impedance
level required. An electrometer tube was considered and finally
selected. Tubes of this type are available which have low-
potential electrodes. The low-voltages and low current drain
make them suitable for portable equipment. The extremely small
grid currents (as low as 10^{-17} amperes) permits inserting
very large resistance (on the order of 1000 megohms) in the
grid circuit.

The Victoreen type 5800 tube was incorporated in the
circuit shown in Figure 3.11. This tube has the following
parameters at the operating point: μ =1, r_p = 66 k-ohm, and
g_m = 15 μ-mhos.

The output impedance of the electrometer stage is consider-
ably higher than the input impedance of the following amplifier
stage. To improve this mismatch and at the same time prevent
low frequency loss, a direct coupled emitter follower arrange-
ment is used. The overall gain is approximately 0.5 from 3 to
50 cps. Most of the loss is in the emitter follower.
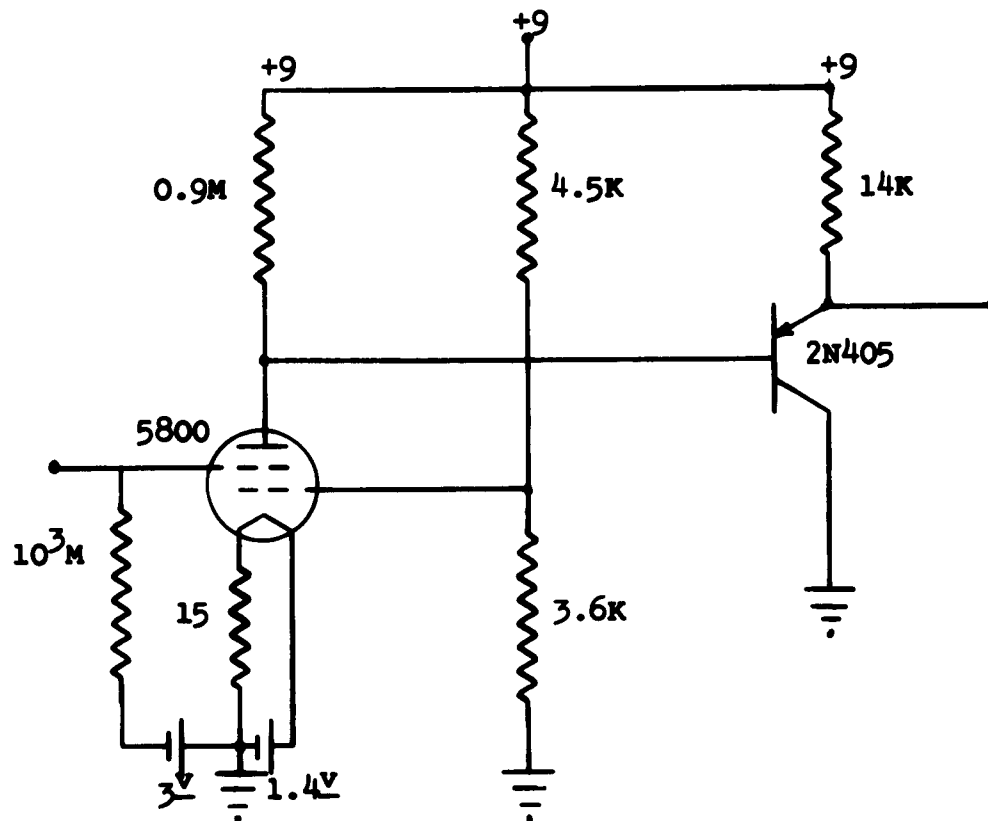
Figure 3.11   Schematic diagram of the pre-amplifier

G.   Antenna

The portability requirement imposed upon the overall system implies that both the weight and the configuration of the antenna must permit ease of handling. Since the loop antenna is independent of shape, it would seem to meet this portability requirement. However, this antenna has a low efficiency and is subject to "night effect" and microseisms. In addition, voltages are induced in this antenna by wind motion.

Assuming 1μ v output from a loop antenna at 10 cps where $\lambda = 3 \times 10^{7}$ meters, calculations shown in Appendix D indicate that a circular loop 10 meters in radius requires 16,000 turns. Calculations for other loop dimensions show that the "area-turns" (AN) product is simply too large to meet the size and weight required for portability. Considering core material to further reduce the AN-product shows that as this product becomes reasonable the weight of the core material becomes excessive.

The capacitance and impedance of a vertical antenna are given in Appendix D. The conclusion that can be drawn here is that the capacitance is quite low and the impedance is very high in the frequency range of interest. Efforts are usually directed to reducing this impedance by increasing the capacitance.

The capacitance of a vertical antenna can be increased by increasing the length or the diameter or both. Increasing the length is more effective. Doubling the length has approximately the same effect as increasing the diameter ten times. Reducing the actual height of the antenna above ground also increases

the capacitance. In addition to altering the dimensions and
height, the vertical antenna can be top-loaded with inductance
and/or capacitance to lower the impedance. However, this
method is not conducive to portability.

A Hall-effect device was briefly considered as a sensor or
antenna. While this device is relatively independent of
frequency it is considerably noisier than either a vertical or
a loop antenna.

All factors considered, the vertical antenna was finally
selected. The antenna completely assembled and erected is
shown in Figure 3.12. The 30 ft. overall length telescope into
a portable length of 10 ft. The 4.5 inch insulator is permanently
mounted on the base plate. The bottom of the antenna is bolted
to the insulator fitting for raising and lowering. Four copper
rods are used as stakes for the nylon guy lines. These rods and
the base plate are electrically connected and serve as the ground
system.

Calculations given in Appendix D show that the antenna
capacitance is approximately 93 fd. A graph of antenna
reactance as a function of frequency is also presented in
Appendix D (Figure D3). It can be seen from this graph that
the antenna coupling device should have a high input impedance.

Figure 3.12   The Antenna

4. Final System Design and Performance

A. Description of the System

The data-collecting system is shown diagrammatically in
Figure 4.1 and schematically in Figure 4.2. Referring to
these figures it can be seen that the 1000 cps sinusoidal
oscillator drives the sync head and the multivibrator. The
sync head energizes the sync-track on the duo-track magnetic
tape. In the playback mode, the sync-track provides a synchro-
nizing signal. The astable multivibrator, synchronized by the
oscillator, provides the necessary square wave to drive the
switch which in turn interrupts the data-channel at the
oscillator rate.

The data signals from the antenna are fed to the amplifier
section when the test-record switch is in the "record" position.
The output of the amplifier section is interrupted or "chopped"
by the switch before being recorded on the data-track of the
tape.

The outputs of the oscillator, multivibrator, switch, and
amplifier section are made available at the test point on the
front panel of the receiver through a test switch. This permits
checking and monitoring the important components of the system.
See Figure 4.3.

In the "test" position of the test-record switch, a 1000
cps test signal from the oscillator, properly attenuated in the
attenuator, is injected into the amplifier section through the
dummy antenna. Since the attenuation factor is constant, the
performance of the amplifier section can be checked at the test
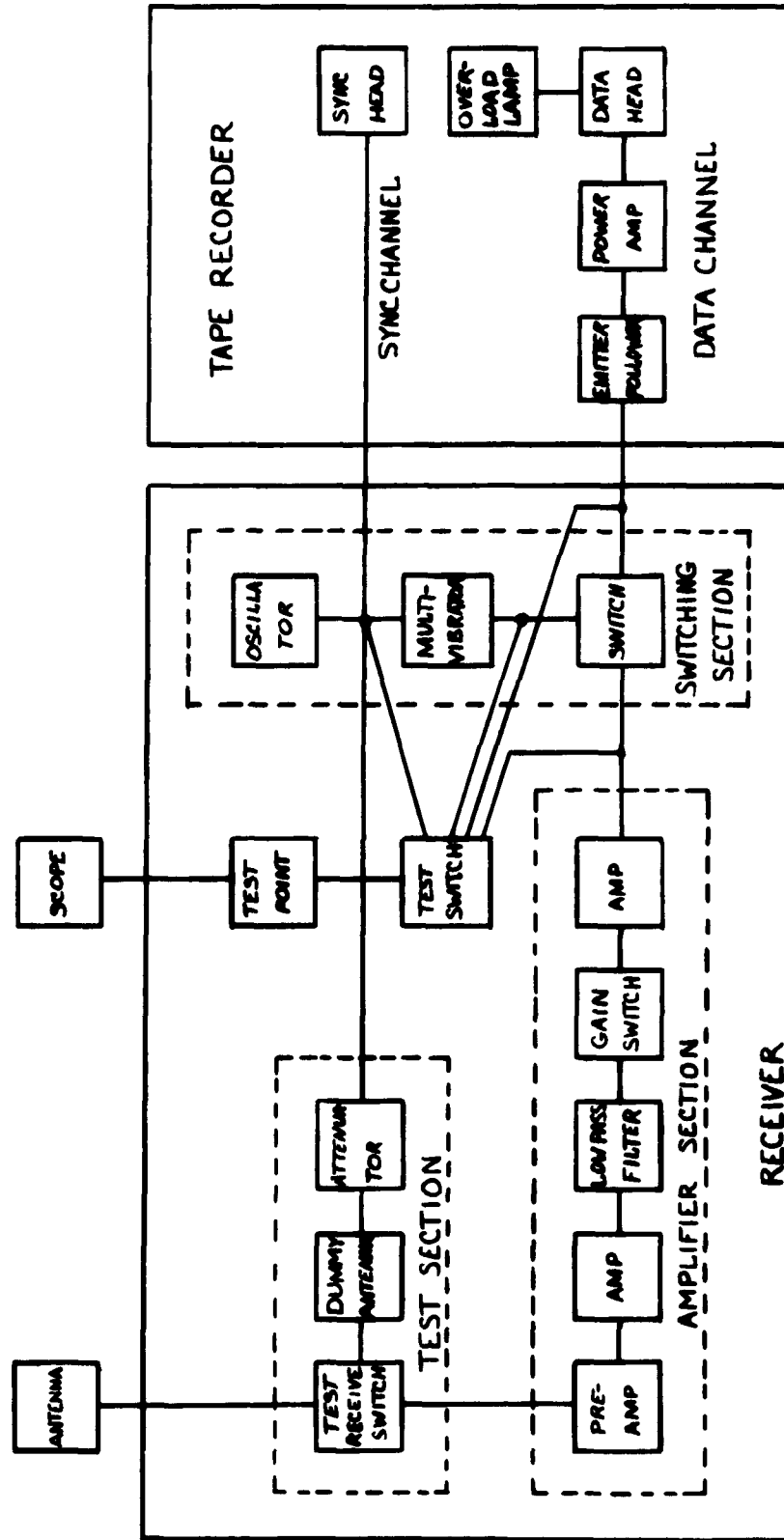
Figure 4.1 Block diagram of data-collecting system

RECEIVER

ANTENNA

TEST SIGNAL

TEST SIGNAL

RECEIVE ← → TEST

PREAMP

AMP #1

GAIN SWITCH

☐ 2N123A
△ 2N169

Fig
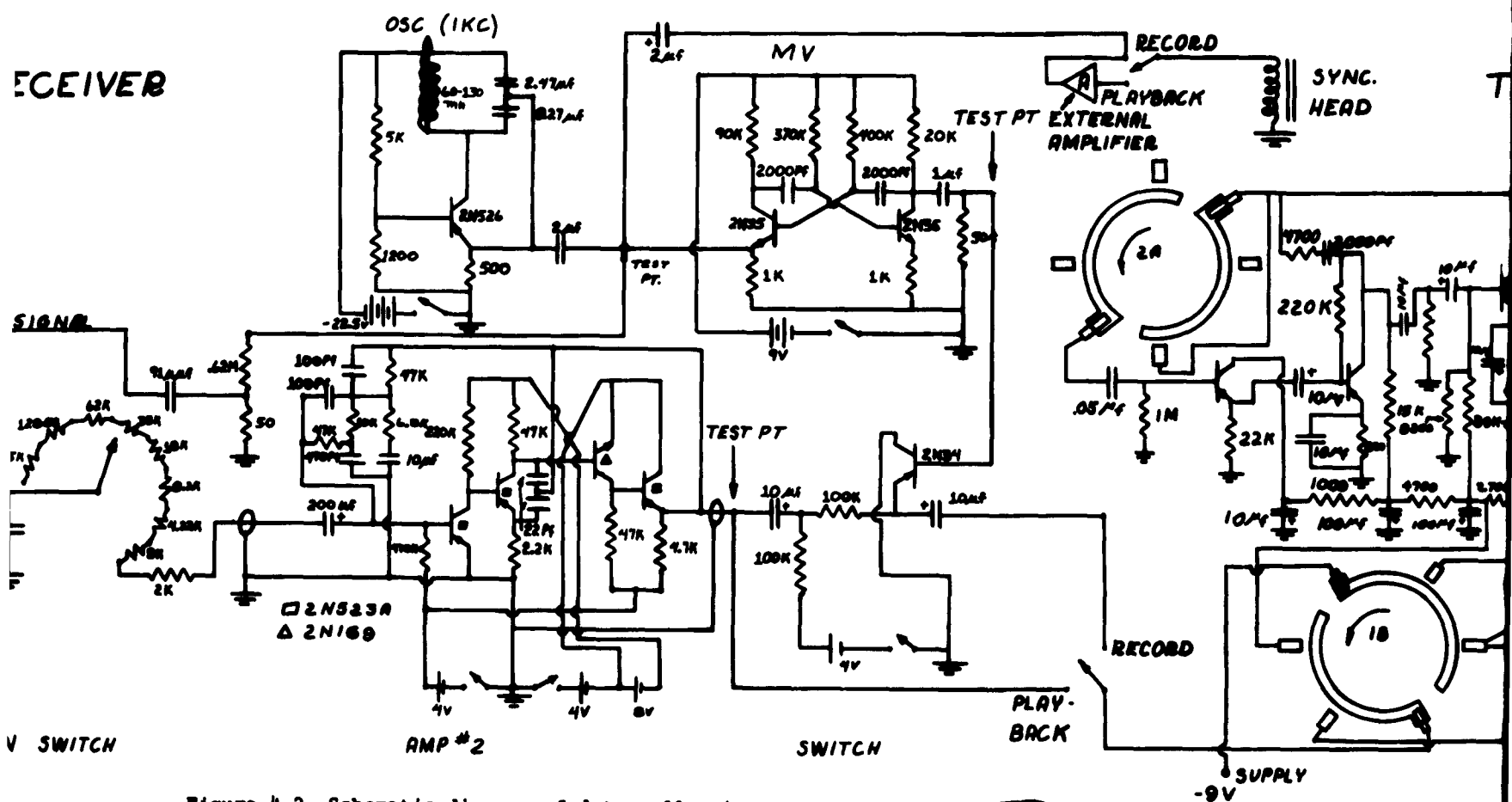
Figure 4.2 Schematic diagram of data-collecting system

STEELMAN
TAPE RECORDER

MV

RECORD
PLAYBACK

TEST PT EXTERNAL
AMPLIFIER

SYNC.
HEAD

RECORD
HEAD

1A

2A

4700 2000PF

220K

6.2K

50K

10M4

.05M4   1M

22K

18K

10M4

1000   4700   2.700

10M4

PLAYBACK

BACK

TEST PT

2N34

10M4   100K   10M4

100K

4V

RECORD

PLAY-
BACK

SWITCH

1B

SUPPLY
-9V

PLAYBACK

RECORD

OFF

FUNCTION SWITCH

ALL TRANSISTORS TYPE 2N405

0.1M4

10

4700

27K

.02M4

1N486

NE-2

1N486

.02M4

10

ng system

Figure 4.2

3
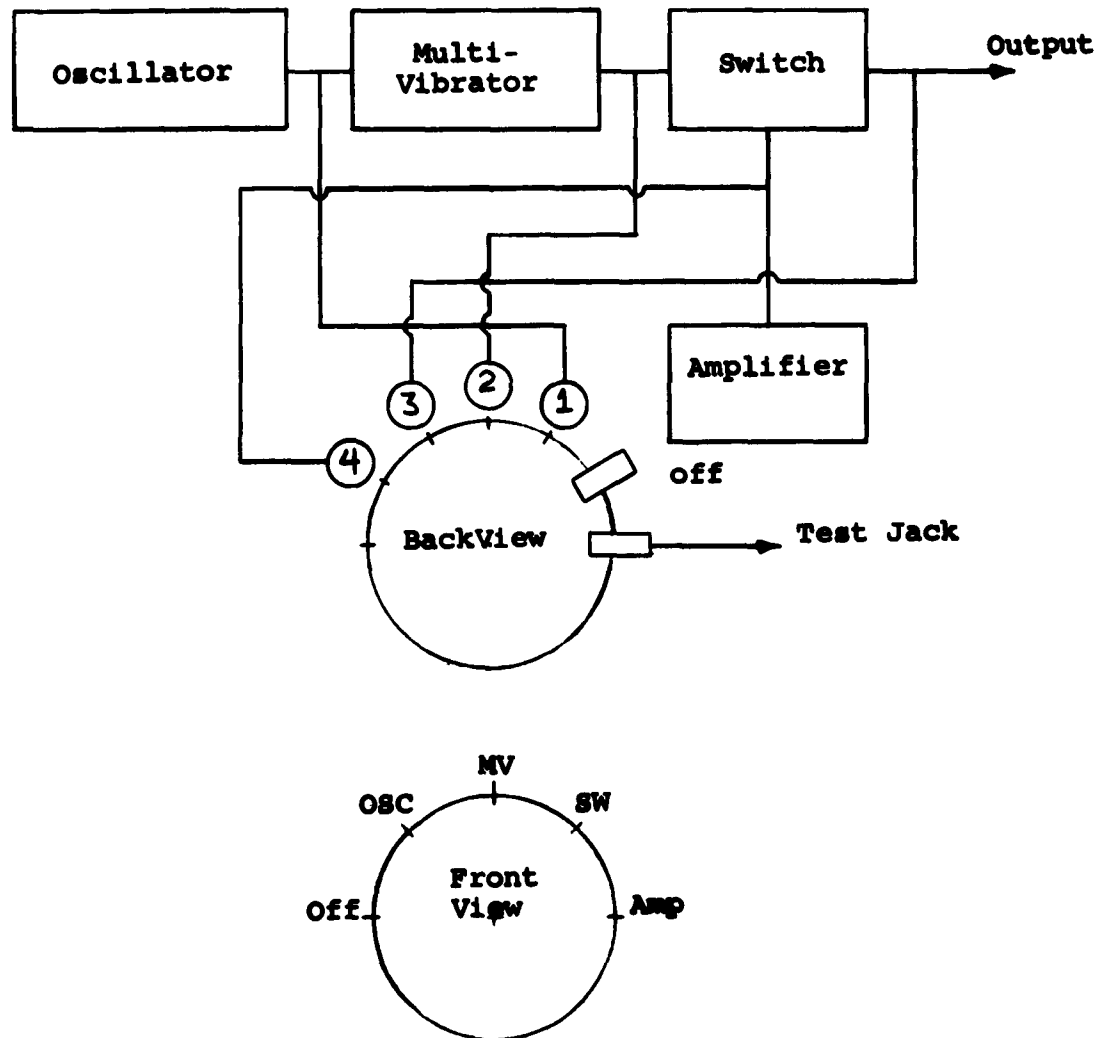
Figure 4.3 Functional diagram of Test Point System

point. A Tektronix Type 321 transistorized portable oscillos-
cope is connected to the test point for checking the system
before and during the data-collecting process.

The batt-test switch provides an additional means of
checking the components in the receiver. This switch permits
measuring the battery voltages under load conditions on the
front panel voltmeter. See Figure 4.4.
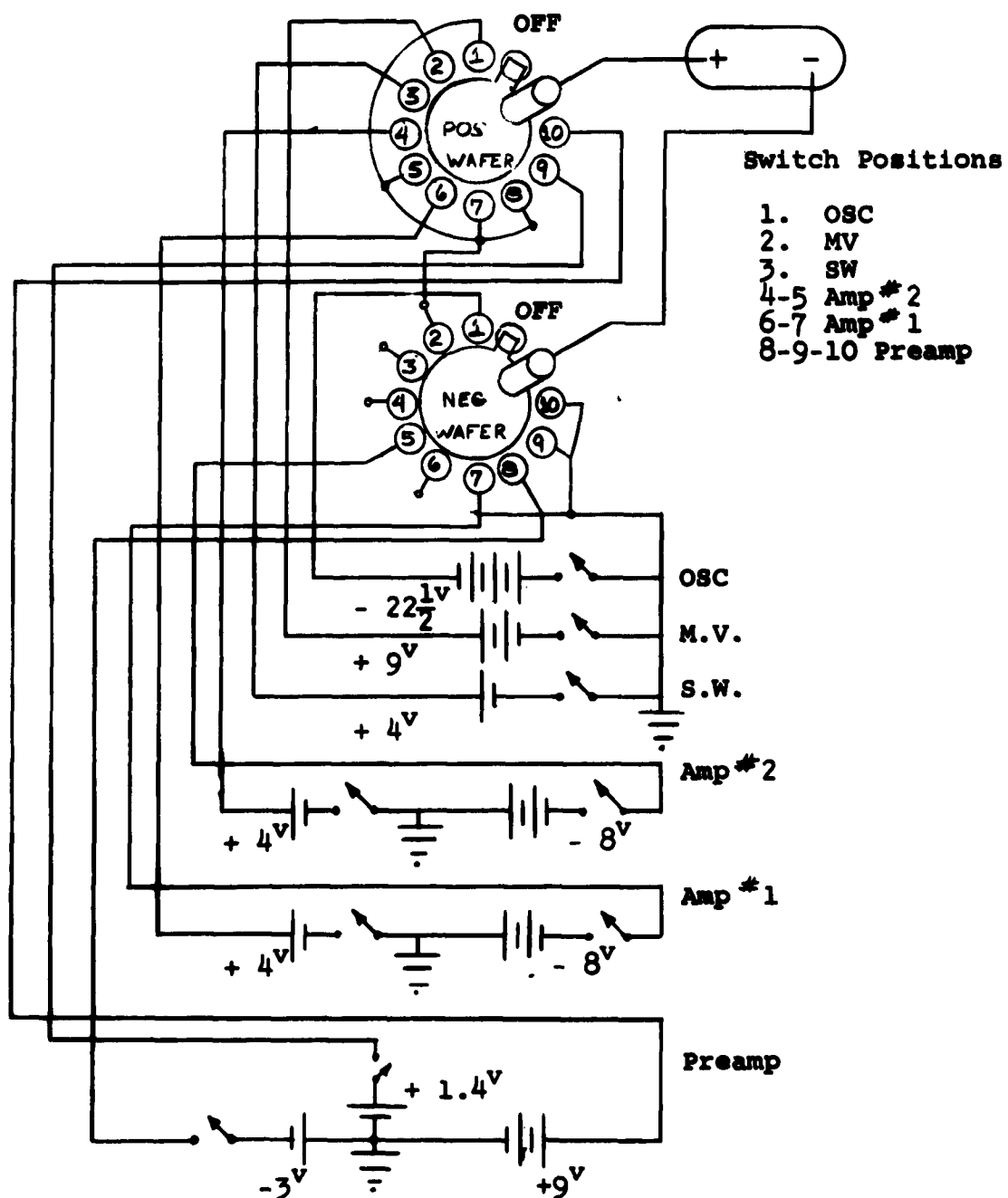
Figure 4.4   Schematic of Battery Test System

B. Overall Performance Tests

The variation of oscillator frequency versus battery voltage with temperature as the parameter has previously been shown in Figure 3.6. A battery voltage of 19.5 volts, down 3 volts from the design value of 22.5 volts, gives a frequency change of 5 cps at 21°C and 9 cps at 46°C. Thus at 21°C the frequency decreases 0.5% and at 46°C, 0.9%.

The oscillator frequency increases approximately 0.1% when the multivibrator is turned on. Subsequently energizing the switch and tape recorder causes no further change in frequency. However, connecting the sync head causes the frequency to increase about 0.2%. This "pulling" effect is independent of the oscillator battery voltage.

The magnitude of the oscillator output is relatively independent of the multivibrator, switch, and sync head. In other words, there are no "loading" effects on amplitude. The mechanical stability is verified by the fact that there was no discernible frequency change after four field trips.

Synchronization of the multivibrator is maintained throughout the multivibrator and oscillator battery voltage ranges 6.4 to 9.0 and 18 to 22.5 volts, respectively. With the multivibrator and switch battery voltages equal to or greater than 6.4 and 3.5 volts respectively, variations of the oscillator battery voltage (18 to 22.5 volts) have no influence on the amplitude of the switch output. This is another way of saying that although the magnitude of the multivibrator output is a function of battery voltage, this output does not effect

the switch output provided this battery voltage is equal to or greater than 6.4 volts. Actually this battery voltage is normally 7.3 volts and because of light loading does not vary appreciably from this value. Maintaining the battery voltage of the switch equal to or greater than 3.5 volts ensures proper switching.

Thus by maintaining the battery voltages on the oscillator, multivibrator, and switch equal to or greater than 19.5, 7.3, and 3.7 volts, respectively, proper performance of the switching section is assured. Under these conditions the output of the switch is maintained at 0.5 volts (peak-to-peak).

The design voltage for the data-channel in the tape recorder is 8.04 volts due to 6 batteries at 1.34 volts each. Under these conditions a sinusoid of 0.52 volts (rms) is required to light the overload lamp in the tape recorder. Tests show (Figure 4.5) that when the battery voltage reduces to 6.6 volts a sinusoid of 0.67 volts (rms) is required to light this overload lamp. In the test procedure, an adjustable fraction of the oscillator output is injected into the tape recorder data-channel, the amplitude of this voltage is not only an indication of the battery voltage but also an indication of the data-channel operation.

The change in signal voltage from 0.52 to 0.67 volts represents a 3 db drop in the data-channel gain. However, under actual field conditions the injected voltage is relatively constant at 0.52 volts with a very rapid and noticeable change when the mercury batteries become exhausted.
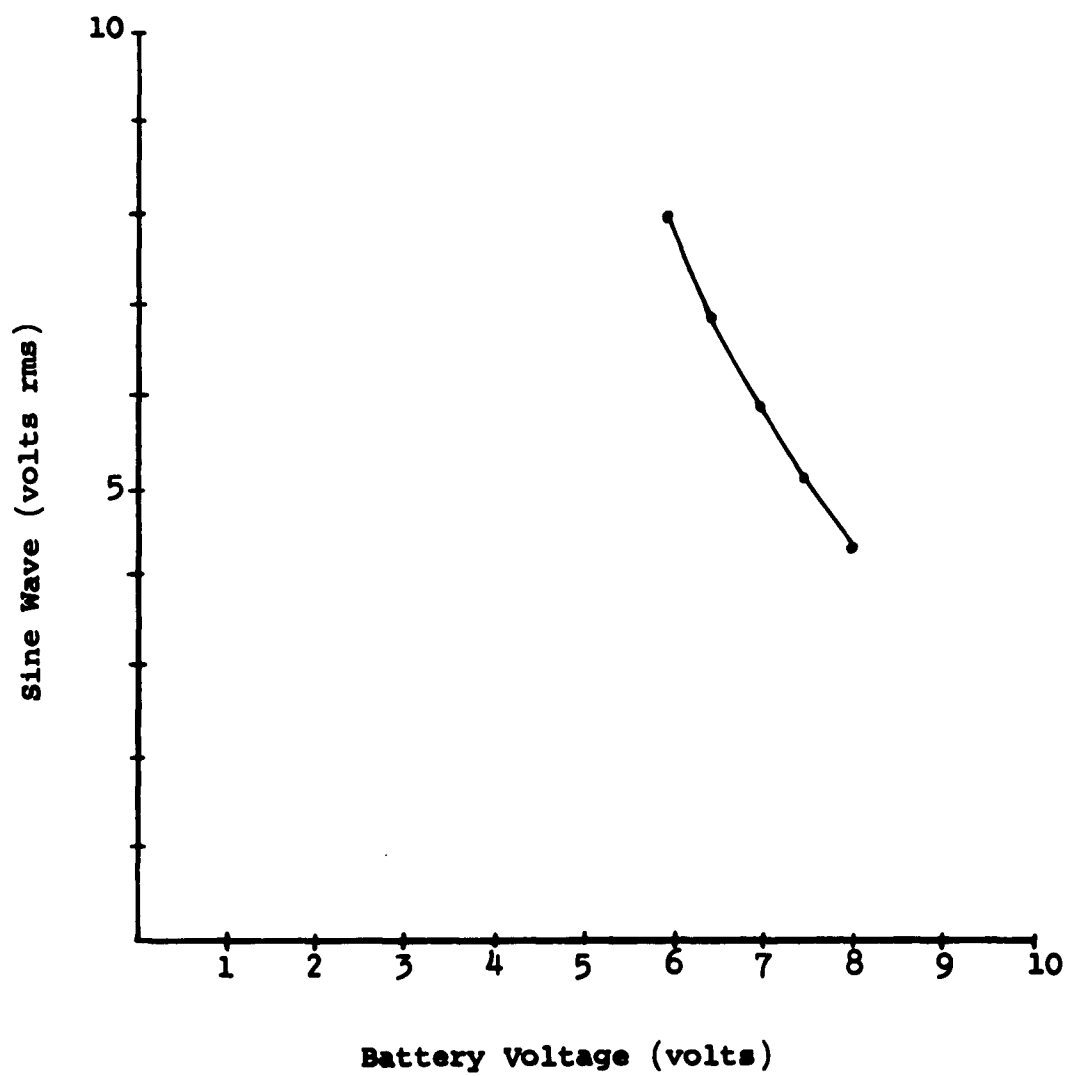
Figure 4.5 Tape recorder amplifier input versus battery
voltage

Since 13 volts is required at the driving side of the output transformer to light the overload lamp, the voltage gain through the data-channel of the tape recorder is approximately 17. This, of course, includes the gain of the emitter follower which is approximately 0.9. The overload lamp circuit is itself independent of the battery voltage and therefore constitutes a relatively constant reference.

The attenuator, dummy antenna, and test-record switch comprise the test section. The attenuator is essentially a voltage divider permanently connected to the oscillator output. The output of this divider is 8.06×10^{-5} that of the oscillator. The dummy antenna is a 93 $\mu\mu$f capacitor which is electrically equivalent to the antenna. When the test-record switch is in the "test" position the output from the divider is injected into the amplifier section through the dummy antenna.

The output of the amplifier section and the oscillator can be measured at the test point on the front panel by using the test switch. Thus, in the "test" position the gain of the amplifier section is readily determined by the relation

$$ k = \frac{e_o \text{ (amplifier section)}}{e_o \text{ (oscillator) } 8.06 \times 10^{-5}} . $$

The gain of the amplifier section for the various positions of the gain switch is shown in Table 4-I. The performance of the amplifier section is checked by determining the gain at positions 1, 5, and 9. With all battery voltages at design values, the gain at positions 1, 5, and 9 is 47.69, 627, and 6535, respectively. Permitting a 3 db reduction in gain, these become 35.5, 467, and 4865, respectively.

Position	Gain
1	47.6
2	83.3
3	157.
4	334.
5	547.
6	1006.
7	2080.
8	3640.
9	5700.

Table 4-I   Gain switch positions

In data-collecting, position 1 of the gain switch is used almost exclusively to prevent saturating or overdriving the switch. In this position the gain is 35.5 to 47.69. This upper limit is with external supplies giving the required design voltages. The gain never exceeds 41 with fresh batteries. Measurements with the test circuit show a gain of 36 to 41, a 1.2 db variation. The usual reading is 36 or 37.

Since the test procedure employs 1000 cps for gain determination, some method of correlating this gain with the actual frequency response is necessary. The frequency response, when the gain is 36 according to the test circuit, is shown in Figure 4.6. This response is the result of injecting signals through the dummy antenna at three voltage levels--70, 44, and 5 mv (rms). The 70 and 44 mv input signals give 100 and 50% saturation of the switch respectively. The 5 mv signal was the minimum obtainable from the signal generator without external voltage division. External voltage division can be done but not without sacrificing accuracy due to 60 cps pickup.
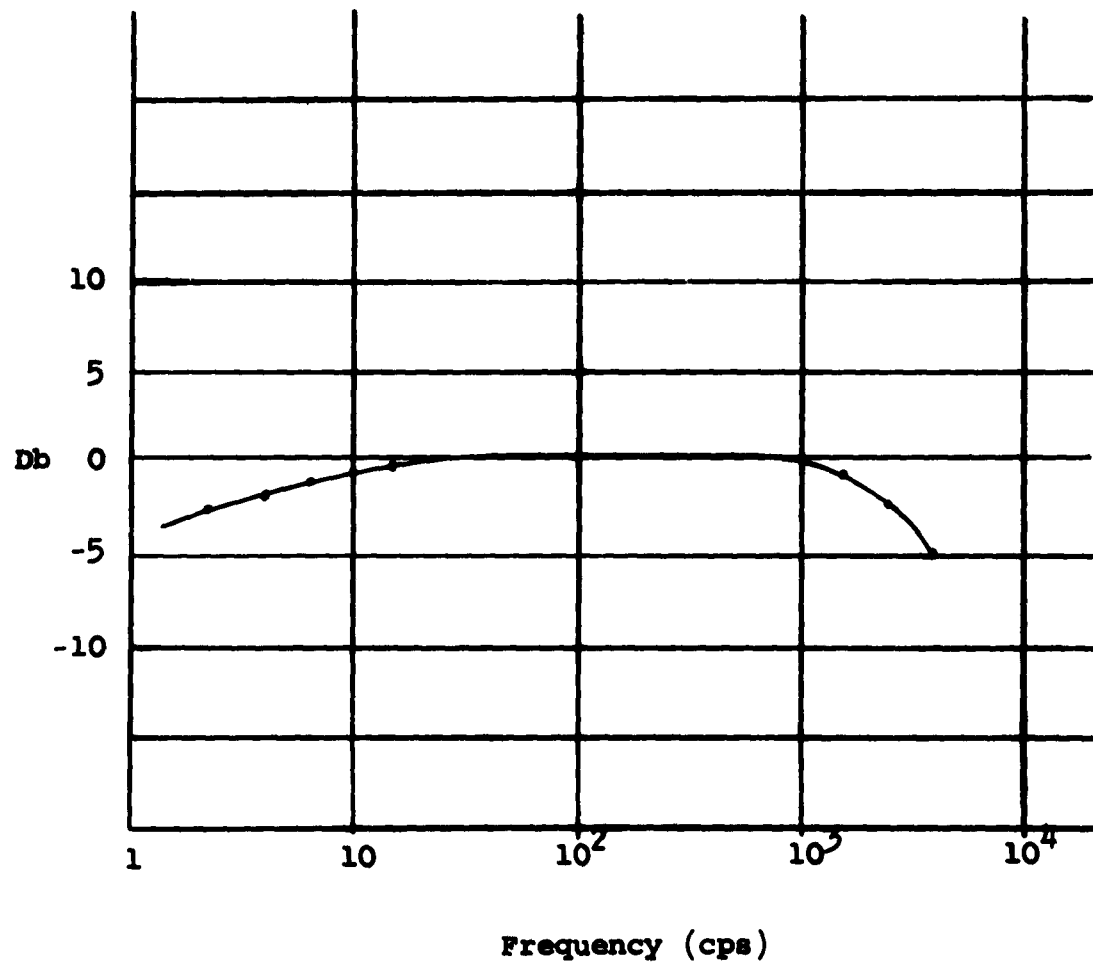
Figure 4.6 Frequency response of receiver

C. Design Considerations

The system for collecting data actually evolved from a series of engineering considerations. The objective to secure electromagnetic noise-data in the 0 to 50 cps region suggested remote sites free from man-made interference. This, in turn, required that the equipment be portable. The speed and response characteristics of the portable tape recorder motivated the synchronizing and switching technique.

The test circuit which finally evolved was based on a compromise method of calibration. Recording a calibration signal simultaneously with the data, or prior to the data, would require another oscillator in the 0 to 50 cps range or frequency division from the 1000 cps oscillator. However, either method was not compatible with compactness and portability. The solution was to reduce the magnitude of the 1000 cps oscillator output and apply it to the data-taking system through a dummy antenna. By adhering to certain gain limitations, the response to this test signal can be correlated with the response to signals in the 0 to 50 cps region.

Other considerations included the gain switch, the low pass filter, and the tape recorder. The 9-position gain switch evolved from a series of field test on the levels of the data-signals. The low pass filter provides a "roll-off" of the response at 2000 cps. This ensures against the possibility of strong high-frequency signals overloading the receiver. The extensive modifications necessary to adapt the tape recorder to the system have been previously discussed.

5. Data-Collecting Site

The selection of the data-collecting site was based upon
several requirements. The most important requirement was
freedom from man-made interference. While this, to a certain
extent, implies a remote location, distance and traveling time
were to be minimized. Finally the site must be accessible by at
least a jeep-type vehicle.

An initial survey of available maps indicated that the
distance factor was favored by the mesa area between the Rio
Grande and the Manzano Mountains southeast of Albuquerque. The
approach to this area is via Highway 47 which runs along the
valley on the eastside of the river. Since the east mesa rises
300-500 feet from the valley rather abruptly, access routes
were limited and in some case quite primitive.

The latest available maps of this area were based on
1952-54 information. As a result, the initial survey trip
disclosed that there was no assurance that various landmarks and
primitive roads existed as shown. This was not particularly
unusual in itself, but it did indicate that a careful investiga-
tion of all landmarks must be made before the site was finally
selected. As a result of this policy, a water well, driven by
a gasoline engine, was discovered. This disclosure had a
direct bearing on site finally selected.

Several approaches to the mesa were made from various
points along Highway 47. These were too far and involved too
much travel time. The only two approaches which seemed to be
suitable were on the Isleta Indian Reservation. Permission to

explore this section of the mesa and to use a site, later found
there, was obtained from Governor Esquipula Jojola, Governor
of Isleta Pueblo.

The area shown in Figure 5.1 is within the Isleta Reserva-
tion. The north and south boundaries of the reservation are 4
and 6 miles, respectively, from the site. There is a gradually
rising elevation to the foot of the Manzano Mountains 13 miles
to the east of Highway 47. This area is devoid of trees except
where labelled on the map. A scrub tree (height less than 3
feet) area begins approximately 2 miles west of the mountains.
A power line runs roughly north and south along Highway 47 and
the west side of the mesa. The dominant feature of this area
is Hells Canyon which extends from the Manzano Mountains to the
Rio Grande River. The character of the terrain varies quite
markedly on either side of this canyon.

The area south of the canyon was immediately rejected as
a site location. Here the terrain is very sandy and traveling
is difficult. In addition, the distance is excessive whether
entrance to the area is made from Isleta or from Chical Indian
School. Nevertheless this area was investigated in order to
verify landmarks on the maps. The gasoline engine driven well
was discovered on this trip.

On the north side of the canyon the terrain is, of course,
sandy but is much firmer. The area east of Hubbell Springs
was unsuitable because of the proximity to the mountains and
possible mining activity. The site finally selected was on
the north rim of Hells Canyon. Here the terrain is slightly
elevated, free from scrub trees, and quite firm. It is about
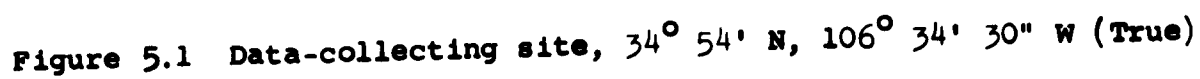
Figure 5.1 Data-collecting site, 34° 54' N, 106° 34' 30" W (True)

8.8 miles from the Isleta turn-off and 20.8 miles from the city of Albuquerque. It is shown in Figure 5.2 that the distance to the nearest power line is 4 miles and to the gasoline-engine well is 2.35 miles.

The rough condition of the road from Isleta turn-off to the site necessitated packaging the equipment in wooden boxes padded with 3 inches of packing material to protect the equipment from shock. A total of 2,000 miles was travelled on surveying and data-collecting trips.

The arrangement of the equipment at the recording site is shown in Figure 5.3. The small tarpaulin was required to keep the direct rays of the sun off the equipment. The temperature under this tarpaulin, which was monitored continuously, varied from 72° to 99°F.
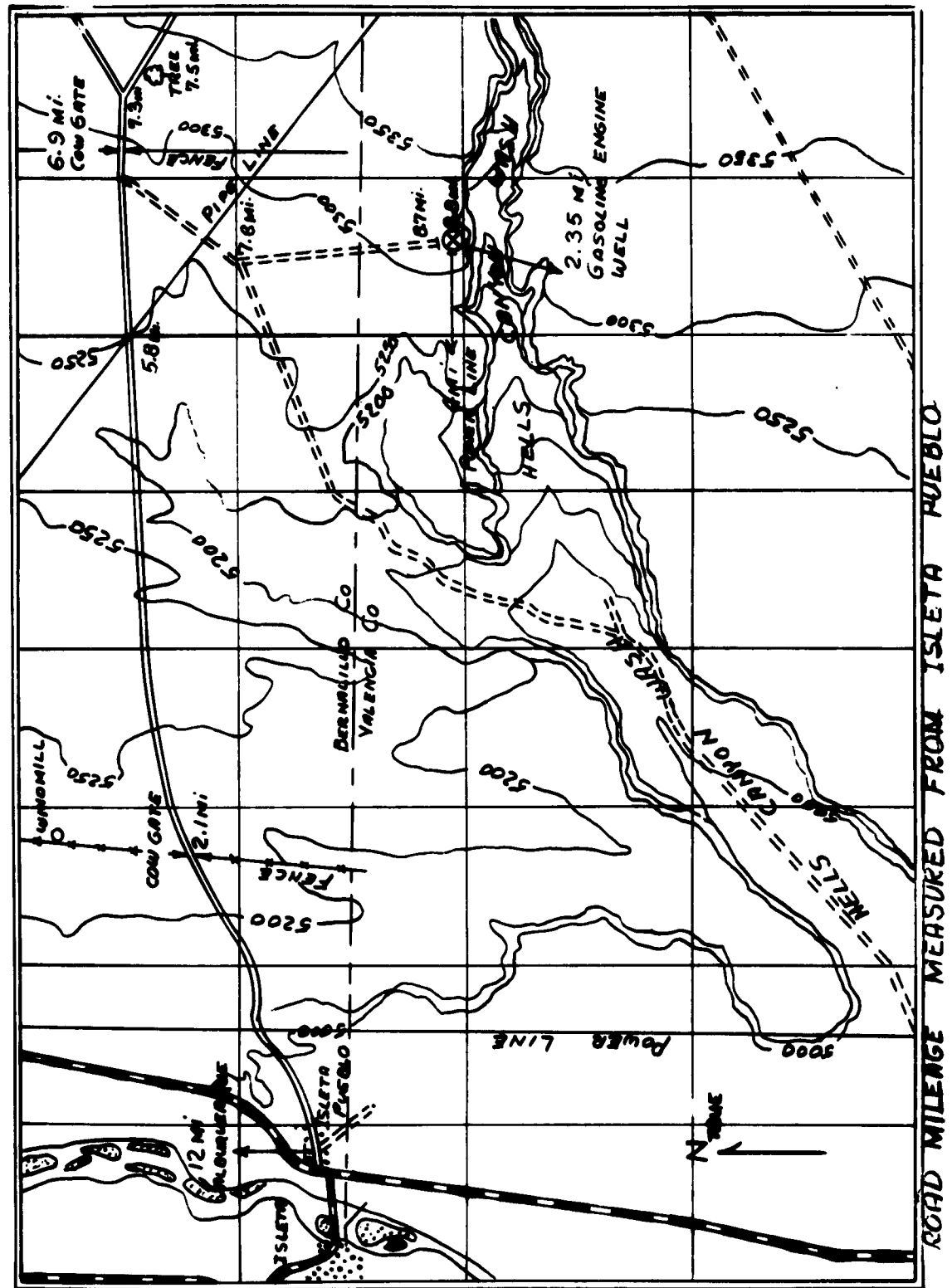
Figure 5.2 Site location relative to Isleta Pueblo
and Albuquerque, New Mexico
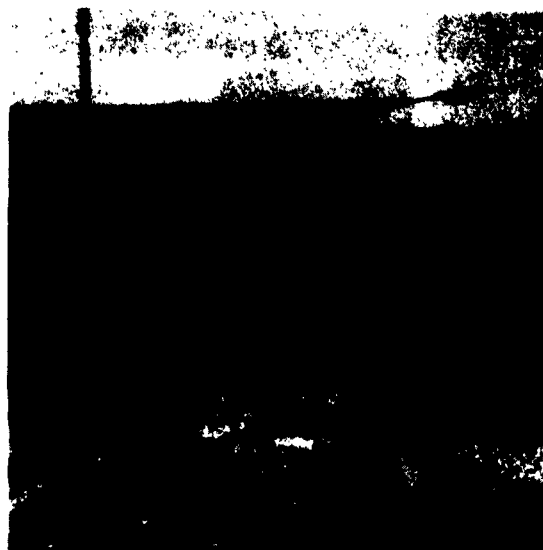
Figure 5.3   Data-collecting equipment at the site.

6. Data Samples

The data was recorded during daylight hours from August 1 to September 8, 1961, and during evening hours from September 11 to September 15, 1961. During this period, 240 rolls of magnetic tape were recorded. Since the time involved precludes any observable seasonal effect, the primary interest is in the diurnal variations of the mean values of field strength.

As can be seen in Figure 2.2, the data-processing system is essentially a filtering system. A particular frequency is selected by the selective amplifier, rectified, and integrated. Five similar circuits are connected to the output of the low-pass filter. This arrangement permits processing five different frequencies simultaneously. The output voltage of the integrator is expressed as a mean value over the integration period. Since the gain of the recording and processing systems are known, the mean value is restated as the mean peak value of the field strength in millivolts per meter (mv/m).

The duration of each magnetic tape is 32 minutes. The mean peak value of field strength for each frequency is consider-ed as representative of the noise activity at that frequency during the hourly period in which the roll of tape was taken. Thus the basic unit for plotting purposes is the mean peak value of field strength per frequency per hour.

No attempt is made here to discuss the data samples shown in Figure 6.1 to 6.3. These samples are simply presented to show the manner in which the data will be plotted when completely processed.
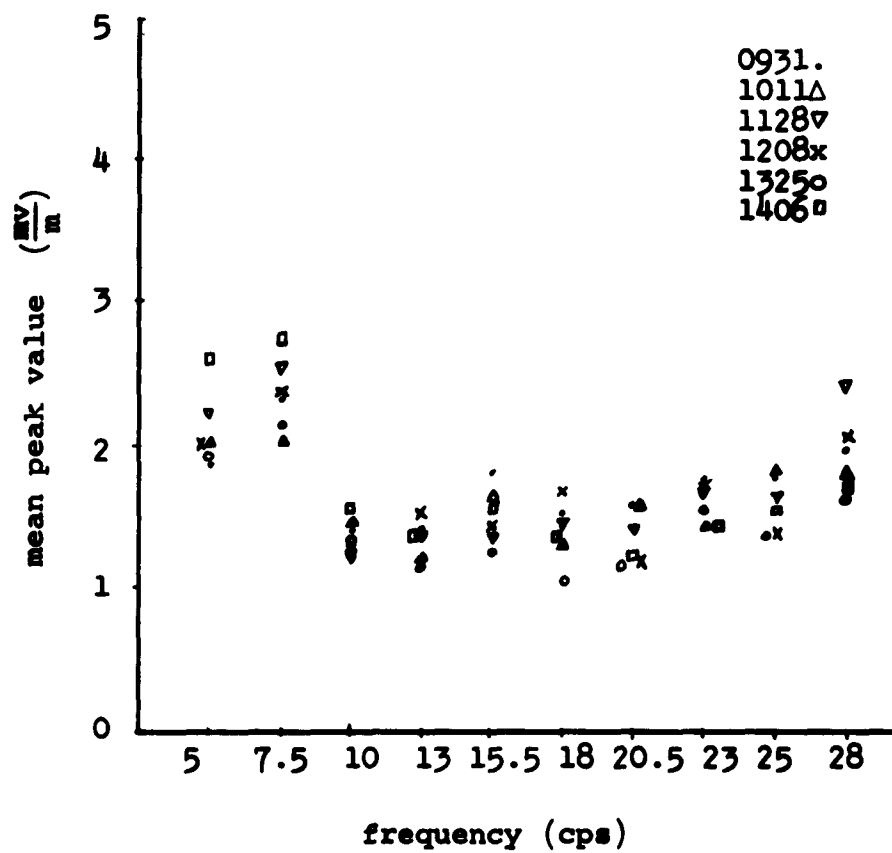
Figure 6.1 Hourly recordings of atmospheric noise field
strength versus frequency from 0900 to 1500
(MST) on August 21, 1961
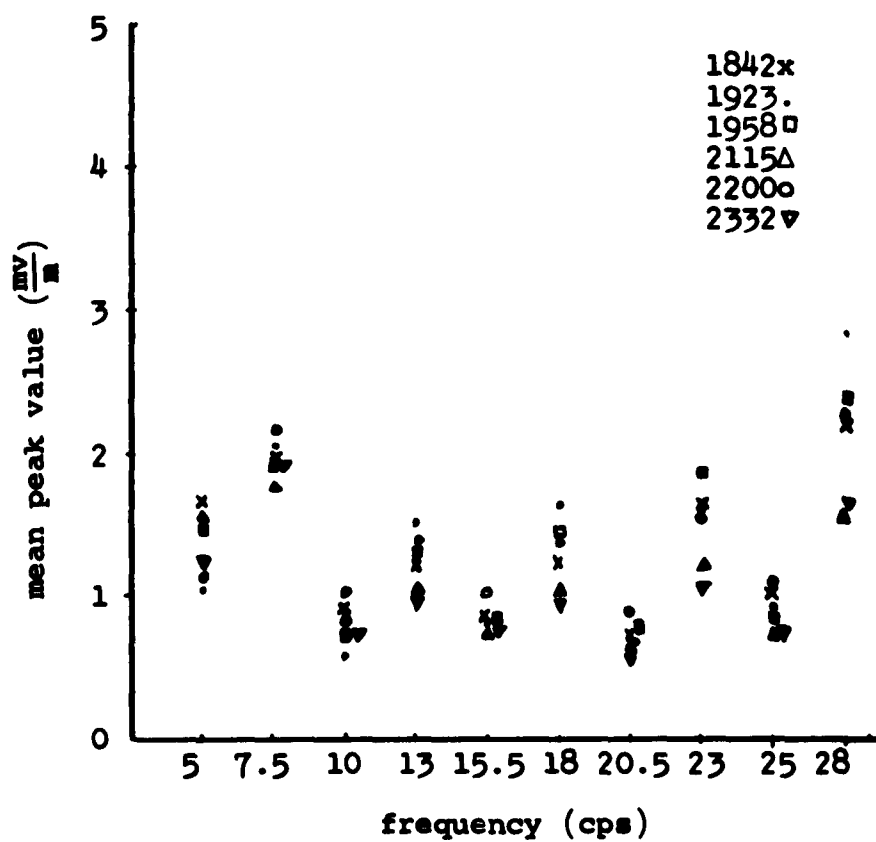
Figure 6.2 Hourly recordings of atmospheric noise field
strength versus frequency from 1800 to 2400
(MST) on September 15, 1961
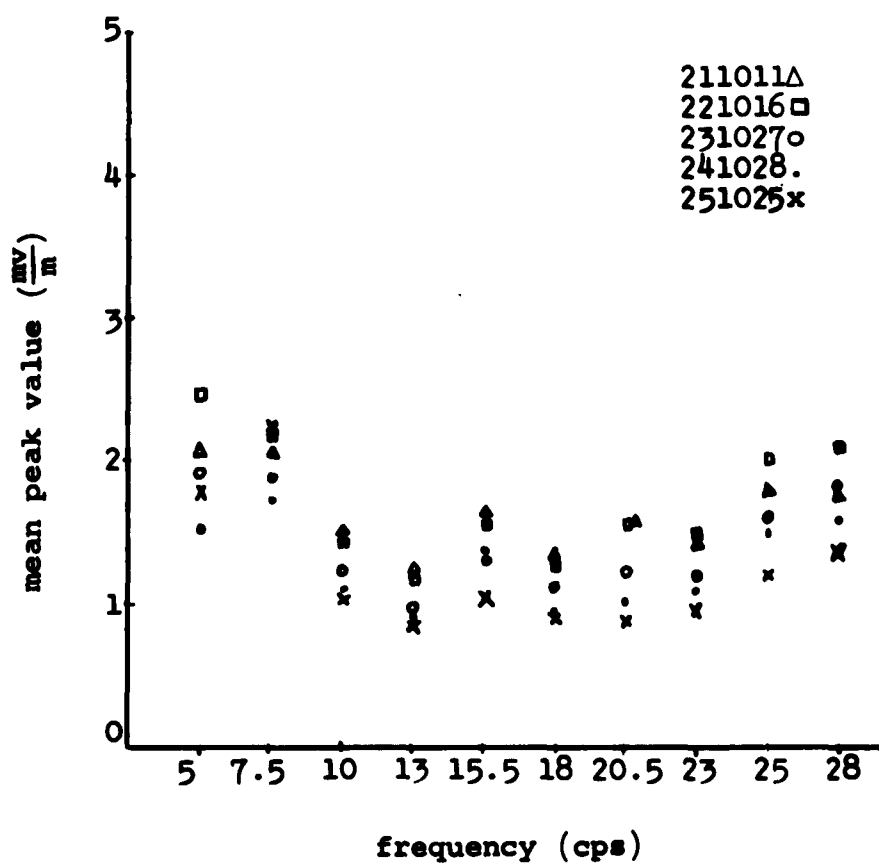
Figure 6.3 Atmospheric noise field strength versus frequency
during the hour 1000 to 1100 (MST) for the week
August 21-25, 1961

7. Conclusions

The purpose of this investigation is to develop instrument-
ation to secure noise data in the 3 to 50 cps portion of the
spectrum and, at the same time, to seek evidence of the Schumann
frequencies in this region. The instrumentation used in this
investigation is discussed fully in Chapter 4. Briefly, a
frequency translation technique is employed during recording.
During playback the data is again translated and restored to its
normal position in the spectrum. A test signal is used to
ensure that in the record mode the gain is maintained within
1.2 db. Under this restriction, test tapes recorded at
frequencies in the 3 to 50 cps range indicate the gain from the
antenna input during record to the receiver output during play-
back. The overall response in this frequency range is the
response of the receiver, i.e., within 3 db.

During data processing, the inputs of 10 filters are
connected to the receiver. The output of each of these 10
filters is amplified, rectified, and integrated. The gain of
each filter channel is carefully determined so that the output
of each integrator can be put in terms of the input to the
filter channel. Since the filter input is the receiver output
and the gain from the antenna to the receiver output is known,
the integrator output can be expressed in terms of the antenna
input. Considering the effective height of the antenna, this
antenna input can be denoted in field strength units.

In the complete recording and recovery process, the noise
data is subjected to two variations with known limits. These

variations are due to the frequency response of the receiver and changes in the receiver gain. Thus the data from a particular tape will vary as the response in Figure 4.6, while the data from different tapes will be within 1.2 db at the most. Samples of the noise data are presented in Chapter 6.

The system for data-collecting described in this paper was utilized during the daylight hours from August 1 to September 8, 1961 and during the evening hours from September 11 to September 15, 1961. In addition to these operational periods, that portion of the system involved in data-processing has been in daily (8 to 11 hours) continuous operation since November 25, 1961.

The data-samples are shown in Chapter 6 to demonstrate the manner in which the data will be plotted in a subsequent report. This report will be issued when the data have been completely processed. While nothing conclusive can be drawn from these samples, it is interesting to note that the greater activity in the 5 to 10 cps region agrees with the findings of Fitchen, et al. [1961], Balser and Wagner as reported by Raemer [1961], and Maple [1961].

Appendix A

Twin-T Filters

General Network Analysis

We shall discuss here the general approach of network analysis in considering the twin-T filter.

The single "T" network shown in Figure A1
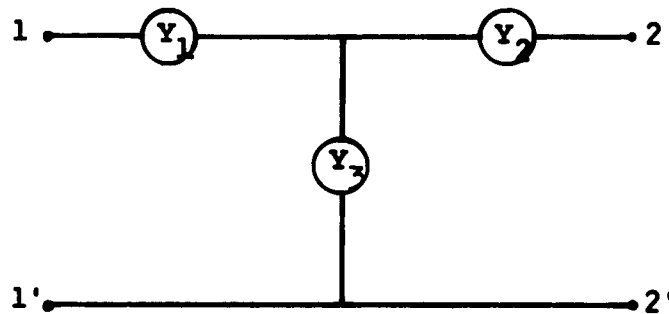
Figure A1   A "T" network

may be considered using the "y" or "short-circuit" parameters. The equations for this network take the form

$$y_{11}V_1 + y_{12}V_2 = I_1$$
$$y_{21}V_1 + y_{22}V_2 = I_2$$

$$(A-1)$$

where

$$y_{11} = \left.\frac{I_1}{V_1}\right|_{V_2 = 0} ; \quad y_{12} = \left.\frac{I_1}{V_2}\right|_{V_1 = 0}$$
$$y_{21} = \left.\frac{I_2}{V_1}\right|_{V_2 = 0} ; \quad y_{22} = \left.\frac{I_2}{V_2}\right|_{V_1 = 0}$$

$$(A-1a)$$

Equations (A-1) may be written in Matrix form

$$
\begin{vmatrix} y_{11} & y_{12} \\ y_{21} & y_{22} \end{vmatrix} \begin{vmatrix} V_1 \\ V_2 \end{vmatrix} = \begin{vmatrix} I_1 \\ I_2 \end{vmatrix} ,
\tag{A-2}
$$

which is easier to manipulate to obtain other circuit parameters such as "z."

If the circuit elements are combined in impedance form the circuit equations take the form

$$
\begin{aligned}
z_{11}I_1 + z_{12}I_2 &= V_1 \\
z_{21}I_1 + z_{22}I_2 &= V_2
\end{aligned}
\tag{A-3}
$$

where

$$
z_{11} = \frac{V_1}{I_1}\bigg|_{I_2 = 0} ; \quad z_{12} = \frac{V_1}{I_2}\bigg|_{I_1 = 0}
$$

$$
z_{21} = \frac{V_2}{I_1}\bigg|_{I_2 = 0} ; \quad z_{22} = \frac{V_2}{I_2}\bigg|_{I_1 = 0}
\tag{A-3a}
$$

Equations (A-3a) define the "z" parameters on the "open circuit" basis. Equation (A-3) can be put in matrix form

$$
\begin{vmatrix} z_{11} & z_{12} \\ z_{21} & z_{22} \end{vmatrix} \begin{vmatrix} I_1 \\ I_2 \end{vmatrix} = \begin{vmatrix} V_1 \\ V_2 \end{vmatrix} .
\tag{A-4}
$$

Although equation (A-2) is more convenient in combining two circuits in parallel since admittances are additive, it is desirable to use equations (A-4) for series connections. The "z" parameters may be found directly from the "y" parameters--matrix (A-4) can be obtained from matrix (A-2), and vice versa.

Given the y-matrix, the determinant is

$$\Delta y = y_{11}y_{22} - y_{12}y_{21} \tag{A-5}$$

Defining Δ_{ij} as the cofactor of element α_{ij}, we have

$$\Delta_{ij} = (-1)^{i+j} M_{ij} \tag{A-6}$$

where M_{ij} is the minor of element α_{ij} [1] and

$$\begin{vmatrix} \Delta_{11} & \Delta_{12} \\ \Delta_{21} & \Delta_{22} \end{vmatrix} \tag{A-7}$$

where

$$\Delta_{11} = y_{22} \qquad \Delta_{21} = - y_{21}$$

$$\Delta_{12} = -y_{12} \qquad \Delta_{22} = y_{11} .$$

Dividing each element of (A-7) by Δy and transposing, (A-2) becomes

---

[1] Seshu S. and N. Balabanian, Linear Network Analysis, John Wiley and Sons, Inc., 1959.

$$\left| \begin{array}{c} V_1 \\ \\ V_2 \end{array} \right| = \frac{1}{\Delta y} \left| \begin{array}{cc} \Delta_{11} & \Delta_{21} \\ \\ \Delta_{12} & \Delta_{22} \end{array} \right| \left| \begin{array}{c} I_1 \\ \\ I_2 \end{array} \right| \qquad \text{(A-8)}$$

where $z_{11} = \dfrac{\Delta_{11}}{\Delta y}$, $z_{21} = \dfrac{\Delta_{12}}{\Delta y}$, etc.

Matrix (A-3) can then be written

$$\left| \begin{array}{c} V_1 \\ \\ V_2 \end{array} \right| = \left| \begin{array}{cc} z_{11} & z_{12} \\ \\ z_{21} & z_{22} \end{array} \right| \left| \begin{array}{c} I_1 \\ \\ I_2 \end{array} \right| \qquad \text{(A-9)}$$

where $z_{11} = \dfrac{V_1}{I_1}\bigg|_{I_2 = 0}$; $z_{21} = \dfrac{V_2}{I_1}\bigg|_{I_2 = 0}$, and so on.

Defining the voltage transfer function (g_{21}) to be

$$g_{21} = \frac{V_2}{V_1}\bigg|_{I_2 = 0} ,$$

we see that

$$g_{21} = \frac{V_2}{V_1}\bigg|_{I_2 = 0} = \frac{z_{21}}{z_{11}} = \frac{\dfrac{-y_{21}}{\Delta y}}{\dfrac{y_{22}}{\Delta y}} = \frac{-y_{21}}{y_{22}} . \qquad \text{(A-10)}$$

Circuits in Parallel

The admittances for circuit shown in Figure A1 are defined in equations (A-1a). Putting these admittances in terms of the admittance of the circuit elements we have

78

$$y_{11} = \frac{Y_1(Y_2 + Y_3)}{Y_1 + Y_2 + Y_3} \; , \qquad\qquad\qquad \text{(A-11a)}$$

$$y_{22} = \frac{Y_2(Y_1 + Y_3)}{Y_1 + Y_2 + Y_3} \; , \qquad\qquad\qquad \text{(A-11b)}$$

$$\text{and } y_{12} = y_{21} = \frac{-Y_1 Y_2}{Y_1 + Y_2 + Y_3} \qquad\qquad \text{(A-11c)}$$

Equation (A-11a) and (A-11b) can be obtained by inspection. The equations (A-11c) are found by solving the loop equations. To obtain the results indicated here, and in subsequent developments, y_{12} and y_{21}, are determined by assuming the loop currents in the same direction in the shunt branch.

Now we consider the total admittances when two circuits are in parallel (Figure A2).
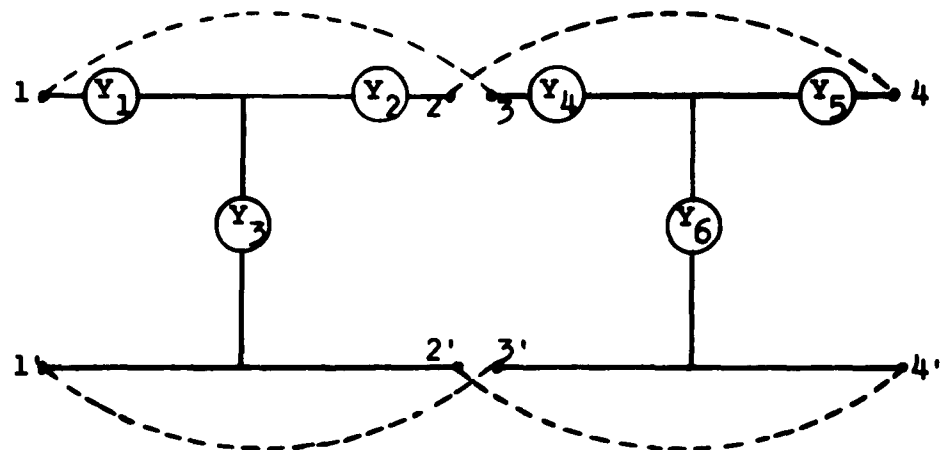
Figure A2   Two "T" networks in parallel

Since admittance in parallel are additive, the total admittances for the circuit in Figure A2 are

$$Y_{11} = \frac{Y_1(Y_2 + Y_3)}{Y_1 + Y_2 + Y_3} + \frac{Y_4(Y_5 + Y_6)}{Y_4 + Y_5 + Y_6} \quad , \tag{A-12a}$$

$$Y_{22} = \frac{Y_2(Y_1 + Y_3)}{Y_1 + Y_2 + Y_3} + \frac{Y_5(Y_4 + Y_6)}{Y_4 + Y_5 + Y_6} \quad , \tag{A-12b}$$

and $$Y_{12} = Y_{21} = \frac{-Y_1 Y_2}{Y_1 + Y_2 + Y_3} - \frac{Y_4 Y_5}{Y_4 + Y_5 + Y_6} \quad . \tag{A-12c}$$

The voltage transfer function (g21) for the two circuits in parallel can be obtained by using equations (A-12b) and (A-12c) in equation (A-10).

Twin-T Network

Consider the two "T" networks shown in Figure A2 and Figure A3. The individual admittances of the
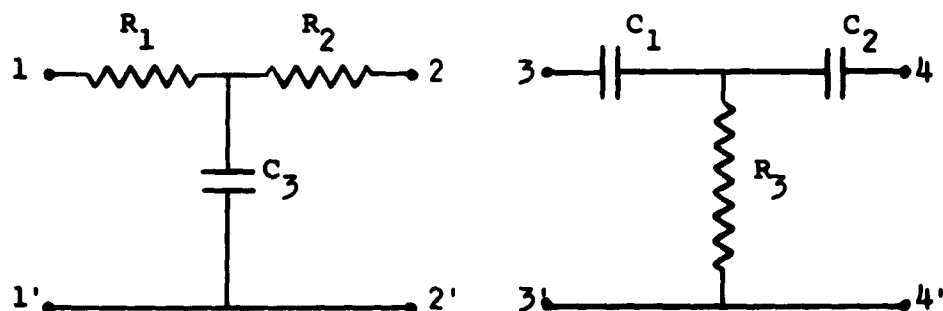
Figure A3   T networks with R and C elements

circuit elements of Figure A3 are seen to be

$$Y_1 = \frac{1}{R_1} \qquad\qquad Y_4 = sC_1$$

$$Y_2 = \frac{1}{R_2} \qquad\qquad Y_5 = sC_2 \qquad\qquad (A-13)$$

$$Y_3 = sC_3 \qquad\qquad Y_6 = \frac{1}{R_3}$$

in the Laplace transform frequency domain. Putting the circuits in Figure A3 in parallel we have Figure A4.
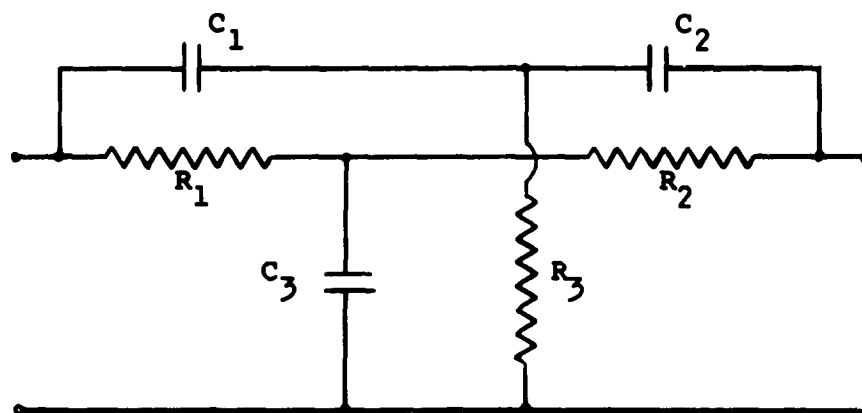
Figure A4   Twin-T network

The voltage transfer function (g21) of Figure A2 is obtained by substituting (A-12b) and (A-12c) into (A-10)

$$g_{21} = \frac{Y_1 Y_2 (Y_4 + Y_5 + Y_6) + Y_4 Y_5 (Y_1 + Y_2 + Y_3)}{Y_2 (Y_1 + Y_3)(Y_4 + Y_5 + Y_6) + Y_5 (Y_4 + Y_6)(Y_1 + Y_2 + Y_3)}$$

$$(A-14)$$

Substituting (A-13) into (A-14) gives

$$g21 = \frac{\frac{1}{R_1} \cdot \frac{1}{R_2}\left[sC_1 + sC_2 + \frac{1}{R_3}\right] + (sC_1)(sC_2)\left[\frac{1}{R_1} + \frac{1}{R_2} + sC_3\right]}{\frac{1}{R_2}\left(\frac{1}{R_1} + sC_3\right)\left[sC_1 + sC_2 + \frac{1}{R_3}\right] + sC_2\left(sC_1 + \frac{1}{R_3}\right)\left[\frac{1}{R_1} + \frac{1}{R_2} + sC_3\right]}$$

$$(A\text{-}15)$$

Now simplifying (A-15), we have

$$g21 = \frac{(sR_3C_1 + sR_3C_2 + 1) + (s^2C_1C_2R_2R_3 + s^2C_1C_2R_1R_3 + s^3C_1C_2C_3R_1R_2R_3)}{(1 + sC_3R_1)(sC_1R_3 + sC_2R_3 + 1) + (s^2C_1C_2R_3 + sC_2)(R_2 + R_1 + sC_3R_1R_2)}$$

and

$$g21 = \frac{1 + s^2C_1C_2R_2R_3 + s^2C_1C_2R_1R_3 + sR_3C_1 + sR_3C_2 + s^3C_1C_2C_3R_1R_2R_3}{(1 + sC_3R_1)(1 + sC_1R_3 + sC_2R_3) + (s^2C_1C_2R_3 + sC_2)(R_2 + R_1 + sC_3R_1R_2)} \; .$$

Now substituting

$$s = j\omega$$

and $s^2 = -\omega^2$

the transfer function becomes

$$g21 = \frac{\left[1 - \omega^2C_1C_2R_2R_3 - \omega^2C_1C_2R_1R_3\right] + j\left[\omega R_3C_1 + \omega R_3C_2 - \omega^3C_1C_2C_3R_1R_2R_3\right]}{(1 + j\omega C_3R_1)(1 + j\omega C_1R_3 + j\omega C_2R_3) + (-\omega^2C_1C_2R_3 + j\omega C_2)(R_2 + R_1 + j\omega C_3R_1R_2)} \; .$$

$$(A\text{-}16)$$

The numerator of g21 in (A-16) has the form

$$\alpha + j\beta$$

If g21 = 0, then $\alpha = \beta = 0$. We then have

$$\alpha = 1 - \omega^2C_1C_2R_2R_3 - \omega^2C_1C_2R_1R_3 = 0$$

$$\omega^2_o = \frac{1}{(R_1 + R_2)C_1C_2R_3}$$

$$(A\text{-}17)$$

and

$$\beta = \omega R_3 C_1 + \omega R_3 C_2 - \omega^3 C_1 C_2 C_3 R_1 R_2 R_3 = 0$$

(A-18)

$$\omega_o^2 = \frac{C_1 + C_2}{C_1 C_2 C_3 R_1 R_2} \; .$$

Combining (A-17) and (A-18)

$$\frac{1}{(R_1 + R_2)C_1 C_2 R_3} = \frac{C_1 + C_2}{C_1 C_2 C_3 R_1 R_2}$$

(A-19)

Separating variables,

$$\frac{\dfrac{R_1 R_2}{R_1 + R_2}}{R_3} = \frac{C_1 + C_2}{C_3} = n$$

(A-20)

where n is a real number $[o, \infty]$.

If we let

$$R_1 = R_2 = R$$

(A-21)

and $C_1 = C_2 = C$,

equation (A-20) becomes

$$\frac{R}{2R_3} = n = \frac{2C}{C_3}$$

(A-22)

By substituting the equalities (A-21) and (A-16),

g21 becomes

$$g21 = \frac{(1 - \omega^2 C^2 RR_3 - \omega^2 C^2 RR_3) + j(\omega R_3 C + \omega R_3 C - \omega^3 C^2 C_3 R^2 R_3)}{(1 + j\omega C_3 R)(1 + j\omega CR_3 + j\omega CR_3) + (-\omega^2 C^2 R_3 + j\omega C)(R + R + j\omega C_3 R^2)}$$

(A-23)

According to (A-22)

$$R_3 = \frac{R}{2n} \quad \text{and} \quad C_3 = \frac{2C}{n} \quad . \tag{A-24}$$

Relations (A-24) in (A-23) give

$$g21 = \frac{(1-\omega^2\frac{2C^2R^2}{2n} - \omega^2\frac{2C^2R^2}{2n}) + j(\omega\frac{CR}{2n} + \omega\frac{CR}{2n} - \omega^3\frac{C^3R^3}{n^2})}{(1+j\omega\frac{R2C}{n})(1 + j\omega\frac{CR}{2n} + j\omega\frac{CR}{2n}) + (-\omega^2\frac{2C^2R}{2n} + j\omega C)(R+R+j\omega\frac{R^2}{n}2C)} \tag{A-25}$$

Collecting terms,

$$g21 = \frac{(1 - \omega^2\frac{C^2R^2}{n}) + j(\frac{\omega CR}{n} - \omega^3\frac{R^3C^3}{n^2})}{(1 + j\omega\frac{2RC}{n})(1 + j\omega\frac{RC}{n}) + (-\omega^2\frac{RC^2}{2n} + j\omega C)(2R + j\omega\frac{2R^2C}{n})} \tag{A-26}$$

If $R_1 = R_2 = R$ and $C_1 = C_2 = C$, equation (A-17) becomes

$$\omega_o^2 = \frac{1}{2RC^2R_3} \tag{A-27}$$

and (A-18) becomes

$$\omega_o^2 = \frac{2C}{C^2R^2C_3} \quad . \tag{A-28}$$

Substituting equations (A-24) into (A-27) and (A-28) we have

$$\omega_o^2 = \frac{n}{R^2C^2} \tag{A-29}$$

and $\omega_o^2 = \frac{n}{R^2C^2}$ respectively. $\tag{A-30}$

From (A-29) or (A-30)

$$R^2 C^2 = \frac{n}{\omega_o^2} \; ,$$

$$RC = \frac{\sqrt{n}}{\omega_o} \; ,$$

(A-31)

$$\text{and} \quad R^3 C^3 = \frac{n\sqrt{n}}{\omega_o^3} \; .$$

Substituting equations (A-31) in (A-26),

$$g21 = \frac{(1 - \frac{\omega^2}{\omega_o^2}) + j(\frac{\omega}{\omega_o}\frac{1}{\sqrt{n}} - \frac{\omega^3}{\omega_o^3}\frac{1}{\sqrt{n}})}{(1 + j\frac{\omega}{\omega_o}\frac{2}{\sqrt{n}})(1 + j\frac{\omega}{\omega_o}\frac{1}{\sqrt{n}}) + (\frac{\omega^2}{\omega_o^2}\frac{1}{2R} + j\frac{\omega}{\omega_o}\frac{\sqrt{n}}{R})(\frac{2\sqrt{n}}{C\omega_o} + j\frac{\omega}{\omega_o^2}\frac{2}{C})}$$

(A-32)

Letting $\rho = \frac{\omega}{\omega_o}$, equation (A-32) becomes,

$$g21 = \frac{(1 - \rho^2) + j(\frac{\rho}{\sqrt{n}} - \frac{\rho^3}{\sqrt{n}})}{(1 + j\rho\frac{2}{\sqrt{n}})(1 + j\rho\frac{1}{\sqrt{n}}) + (-\frac{\rho^2}{2R} + j\rho\frac{\sqrt{n}}{R})(\frac{2\sqrt{n}}{\omega_o C} + j\rho\frac{2}{\omega_o C})}$$

(A-33)

Expanding the denominator gives,

$$g21 = \frac{(1 - \rho^2) + j\frac{\rho}{\sqrt{n}}(1 - \rho^2)}{(1 + j\frac{2\rho}{\sqrt{n}} + j\frac{\rho}{\sqrt{n}} - \frac{2\rho^2}{n}) + (-\frac{\rho^2\sqrt{n}}{RC\omega_o} + j\frac{\rho 2n}{RC\omega_o} - j\frac{\rho^3}{RC\omega_o} - \frac{\rho^2 2\sqrt{n}}{RC\omega_o})}$$

(A-34)

Now $RC\omega_o = \sqrt{n}$ from (A-31). Using this relation,
equation (A-34) becomes

$$g21 = \frac{(1 - \rho^2) + j\frac{\rho}{\sqrt{n}}(1 - \rho^2)}{1 + j\frac{2\rho}{\sqrt{n}} + j\frac{\rho}{\sqrt{n}} - \frac{2\rho^2}{n} - \rho^2 + j\rho 2\sqrt{n} - j\frac{\rho^3}{\sqrt{n}} - \rho^2 2}$$

$$(A-35)$$

Factoring the numerator and rearranging the denominator, (A-35) becomes

$$g21 = \frac{(1 - \rho^2)(1 + j\frac{\rho}{\sqrt{n}})}{1 - \rho^2 + j\frac{\rho}{\sqrt{n}} - j\frac{\rho^3}{\sqrt{n}} - 2\rho^2 - 2\frac{\rho^2}{n} + j2\rho\sqrt{n} + j\frac{2\rho}{\sqrt{n}}}$$

$$(A-36)$$

Now we operate on the denominator of (A-36) and obtain

$$\left[(1 - \rho^2) + j\frac{\rho}{\sqrt{n}}(1 - \rho^2)\right] + \left[-2\rho^2 - \frac{2\rho^2}{n} + j(2\rho\sqrt{n} + \frac{2\rho}{\sqrt{n}})\right] ,$$

$$\left[(1 - \rho^2) + j\frac{\rho}{\sqrt{n}}(1 - \rho^2)\right] + j2\rho\left[j\rho + j\frac{\rho}{n} + (\sqrt{n} + \frac{1}{\sqrt{n}})\right] ,$$

$$\left[(1 - \rho^2) + j\frac{\rho}{\sqrt{n}}(1 - \rho^2)\right] + j2\rho(\sqrt{n} + \frac{1}{\sqrt{n}})(1 + j\frac{\rho}{\sqrt{n}}) ,$$

$$(1 + j\frac{\rho}{\sqrt{n}})(1 - \rho^2) + j2\rho(1 + j\frac{\rho}{\sqrt{n}})(\sqrt{n} + \frac{1}{\sqrt{n}}) ,$$

$$(1 + j\frac{\rho}{\sqrt{n}})\left[(1 - \rho^2) + 2j\rho(\sqrt{n} + \frac{1}{\sqrt{n}})\right] ,$$

and

$$(1 + j\frac{\rho}{\sqrt{n}})\left[(1 - \rho^2) + j2\rho(\frac{n + 1}{\sqrt{n}})\right] . \qquad (A-37)$$

Now putting the denominator (A-37) back into (A-36) we have

$$g21 = \frac{(1 - \rho^2)(1 + j\frac{\rho}{\sqrt{n}})}{(1 + j\frac{\rho}{\sqrt{n}})\left[(1 - \rho^2) + j2\rho(\frac{n + 1}{\sqrt{n}})\right]} \qquad (A-38)$$

Dividing the numerator and denominator by "- $(1 + j\frac{\rho}{\sqrt{n}})$," (A-38) becomes

$$g21 = \frac{\rho^2 - 1}{(\rho^2 - 1) - j2\rho(\frac{n + 1}{\sqrt{n}})} \, . \tag{A-39}$$

The optimum "n" will be that which gives the steepest slope of $\left|g21\right|$ at ω_o. Now

$$\left|g21\right| = \frac{\rho^2 - 1}{\left[(\rho^2 - 1)^2 + 4\rho^2(\frac{n + 1}{\sqrt{n}})^2\right]^{1/2}} \tag{A-40}$$

and

$$\frac{\partial}{\partial \rho} \left|g21\right| = \frac{-\frac{(\rho^2-1)}{2}\left[4\rho(\rho^2-1) + 8\rho\frac{(n+1)^2}{n}\right] + 2\rho\left[(\rho^2-1)^2 + 4\rho^2\frac{(n+1)^2}{n}\right]}{\left[(\rho^2-1)^2 + 4\rho^2(\frac{n+1}{\sqrt{n}})^2\right]^{3/2}} \tag{A-41}$$

Relation (A-41) can be simplified by recalling that when $\omega = \omega_o$, $\rho = 1$ since $\rho = \frac{\omega}{\omega_o}$. Using this, (A-41) becomes

$$\left.\frac{\partial \left|g21\right|}{\partial \rho}\right|_{\rho = 1} = \frac{\sqrt{n}}{n + 1} \, . \tag{A-42}$$

The optimum "n" will maximize (A-42). Therefore

$$\frac{d}{dn} \left(\left.\frac{\partial \left|g21\right|}{\partial \rho}\right|_{\rho = 1}\right) = \frac{-\sqrt{n} + \frac{1}{2}n^{-\frac{1}{2}}(n + 1)}{(n + 1)^2} = 0 \tag{A-43}$$

and n = 1. $\tag{A-44}$

For this value of n, the steepest slope of $\left|g21\right|$, (A-42) will be

$$\left.\frac{\partial \left|g21\right|}{\partial \rho}\right|_{\substack{\rho = 1 \\ n = 1}} = \pm \frac{1}{2} \tag{A-45}$$

Also for n = 1,

$$R_3 = \frac{R}{2} \quad \text{and} \quad C_3 = 2C \qquad \qquad \text{(A-46)}$$

from (A-24).

If we let n = 2, however, the slope will be $\pm$ 0.472 but C_3 = C. Thus for a light sacrifice in slope, we are able to have $C_1 = C_2 = C_3$ which permits continuous variable tuning. Letting n = $\frac{1}{2}$, the slope will again be $\pm$ 0.472 but $R_1 = R_2 = R_3$.

The gain (β) of a twin-T network with zero input impedance, infinite output impedance, and n = 1 has been shown to be[2]

$$\beta = \frac{1}{1 - j\dfrac{4\rho}{\rho^2 - 1}} \qquad \qquad \text{(A-47)}$$

where

$$\rho = \frac{\omega}{\omega_o} = \frac{f}{f_o} . \qquad \qquad \text{(A-48)}$$

The term

$$\frac{4\rho}{\rho^2 - 1} \qquad \qquad \text{(A-49)}$$

indicates the manner in which the magnitude and phases of "β" varies with "ρ." When ρ = 0, (A-49) vanishes and

$$|\beta| = 1.$$

However when (A-49) is equal to unity,

$$|\beta| = \frac{\sqrt{2}}{2} ,$$

---

[2]Valley, G. E. Jr. and H. Wallman, Vacuum Tube Amplifiers, Vol. 18, Radiation Laboratory Series, McGraw-Hill Book Company, Inc., 1948.

and the response is 3 db down from $f = \rho = 0$ which is taken here as the reference. Thus at the 3 db points

$$\frac{4\rho}{\rho^2 - 1} = 1$$

and $\rho \approx \frac{1}{4}$

or $\frac{f}{f_o} \approx \frac{1}{4}$. $\qquad\qquad$ (A-50)

Equation (A-47) may now be written as

$$\beta = \frac{1}{1 - j\dfrac{4}{\left(\dfrac{f}{f_o} - \dfrac{f_o}{f}\right)}} = \frac{1}{1 - j\dfrac{4f_o}{\left(f - \dfrac{f_o^2}{f}\right)}} , \qquad\qquad (A-51)$$

in which the frequencies at the $\frac{1}{2}$-power points are

$$f_2 = \frac{f_o^2}{f} \qquad\qquad (A-52)$$

and $f_1 = f$

Defining

$$Q = \frac{f_o}{f_2 - f} ,$$

then

$$Q = \frac{f_o}{\dfrac{f_o^2}{f} - f} = \frac{ff_o}{f_o^2 - f^2} , \qquad\qquad (A-53)$$

Using (A-50) and putting Q in terms of "f"

$$Q = \frac{4f^2}{16f^2 - f^2} \approx \frac{1}{4} \qquad\qquad (A-54)$$

or $\quad 4 = \frac{1}{Q}$.

Substituting this last relation into (A-51) gives

$$\beta = \cfrac{1}{1 - j \cfrac{1}{Q(\frac{f}{f_o} - \frac{f_o}{f})}} = \cfrac{1}{1 - j \cfrac{1}{\frac{Q}{f_o}(f - \frac{f_o^2}{f})}} . \qquad \text{(A-55)}$$

We now show that "β" possesses geometric symmetry by considering the bracketed term in (A-55)

$$(f - \frac{f_o^2}{f}) \qquad\qquad \text{(A-56)}$$

which is equal to $(f_1 - f_2)$ by equations (A-52).

In a geometric progression

$$a_1 + a_1 r + a_1 r^2 + \dots a_1 r^{n-1} \qquad \text{(A-57)}$$

the ratio between successive terms is "r," and the general expression for the nth term is

$$a_n = a_1 r^{n-1} .$$

Thus the relation between the ordered frequencies f_1, f_x, and f_2 is

$$f_2 = f_1 r^2$$

or

$$r^2 = \frac{f_2}{f_1}$$

and by (A-52)

$$r^2 = \frac{\frac{f_o^2}{f}}{f} = \frac{f_o^2}{f^2} . \qquad\qquad \text{(A-58)}$$

By referring to (A-57) we see that

$$f_x = f_1 r = f. \ (\frac{f_o}{f}) = f_o \qquad (A-59)$$

since $f_1 = f$ by (A-52).

Because the geometric mean of f_2 and f_1 is f_o, the $|\beta|$ will be symmetric about the null frequency (f_o) when plotted against the logrithm of frequency or the logrithm of the frequency ratio "r."

Since

$$r = \frac{1}{\rho} \qquad (A-60)$$

by (A-50) and (A-58), it is more meaningful to use "ρ" as the parameter in plotting. From (A-48) we have

$$f = \rho f_o$$

which becomes

$$f_1 = \frac{1}{4} f_o \qquad (A-61)$$

$$f_2 = 4 f_o$$

after substituting (A-50) and (A-52).

Considering equation (A-47), the phase angle of β is

$$\Theta = \tan^{-1} \frac{4\rho}{\rho^2 - 1} . \qquad (A-62)$$

An examination of this relation shows that Θ varies from 0 to $-\frac{\pi}{2}$ as ρ varies from 0 to 1, and from $\frac{\pi}{2}$ to 0 as ρ varies from 1 to ∞. Figure A5 shows the $|\beta|$ and Θ as functions of ρ.
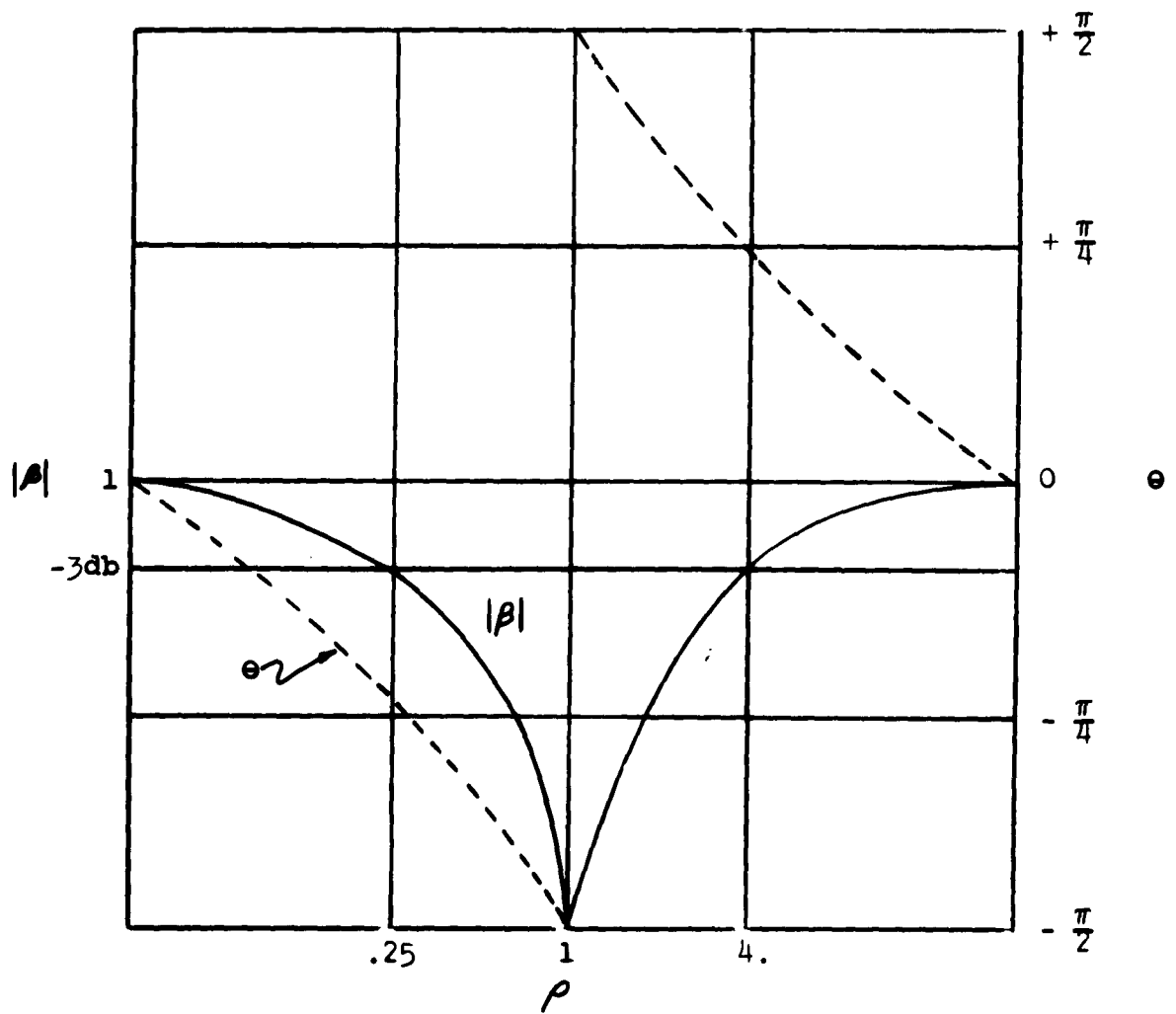
Figure A5 $|\beta|$ versus ρ

The input and output impedances affect the symmetry of the overall response.[3] The equation for β, (A-55), will not be affected directly since the external impedances are intentionally related to "r" and "n" of the network to insure that the response is equal to $f = 0$ and $f = \infty$.

Consider the twin-T network in Figure A6 which is driven by a source with finite impedance (R_1) and which operates into a load (R_L).
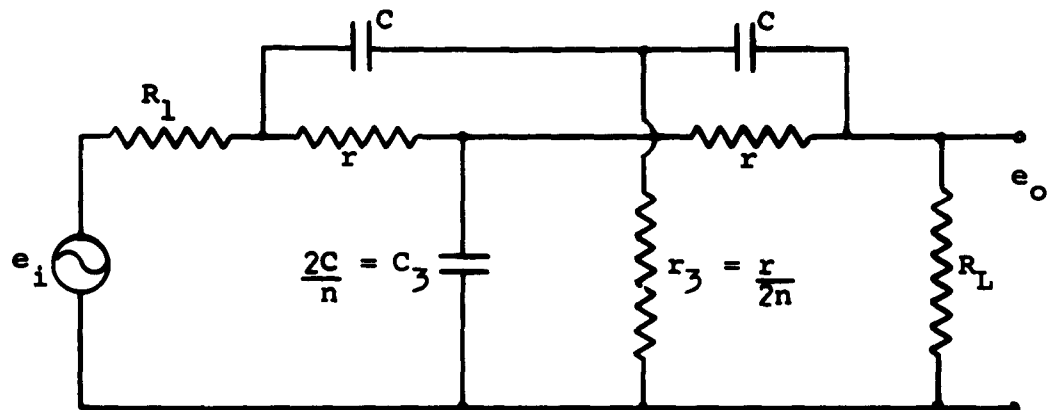
Figure A6   Twin-T network with voltage
source and load

When the frequency is zero, Figure A6 reduces to the equivalent circuit shown in Figure A7.

---

[3]Cowles, L. G., "Parallel - T Resistance Capacitance Networks," Proc. I.R.E., No. 12, Dec., 1952, p. 1712.
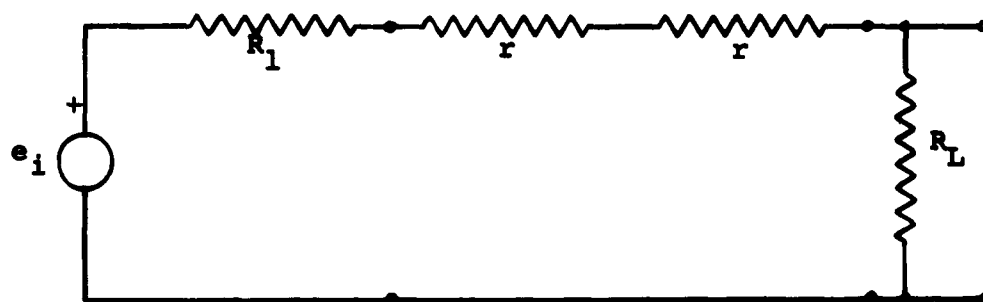
Figure A7   D-C equivalent circuit of twin-T
            network with source and load

The overall gain of this circuit is

$$\frac{e_O}{e_i} = \frac{R_L}{R_1 + 2r + R_1} \quad . \qquad\qquad (A\text{-}63)$$

As f tends to ∞, the circuit of Figure A6 becomes equivalent to that shown in Figure A8.
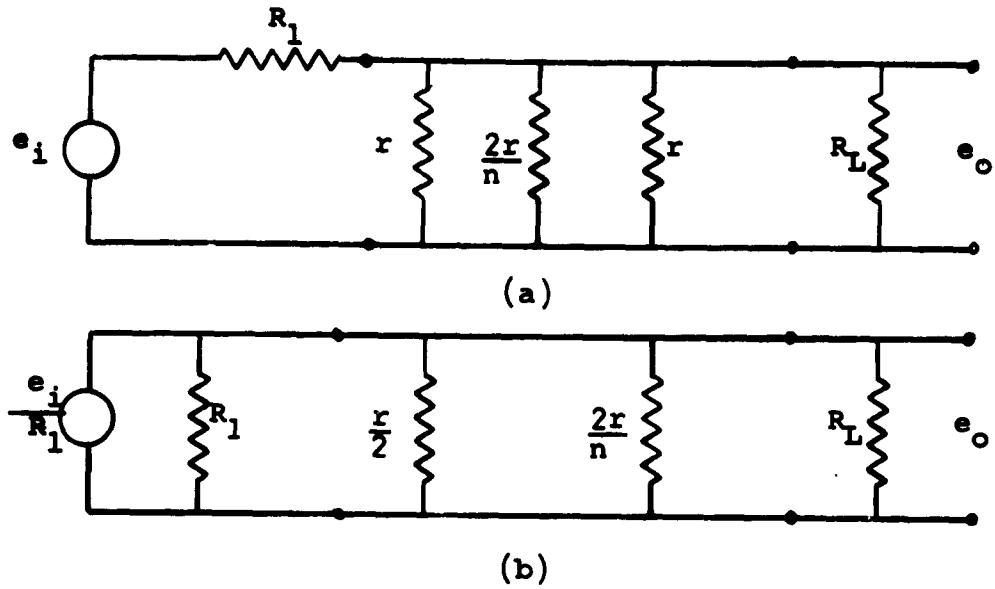
Figure A8   High frequency equivalent circuit of
twin-T network with source   and load

The overall gain is determined by

$$e_o\left[\frac{1}{R_L} + \frac{2}{r} + \frac{2n}{r} + \frac{1}{R_1}\right] = \frac{e_i}{R_1}$$

(A-64)

$$\frac{e_o}{e_i} = \frac{rR_L}{rR_L + rR_1 + R_1R_L(2n + 2)}$$

Equating (A-63) and (A-64), and solving for R_1 and
R_L we obtain

$$\frac{rR_L}{rR_L + rR_1 + R_1R_L(2n + 2)} = \frac{R_L}{R_1 + 2r + R_L}$$

$$R_1R_L^2(2n + 2) = 2r^2R_L$$

(A-65)

$$R_1R_L = \frac{r^2}{n + 1} \quad .$$

Equation (A-65) relates the external impedances with the "r" and "n" of the network such that the overall response is symmetric. In general the source impedance should be small compared to "r" and the load impedance should be relatively large.

In addition to the advantage of symmetry itself, satisfying (A-65) also means that the simpler d-c relation (A-63) can be used for determining the overall gain.

Consider the situation in which circuit design has resulted in R_1 being 10 k-ohms and R_L, 2 M-ohms. By relation (A-65), with $n = 1$,

$$(10^4) \ 2 \ (10^6) = \frac{r^2}{2}$$

$$r = 2 \ (10^5).$$

The overall gain from (A-63) is

$$\frac{e_o}{e_i} = \frac{2(10^6)}{10^4 + 4(10^5) + 2(10^6)} = \frac{2}{2.41} \approx 0.83$$

of the gain of the twin-T itself, (β). We are assuming here, and reasonably so, that for the value of "r" found above, the values of C, C_3, and r_3 are practicable and can satisfy the null frequency equation for a specific "f_o."[4]

---

[4]White, Gifford, "Design and Use of RC Parallel-T Networks," IRE Transactions on Audio, Vo. AV-8, Jan-Feb, 1960.

Considering the external impedances, a symmetrical response is obtained by equation (A-65). The series elements of the twin-T are related to the "null" frequency by

$$\omega_o^2 = \frac{n}{r^2 C^2} \tag{A-66}$$

and the series and shunt elements are related by

$$r_3 = \frac{r}{2n} \quad \text{and} \quad C_3 = \frac{2C}{n} \quad . \tag{A-67}$$

It is shown in Figure A9, which is based upon relation (A-66) (with $n = 1$), that for null frequencies in the 0-50 cps region there is a wide range of component values for "r" and "C" which are readily available and practical. In addition, this wide range of component values will accommodate equation (A-65) for many external impedance combinations.
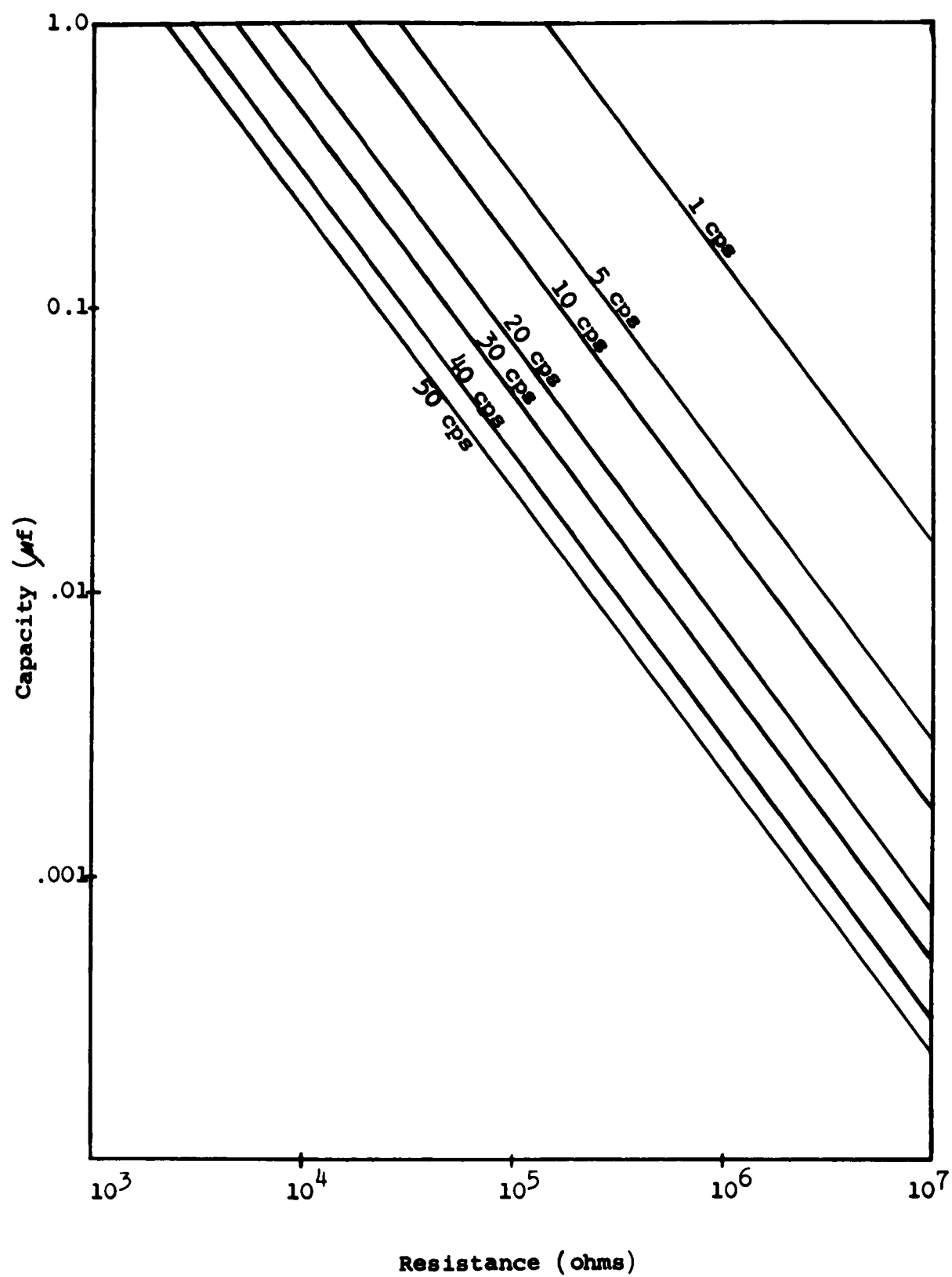
Figure A9. Capacity and resistance for null frequencies 0-50 cps.

Appendix B

Tape Recording

The objective of this article is to demonstrate the influence that varying tape speed has upon the recording and reproduction signals.

Basic Relations

During recording the magnetic material on the tape is exposed to a varying flux across the gap of the recording head. Both tape speed and flux are functions of time. Therefore interaction between the two may be analyzed at one point in space. See figure B1
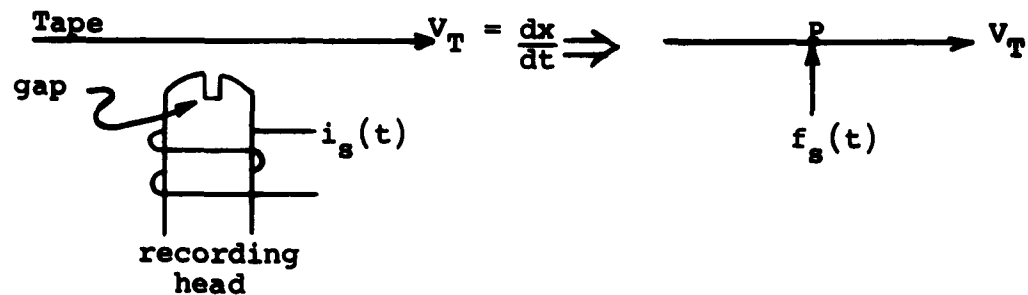
Figure B1   Interaction between tape speed and flux

The flux ϕ at point "P" is proportional to NI. Assuming $i(t)$ is periodic with frequency, f_s, then the instantaneous flux is

$$\phi = \hat{\Phi} \cos \omega_s t. \qquad (B-1)$$

98

The linear velocity of the tape (v_T) is of course

$$v_T = \frac{dx}{dt} \cdot \qquad (B-2)$$

Perhaps the best way to demonstrate the relation of $\phi(t)$ and v_T is to plot both on the same time axis (Figure B2). Assuming that the frequency of the recording signal (f_{sR}) is constant, then the period (T_{sR}) of the signal and wavelength of flux in the gap ($\lambda\phi g$) are constant. Figure B2 shows that the time in one wavelength on the tape (T_T) is equal to the period (T_{sR}) of the signal regardless of the tape velocity during the recording (v_{TR}). However, the space wavelength on the tape (λ_T) is proportional to tape velocity (v_{TR}). To put these relations in mathematical form, we begin by saying that

$$v_{TR} = \frac{x}{t} \cdot \qquad (B-3)$$

Considering one cycle of f_{sR}, then

$$x = \lambda_{TR}$$
$$t = T_{TR} = T_{sR} \qquad (B-4)$$

and

$$v_{TR} = \frac{\lambda_{TR}}{T_T} = \frac{\lambda_{TR}}{T_{sR}} \cdot \qquad (B-5)$$

this last expression says that

$$\lambda_{TR} = T_{sR} v_{TR} \qquad (B-6)$$
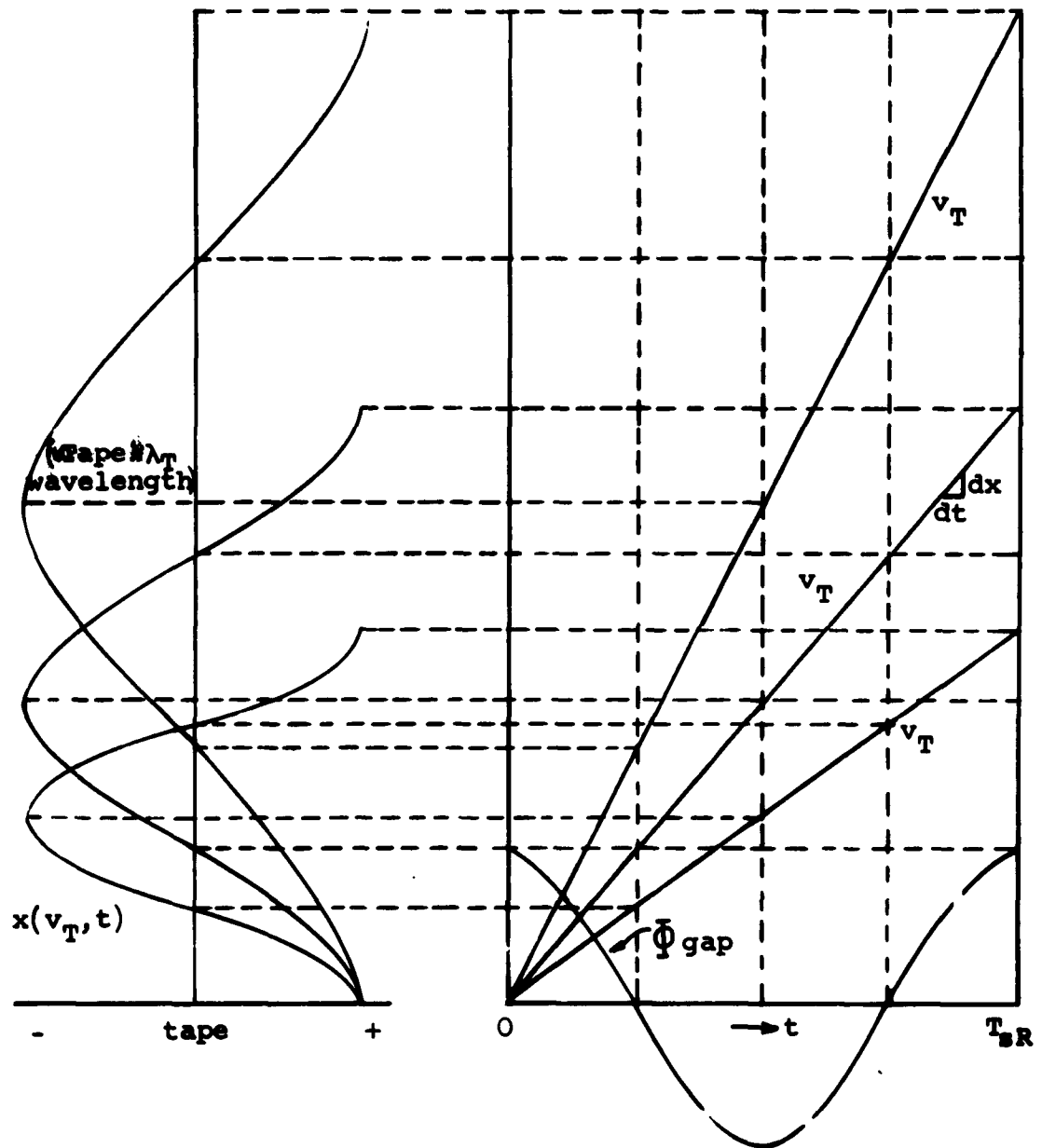
Figure B2   Recording head flux and tape speed
versus time

or that

$$\lambda_{TR} = \frac{v_{TR}}{f_{sR}}$$

since

$$T_{sR} = \frac{1}{f_{sR}} \; . \qquad (B-7)$$

We have assumed that f_{sR} is constant. If we further assume that v_{TR} is constant during the recording process; then from relation $(B-7)$, λ_{TR} will be constant. This appears trivial until we consider the play-back situation. Once λ_{TR} is established on the tape, it is fixed, and in analyzing the play-back situation, it becomes a convenient reference parameter. Thus

$$\lambda_{Tb} = \lambda_{TR} = \lambda_{T} \qquad (B-8)$$

where subscript (R) denotes the recording sequence and subscript (b) denoted the play-back sequence.

The basic relation $(B-7)$ also describes the play-back process. Thus changing the subscripts $(B-7)$ becomes

$$\lambda_{T} = \frac{v_{Tb}}{f_{sb}} \; . \qquad (B-9)$$

The frequency obtained from the tape will be directly proportional to the velocity,

$$f_{sb} = \frac{v_{Tb}}{\lambda_{T}} \qquad (B-10)$$

Or stated in another way,

$$f_{sb} = f_{sR} \qquad\qquad (B-11)$$

if

$$v_{Tb} = v_{TR} \; .$$

Velocity Effects

The mechanism which pulls the tape past the play-back head is basically a rotating device. As a consequence, it is quite conceivable that any variation in tape velocity (v_{Tb}) would be periodic. Thus we shall assume that the tape velocity (v_{Tb}) varies about the correct tape velocity-- the recording velocity (v_{TR})--in a periodic manner (Figure B3). The origin and description of this variation are of no concern at the moment.
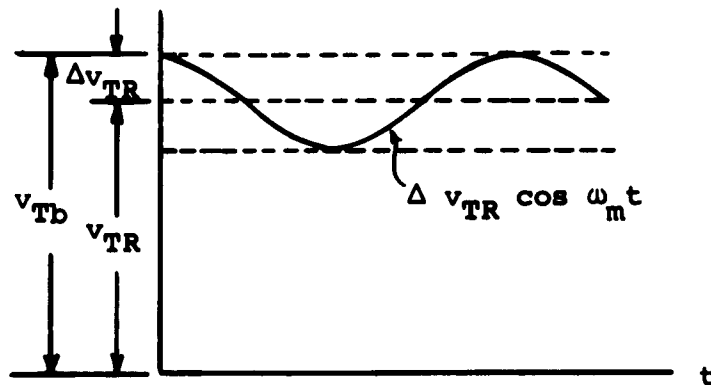
Figure B3   Playback tape speed versus time

Due to the variation tape speed,

$$v_{Tb} = v_{TR} + \Delta v_{TR} \cos \omega_m t. \qquad\qquad (B-12)$$

or by dividing by λ_T

$$\frac{v_{Tb}}{\lambda_T} = \frac{v_{TR}}{\lambda_T} + \frac{\Delta v_{TR}}{\lambda_T} \cos \omega_m t.$$

Recalling (B-8) and (B-10), the above equation reduces to

$$f_{sb} = f_{sR} + \Delta f_{sR} \cos \omega_m t \qquad \text{(B-13a)}$$

$$f_{sb} = f_{sR} \left(1 + \frac{\Delta f_{sR}}{f_{sR}} \cos \omega_m t\right) \qquad \text{(B-13b)}$$

or $\omega_{sb} = \omega_{sR} \left(1 + \dfrac{\Delta \omega_{sR}}{\omega_{sR}} \cos \omega_m t\right).$ \qquad (B-13c)

Equation (B-13a) is shown in Figure B4. Figure B3 and Figure B4 differ in magnitude by a factor of λ_T because of (B-10). However, the ratios are identical:

$$\frac{\Delta v_{TR}}{v_{TR}} = \frac{\Delta f_{sR}}{f_{sR}}. \qquad \text{(B-14)}$$
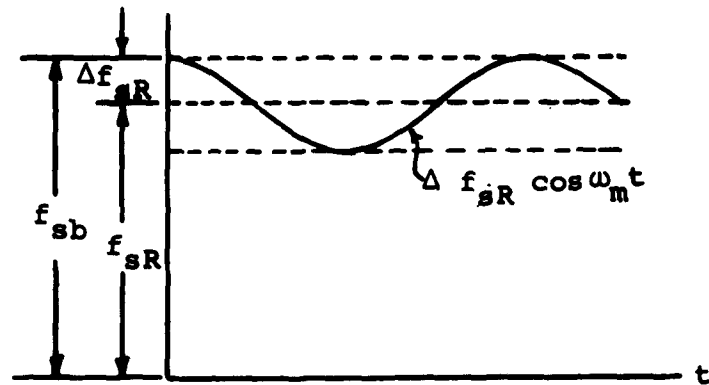
Figure B4   Playback signal frequency versus time

In other words, the percentage change in the tape velocity is equal to the percentage change in the output frequency.

Consider that the output be expressed as

$$f_{sb}(t) = A \cos \Theta(t) . \tag{B-15}$$

By definition $\dfrac{d\Theta}{dt} = \omega$ $\tag{B-16}$

or $\quad \Theta(t) = \displaystyle\int \omega \, dt + C.$

If the angular frequency (ω) is constant, then

$$\Theta(t) = \omega t + \Theta_o$$

and (B-15) assumes the familiar form

$$f_{sb}(t) = A \cos (\omega t + \Theta_o).$$

However, (B-13c) indicates that ω_{sb} is not constant. Therefore (B-16), upon substituting (B-13c), becomes

$$\Theta(t) = \int (\omega_{sR} + \Delta\omega_{sR} \cos \omega_m t) dt$$

$$\tag{B-17}$$

or

$$\Theta(t) = \omega_{sR} t + \frac{\Delta\omega_{sR}}{\omega_m} \sin \omega_m t + \Theta_o$$

Letting the reference time be chosen such that $\Theta_o = 0$, and incorporating (B-17), (B-15) becomes

$$f_{sb}(t) = A \cos \left[\omega_{sR} t + \frac{\Delta\omega_{sR}}{\omega_m} \sin \omega_m t \right] \tag{B-18a}$$

This is the expression for frequency modulation (FM) in which

$$\Delta\omega_{sR} \text{ - the deviation} \tag{B-18b}$$

and

$$\frac{\Delta\omega_{sR}}{\omega_m} = \beta \text{ - the modulation index .} \tag{B-18c}$$

Voltage Output During Playback

The instantaneous output voltage from the playback head is

$$e_o = - N \frac{d\phi}{dt} . \tag{B-19}$$

The flux on the tape is distributed according to

$$\phi_T = \bar{\Phi} \cos 2\pi f_s t \tag{B-20}$$

since it is due to the flux in the gap (B-1). On playback then

$$e_o = N \bar{\Phi} 2\pi f_{sb} \sin 2\pi f_{sb} t \tag{B-21a}$$

or using (B-19)

$$e_o = N \bar{\Phi} 2\pi \frac{v_{Tb}}{\lambda_t} \sin 2\pi \frac{v_{Tb}}{\lambda_T} t . \tag{B-21b}$$

Figure B5 shows the variation of e_o due to f_{sb} or v_{Tb}. Although the curve drops off at the higher frequencies due to losses, it is linear in the frequency range of concern. Thus both magnitude and frequency of e_o are functions of v_{Tb}. However, since NARTB equalization keeps $|e_o|$ constant, only the frequency of e_o changes with v_{Tb}.
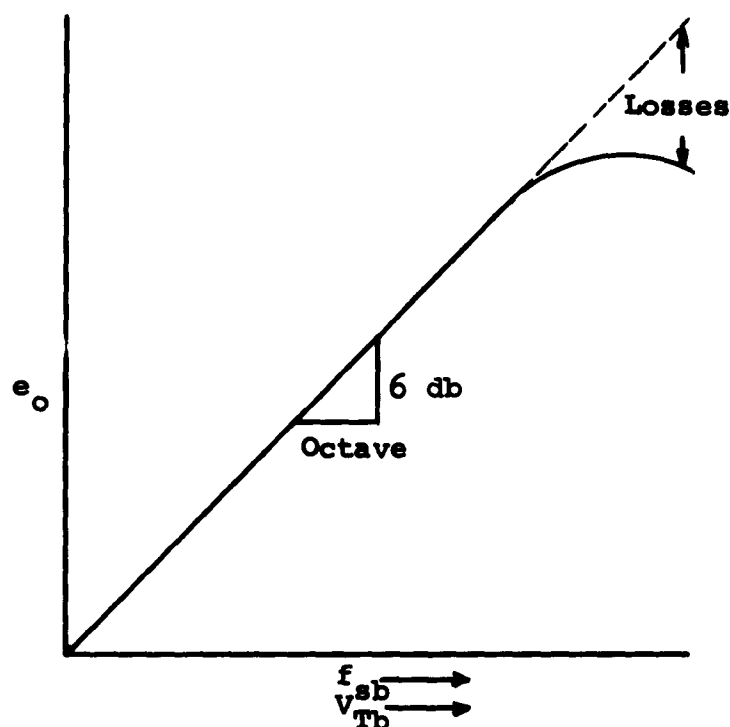
Figure B5   Output voltage versus tape
playback speed

Analysis of Velocity Variations During Playback

Under idealised conditions the recording and playback
velocities are identical; and therefore, the input and
output frequencies are equal. Under these conditions
assume a perfectly symmetric capstan pulls the tape at 7.5
ips. If the radius of the capstan is 0.5 in., then the
angular velocity will be

$$\omega_m = \frac{v_{Tangent}}{r} = \frac{7.5}{0.5} = 15 \quad \text{rad/sec.} \tag{B-22}$$

or the frequency will be

$$f_m = \frac{15}{2\pi} = 2.4 \quad \text{cps.} \tag{B-23}$$

Now we assume that a perfect tape recorded at 7.5 ips, is played back with a non-symmetric capstan (Figure B6).
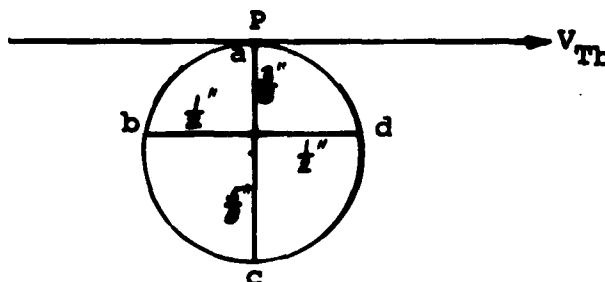
Figure B6   A non-symmetric capstan

Since no other defect is assumed, the angular velocity of this non-symmetric capstan is also 15 rad/sec. The tangential velocity or tape velocity is directly proportional to the radius,

$$v_{Tb} = \omega_m r. \tag{B-24}$$

Figure B6 shows that

$$v_{Tb}(a) = 15\left(\frac{3}{8}\right) = 5.6 \quad \text{ips.} \tag{B-25a}$$

when point "a" is in contact with the tape at "P."   In
a similar manner, as the capstan rotates,

$$v_{Tb}(b) = 15(\tfrac{1}{2}) = 7.5 \text{ ips},\qquad\qquad\text{(B-25b)}$$

$$v_{Tb}(c) = 15(\tfrac{5}{8}) = 9.4 \text{ ips},\qquad\qquad\text{(B-25c)}$$

$$v_{Tb}(d) = 15(\tfrac{1}{2}) = 7.5 \text{ ips},\qquad\qquad\text{(B-25d)}$$

Thus the tape velocity varies about the correct velocity
(7.5 ips) periodically at a frequency of 2.4 cps (B-23)
and amplitude of 1.9 ips (Figure B7).
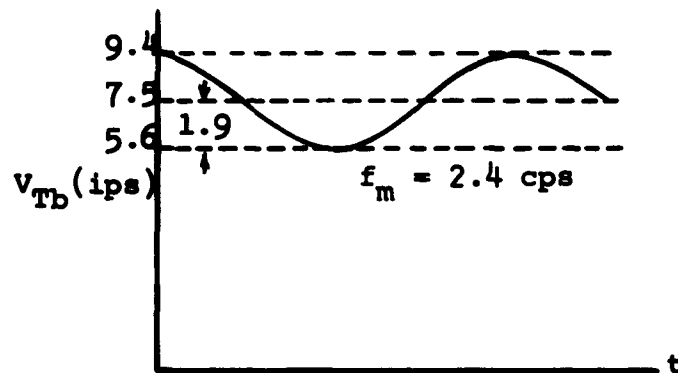
Figure B7   Tape playback speed versus time with
non-symmetric capstan

From relation (B-10), we know that the output frequency
(f_{sb}) is directly proportional to the tape velocity in
playback (v_{Tb}) since the wavelength on the tape (λ_t) is
fixed. Assuming a 1000 cps recording frequency with tape
velocity of 7.5 ips., the tape wavelength is

$$\lambda_T = \frac{v_{TR}}{f_{sR}} = \frac{7.5}{10^3} = 7.5(10^{-3}) \text{ in.} \qquad (B-26)$$

Upon playback

$$f_{sb} = \frac{v_{Tb}}{\lambda_T} = \frac{v_{Tb}}{7.5(10^{-3})} \qquad (B-27)$$

The results using this relation and the values of v_{Tb} (Figure B7) are shown in Table B-I.

v_{Tb}(ips)	f_{sb}(cps)
9.4	1260
7.5	1000
5.6	740
1.9	260

Table B-I   Signal frequencies at various tape speeds during playback

The output frequency (f_{sb}) varies periodically at a frequency of 2.4 cps and amplitude of 260 cps. Figure B8 shows the correspondence indicated in Table B-I. The frequency (f_{sb}) and velocity (v_{Tb}) axis are scaled to include the λ_T factor.
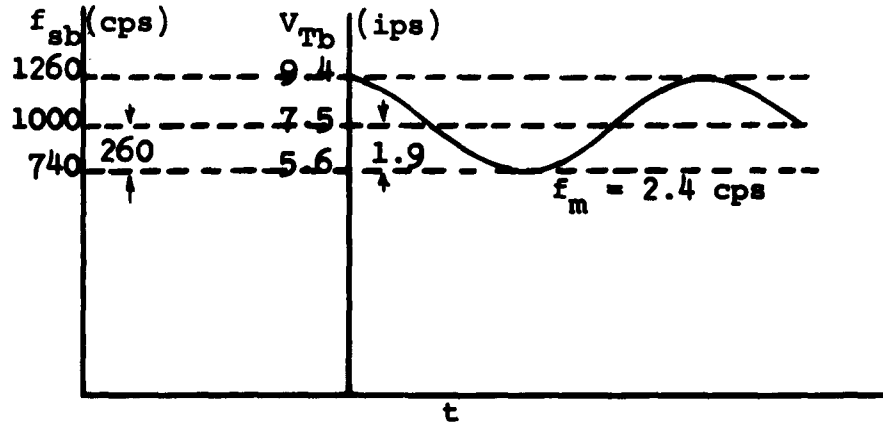
Figure B8   Tape speed and signal frequency versus time during playback

Considering the change in velocity and frequency we have from (B-27)

$$\Delta f_{sb} = \frac{\Delta v_{Tb}}{\lambda_T} .$$

(B-28)

From (B-7) and (B-8), we have

$$\lambda_T = \frac{v_{TR}}{f_{sR}} .$$

(B-29)

Substituting (B-29) into (B-28) gives

$$\frac{\Delta f_{sb}}{f_{sR}} = \frac{\Delta v_{Tb}}{TR} ,$$

(B-30)

which says that the percentage change in the output frequency is equal to the percentage change in the tape velocity. This expression (B-30) is general in that it

says nothing concerning the cause of the varying tape velocity.

In arriving at (B-30), we assumed a non-symmetric capstan. W shall therefore determine the percentage of frequency change in terms of capstan asymmetry. Considering a change in velocity due to asymmetry, relation (B-24) becomes

$$\Delta v_{Tb} = \omega_m \Delta r \tag{B-31}$$

since ω is constant. Substituting (B-24) into (B-31) we have

$$\frac{\Delta v_{Tb}}{v_{TR}} = \frac{\Delta r}{r} \tag{B-32}$$

which from (B-30) gives

$$\frac{\Delta f_{sb}}{f_{sR}} = \frac{\Delta r}{r} \ . \tag{B-33}$$

Appendix C

Modulation

Single-ended Switching

A mechanical or electromechanical switch can be represented by[1]

$$S(t) = \frac{1}{2} + \sum_{\substack{n=1 \\ (odd)}}^{\infty} \frac{\sin \frac{n\pi}{2}}{n\frac{\pi}{2}} \cos n\omega_c t \qquad (C-1)$$

This switching function operating on some signal, e_i, produces an output shown in Figure C1.
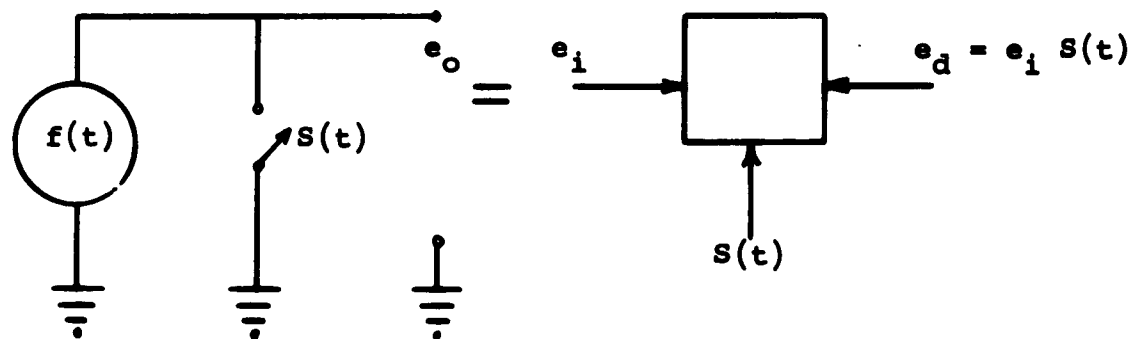
Figure C1   Single-ended switching

---

[1]Schwartz, Mischa, Information Transmission, Modulation, and Noise, McGraw-Hill Book Company, Inc., 1959.

Assuming

$$e_i = a \cos \omega_m t \tag{C-2}$$

$$e_d = e_i S(t) = a \cos \omega_m t \left[\frac{1}{2} + \sum_{\substack{n=1 \\ (\text{odd})}}^{\infty} \frac{\sin \frac{n\pi}{2}}{\frac{n\pi}{2}} \cos n\omega_c t \right] \tag{C-3}$$

where ω_m is the signal or modulating frequency and ω_c is the switching or carrier frequency. Expanding (C-3) and explicitly showing the "n = 1" term

$$e_d = \frac{a}{2} \cos \omega_m t + \frac{2a}{\pi} \cos \omega_m t \cos \omega_c t$$
$$+ a \cos \omega_m t \sum_{\substack{n=3 \\ n \text{ odd}}}^{\infty} \frac{\sin \frac{n\pi}{2}}{\frac{n\pi}{2}} \cos n\omega_c t \tag{C-4}$$

Substituting the trigonometric equivalence for the second term and letting

$$\frac{a}{2} = A \quad \text{and} \quad \frac{a}{\pi} = B, \tag{C-5}$$

equation (C-4) becomes

$$e_d = A \cos \omega_m t + B \left[\cos (\omega_c + \omega_m)t + \cos (\omega_c - \omega_m)t \right]$$
$$+ a \cos \omega_m t \sum_{\substack{n=3 \\ n \text{ odd}}}^{\infty} \frac{\sin \frac{n\pi}{2}}{\frac{n\pi}{2}} \cos n\omega_c t . \tag{C-6}$$

The original signal or data occupies its original position in the spectrum and in addition also becomes side bands about odd harmonics of the switching frequency.

The switching frequency and its harmonics are not present. This is double side band (DSB) modulation or carrier suppressed modulation. See Figure C2.
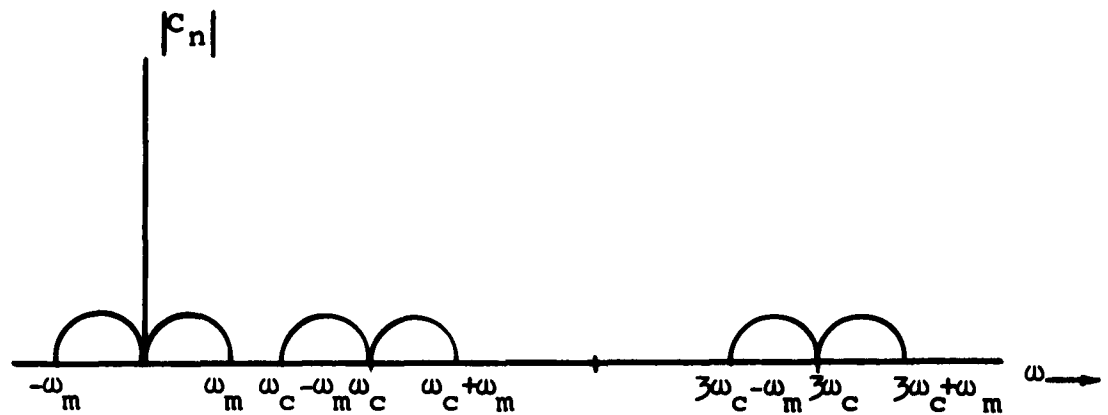
Figure C2   Spectrum of single-ended switching

It is evident from Figure C2 that filtering is made easier by increasing ω_c. Distortion occurs if $\omega_c - \omega_m < \omega_m$. Thus the minimum tolerable ω_c occurs when

$$\omega_c - \omega_m = \omega_m$$

or

$$\omega_c = 2\omega_m.$$

(C-7)

Note here that $f(t)$ has no d-c bias term. In addition, equation (C-4) and (C-6) show that the side bands are generated by the product term $\cos \omega_m t \cos \omega_c t$ which is basically

$$e_i \times \cos \omega_c t \ . \tag{C-8}$$

The response (assuming 100 to 4000 cps) of the tape recorder automatically filters out the ω_m (0-50 cps) in the spectrum. The fact that this occurs is the sole basis for considering switching in the first place. The frequencies above 4,000 cps are also filtered out. As a result the data actually recorded upon the tape will have the spectrum shown in Figure C3.
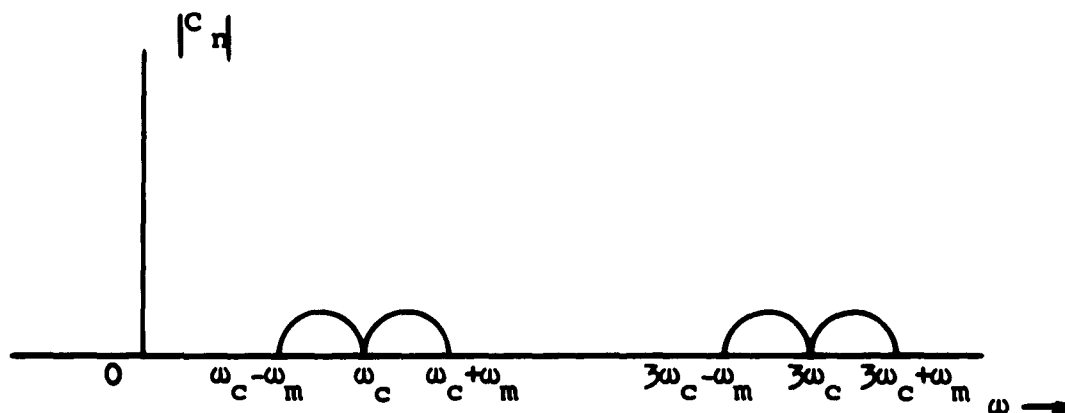
Figure C3   Spectrum of single-ended switching
after filtering by tape recorder

Since the 3rd harmonics are not of interest and only complicate subsequent developments, we consider

$$e_d = B\left[\cos\ (\omega_c + \omega_m)t + \cos\ (\omega_c - \omega_m)t\right] \qquad (C-9)$$

and consider only the spectrum as shown in Figure C4.
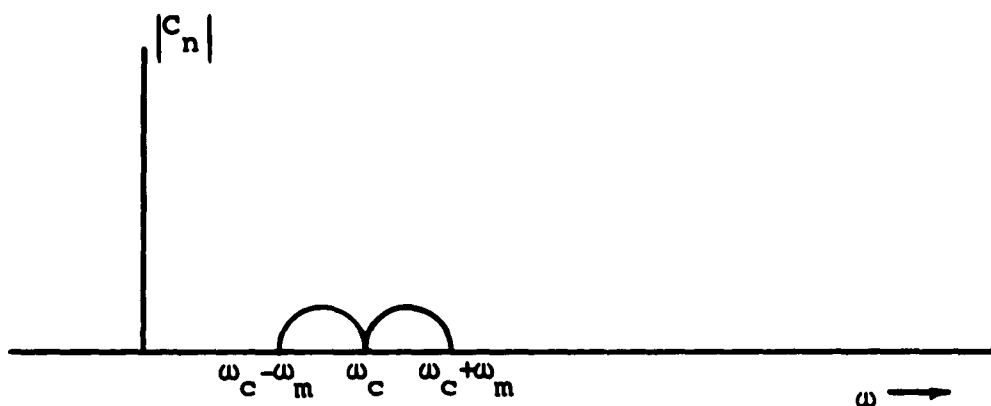
Figure C4   Spectrum of single-ended switching used for analysis

Bi-polar Switching

Bi-polar switching which is depicted in Figure C5 has a switching function $S(t)$ which is balanced with respect to ground as shown in Figure C6. From this

$$S(t) = 2 \sum_{\substack{n = 1 \\ n \text{ odd}}}^{\infty} \frac{\sin \frac{n\pi}{2}}{\frac{n\pi}{2}} \cos n\omega_c t \qquad (C-10)$$
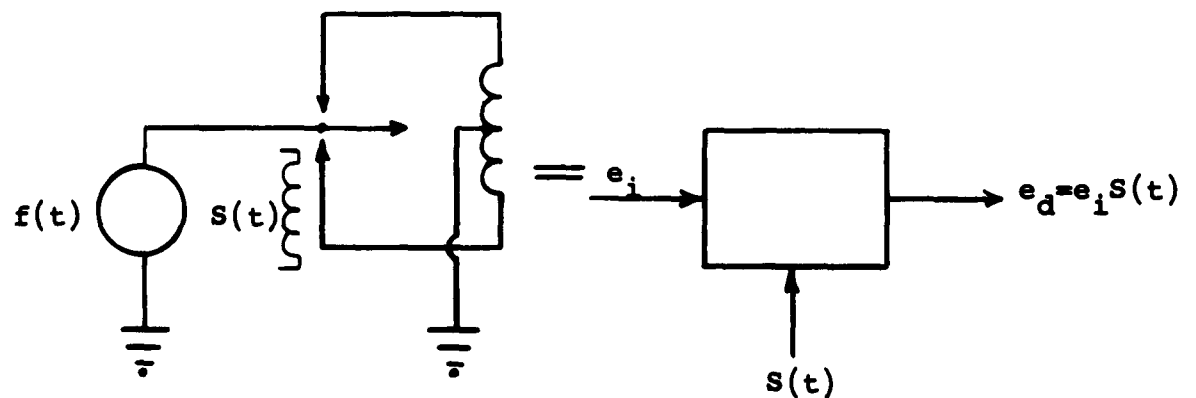
Figure C5   Bi-polar switching
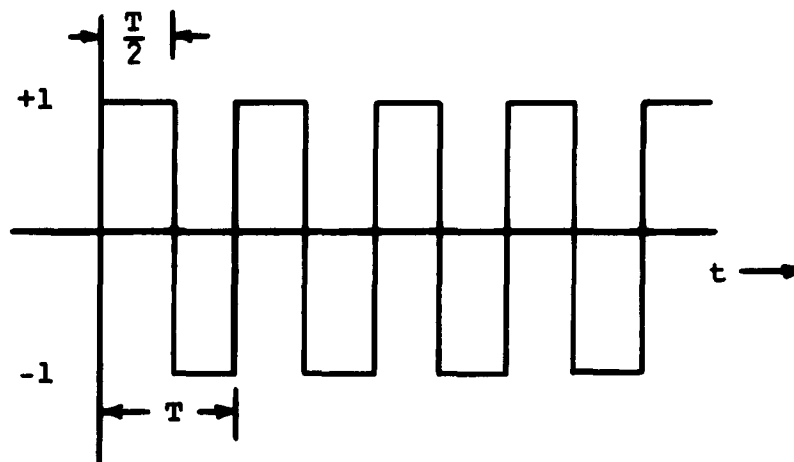
Figure C6   Bi-polar switching function

and assuming $e_i = a \cos \omega_m t$

$$e_d = a \cos \omega_m t \left[2 \sum_{\substack{n = 1 \\ n \text{ odd}}}^{\infty} \frac{\sin \frac{n\pi}{2}}{\frac{n\pi}{2}} \cos n\omega_c t \right]$$

or

$$e_d = \frac{4a}{\pi} \cos \omega_m t \cos \omega_c t$$

$$+ a \cos \omega_m t \left[2 \sum_{\substack{n = 3 \\ n \text{ odd}}}^{\infty} \frac{\sin \frac{n\pi}{2}}{\frac{n\pi}{2}} \cos n\omega_c t \right] \quad \text{(C-11)}$$

The spectrum, Figure C7, is identical with Figure C2, except the ω_m about zero is absent. This is due, of course, to the absence of the d-c term in $S(t)$ equation (C-10). The minimum ω_c occurs when

$$\omega_c - \omega_m = 0$$

or

$$\omega_c = \omega_m .$$

(C-12)

Since we are considering switching at 1 kc and have automatic filtering by the tape recorder, the difference in minimum switching rates and the presence or absence of ω_m spectrum at zero makes no difference here.
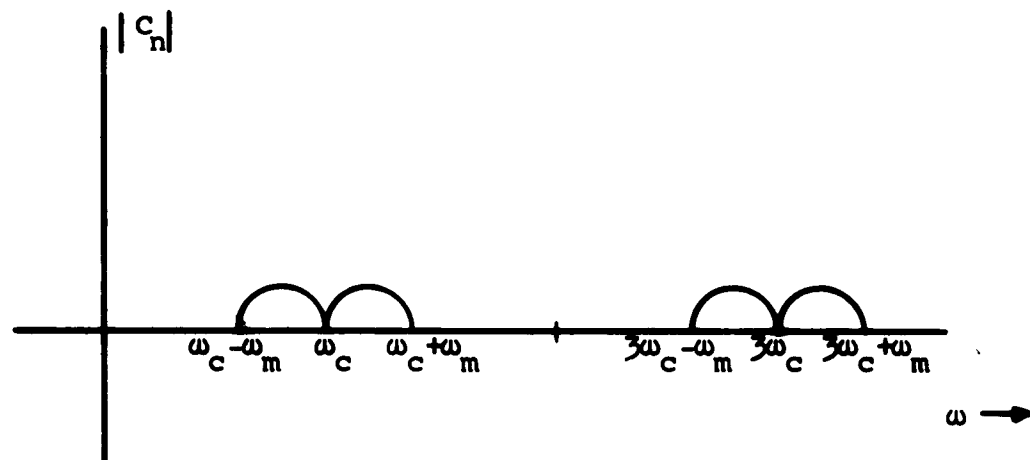
Figure C7   Spectrum of bi-polar switching

Single-ended switching appears the simpler of the two, particularly so, if further inquiry indicates that complete carrier suppression is unnecessary. Bi-polar switching would necessitate exact balancing and, of course, would complicate construction and adjustments.

In this discussion of the two forms of switching, the analysis assumed no d-c bias on the switching device. This, of course, is easily obtainable with reed-type of mechanical switches. However, the upper frequency limit of these switches is far short of 1 kc. To satisfy other requirements, such as portability, lightweight, low battery drain, etc., some form of transistor switching would be desirable.

The typical circuit configuration shown in Figure C8 will now be analyzed. The signal input e_i fluctuates about a positive potential. The connections are made so that
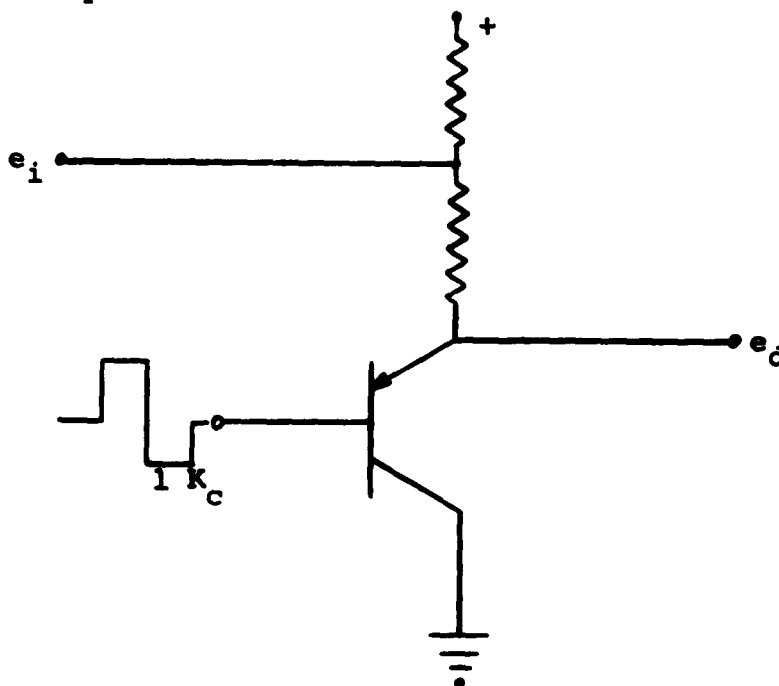
Figure C8   Transistor switch

both positive and negative excursions are preserved. The
switching effect in the presence of the d-c bias can be
symbolized as shown in Figure C9.
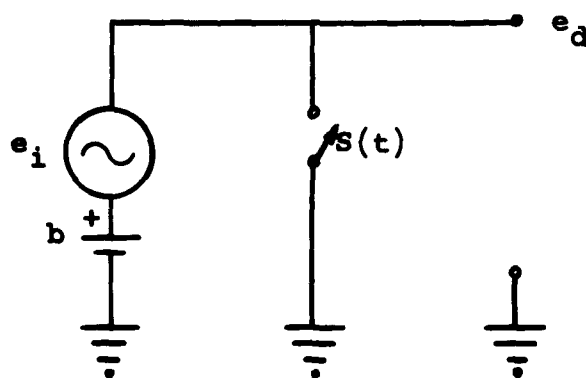
Figure C9   Equivalent circuit for transistor switch

The output voltage then is

$$e_d = \left[b + e_i\right] S(t) \tag{C-13}$$

or with $e_i = a \cos \omega_m t$

$$e_d = \left[b + a \cos \omega_m t\right]\left[\frac{1}{2} + \sum_{\substack{n=1 \\ n \text{ odd}}}^{\infty} \frac{\sin \frac{n\pi}{2}}{\frac{n\pi}{2}} \cos n\omega_c t\right]. \tag{C-14}$$

Expanding (C-14) and showing the "n = 1" terms explicitly

gives

$$e_d = \frac{b}{2} + \frac{a}{2} \cos \omega_m t + \frac{2b}{\pi} \cos \omega_c t + \frac{2a}{\pi} \cos \omega_m t \cos \omega_c t$$

$$+ \left[b + a \cos \omega_m t \right] \sum_{\substack{n = 3 \\ n \text{ odd}}}^{\infty} \frac{\sin \frac{n\pi}{2}}{\frac{n\pi}{2}} \cos n\omega_c t \quad . \quad (C\text{-}15)$$

The d-c term is removed by coupling capacitor and the original data term (2nd term) plus higher ordered terms will be filtered out by the tape recorder. So essentially, (ignoring the 3rd harmonic and side bands) the spectrum recorded on the tape will be

$$e_d = \frac{2b}{\pi} \cos \omega_c t + \frac{2a}{\pi} \cos \omega_m t \cos \omega_c t \quad (C\text{-}16)$$

as shown in Figure C10.
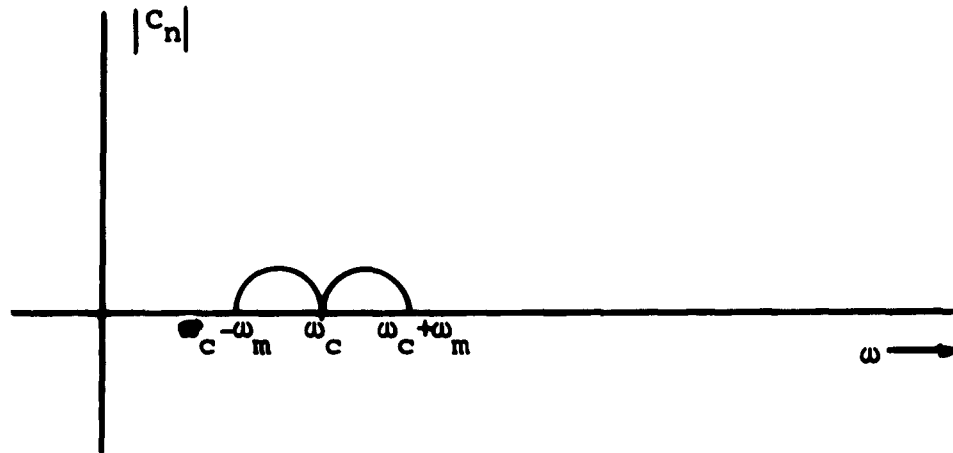
Figure C10   Spectrum of transistor switch after
filtering by tape recorder

This is, of course, Amplitude Modulation (AM). The carrier, $\cos \omega_c t$, is due to the d-c bias.

One way of securing DSB modulation would be to place two such circuits as shown in Figure C8 in push-pull with transformer coupled input and output balanced to ground. This complicates the circuitry, adds to the cost, and adds to the weight.

Demodulation

Demodulation of AM modulation by switching on tape playback is now considered. A circuit identical to Figure C8 is used as the demodulator.

From equation (C-16) the output of the tape recorder will be

$$e_d' = \frac{2b}{\pi} \cos \omega_c' t + \frac{2a}{\pi} \cos \omega_m' t \cos \omega_c' t \qquad (C-17)$$

where $\omega_m' \neq \omega_m$ and $\omega_c' \neq \omega_c$ due to variations in tape speed. The switching function has the same frequency (ω_c) as during modulation. Considering Figure C9, e_i is now e_d and e_d becomes e_o. Therefore

$$e_o = \left[b + e_d \right] S(t) = \left[b + \frac{2b}{\pi} \cos \omega_c' t + \frac{2a}{\pi} \cos \omega_m' t \right.$$
$$\left. \cos \omega_c' t \right] \left[\frac{1}{2} + \sum_{\substack{n=1 \\ n \text{ odd}}} \frac{\sin \frac{n\pi}{2}}{\frac{n\pi}{2}} \cos n\omega_c t \right] \qquad (C-18)$$

and expanding

$$e_o = \frac{b}{2} + \frac{b}{\pi} \cos \omega_c't + \frac{a}{\pi} \cos \omega_m't \cos \omega_c't + \frac{2b}{\pi} \cos \omega_c t$$

$$+ \frac{4b}{\pi} \cos \omega_c't \cos \omega_c t + \frac{4a}{\pi^2} \cos \omega_m't \cos \omega_c't \cos \omega_c t$$

$$+ \left[b + \frac{2b}{\pi} \cos \omega_c't + \frac{2a}{\pi} \cos \omega_m't \cos \omega_c't \right]$$

$$\left[\sum_{\substack{n = 3 \\ n \text{ odd}}}^{\infty} \frac{\sin\frac{n\pi}{2}}{\frac{n\pi}{2}} \cos n\omega_c t \right] .$$

$$(C-19)$$

Equation (C-18) shows that the $\cos \omega_m't$ term, the recovered data, is not isolated.

We expand the sixth term of (C-19), which is the product term, for further consideration.

This term

$$\frac{4a}{\pi^2} \cos \omega_m't \cos \omega_c't \cos \omega_c t \qquad\qquad (C-20)$$

gives

$$\frac{2a}{\pi^2} \cos \omega_m't \left[\cos(\omega_c + \omega_c')t + \cos(\omega_c - \omega_c')t \right]$$

then

$$\frac{a}{\pi^2} \left[2 \cos \omega_m't \left[\cos(\omega_c + \omega_c')t \right] + 2 \cos \omega_m't \left[\cos(\omega_c - \omega_c')t \right] \right]$$

and finally

$$\frac{a}{\pi^2} \left[\cos\left[(\omega_c + \omega_c') + \omega_m'\right]t + \cos\left[(\omega_c + \omega_c') - \omega_m'\right]t \right.$$

$$\left. + \cos\left[(\omega_c - \omega_c') + \omega_m'\right]t + \cos\left[(\omega_c - \omega_c') - \omega_m'\right]t \right] .$$

$$(C-21)$$

Now if $\omega_c' = \omega_c$, equation (C-21) becomes

$$\frac{a}{\pi^2} \left[\cos\ (2\omega_c' + \omega_m')t + \cos(2\omega_c' - \omega_m')t \right.$$

$$\left. + \cos\ \omega_m't + \cos(-\ \omega_m')t \right]$$

or

$$(C-22)$$

$$\frac{2a}{\pi^2}\ \cos\ 2\ \omega_c't\ \cos\ \omega_m't + \frac{2a}{\pi^2}\ \cos\ \omega_m't\ \ .$$

With filtering, equation (C-19) reduces to

$$e_o = \frac{2a}{\pi^2}\ \cos\ \omega_m't \qquad\qquad (C-23)$$

which is the recovered data. Equation (C-23) came from
(C-20) with $\omega_c' = \omega_c$ and with filtering. The assumption
$\omega_c' = \omega_c$ implies $\omega_m' = \omega_m$. Therefore equation (C-23), the
recovered data, is the same as the recorded data. Equation
(C-20) is the only term of consequence, the product term,
in (C-19). Since $\omega_c' = \omega_c$ and $\omega_m' = \omega_m$, equation (C-20)
can be written symbolically

$$e_o = \cos\ \omega_m t\ \cos\ \omega_c t\ \cos\ \omega_c t. \qquad\qquad (C-24)$$

Recalling that the original data was

$$e_i = \cos\ \omega_m t \qquad\qquad (C-25)$$

equation (C-24) becomes

$$e_o = e_i \cos \omega_c t \cos \omega_c t \qquad (C-26)$$

which is the product of the original data, modulation carrier, and demodulation carrier. Thus if the demodulating carrier has the same frequency as the modulating carrier the original data is recovered.

Now let the demodulation carrier differ from modulation carrier by the phase angle "θ." Equation (C-26) becomes

$$e_o = e_i \cos \omega_c t \cos(\omega_c t + \theta) \qquad (C-27)$$

or

$$e_o = \frac{e_i}{2}\left[\cos\left[\omega_c t + (\omega_c t + \theta)\right] + \cos\left[\omega_c t - (\omega_c t + \theta)\right] \right]$$

and

$$e_o = \frac{e_i}{2}\left[\cos\ (2\omega_c t + \theta) + \cos(-\ \theta)\right]$$

and finally

$$e_o = \frac{e_i}{2} \cos(2\omega_c t + \theta) + \frac{e_i}{2} \cos\ \theta\ . \qquad (C-28)$$

After the usual filtering (C-28) reduces to

$$e_o = \frac{e_i}{2} \cos\ \theta \qquad (C-29)$$

and from (C-25)

$$e_o = \frac{1}{2} \cos \omega_m t \cos\ \theta\ . \qquad (C-30)$$

This shows that the recovered data is a function of phase difference between the modulating and demodulating carriers. If $\theta = \pi/2$, the data is, of course, lost.

Thus the requirements for demodulation of AM modu-
lation by switching are that the frequency and phase be
the same for both carriers. These are also the same
requirements for DSB demodulation.

To ensure that the demodulating carrier is always of
the same frequency and in phase with the modulating carrier,
the modulating carrier is recorded as a synchronizing
signal on the second track of the duo-track tape simultane-
ously with the data-modulated carrier on the first track.
In the playback mode, the synchronizing signal becomes the
demodulating carrier. Thus regardless of tape speed
variations, the modulating and demodulating carriers are
always of same frequency and in phase.

These speed variations cause ω_m' to differ from ω_m.
Since the percentage change in the data frequency and the
synchronizing signal are equally proportional to speed
variations, monitoring the synchronizing signal is tanta-
mount to monitoring ω_m'. This monitoring is accomplished
by using filters of same percentage bandpass for the data
frequencies and synchronizing signal. The fact that the
synchronizing signal remains within the filter bandpass
ensures that the data-frequencies are within their filters
and that the data is being recovered. Furthermore, should
the speed variations become excessive, this synchronizing
signal is available as a control signal for a speed
control servo system.

Appendix D

Antenna

On the basis of portability, the loop antenna seems to be the proper type to use for the data-collecting system. Nevertheless, a further inquiry is advisable before the final selection is made.

Initial computations for a loop antenna may be performed by line integration or by Faraday's Law.

Figure D1 shows the antenna configuration and symbolism. Letting $\theta = 0$,

$$e_0 = \int \overline{E} \cdot \overline{dl} = \int_0^h \overline{E} \cdot \overline{k} \, dl + 0 + \int_{-h}^0 \overline{E} \cdot -\overline{k} \, dl + 0$$

$$\text{(D-1)}$$

and

$$e = hE_z e^{-jk(r - \frac{W}{2})} - hE_z e^{-jk(r + \frac{W}{2})}$$

$$= hE_z e^{-jkr} \left[e^{j\frac{kW}{2}} - e^{-j\frac{kW}{2}} \right] = 2jh \, E_z e^{-jkr} \sin \frac{kW}{2} \ .$$

$$\text{(D-2)}$$

Now with $W \ll \lambda$,

$$e = jkWh \, E_z e^{-jkr} \ . \tag{D-3}$$

Since the area is

$$A = Wh \tag{D-4}$$

Side View

(a)

Top View

(b)
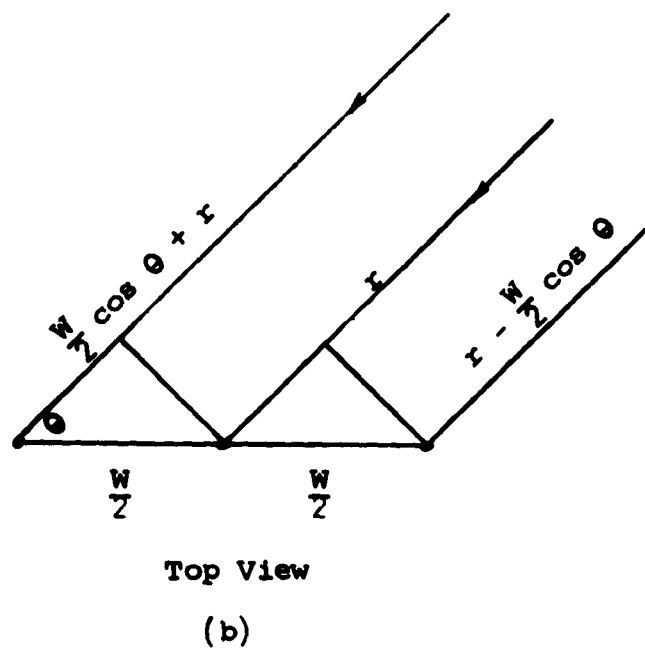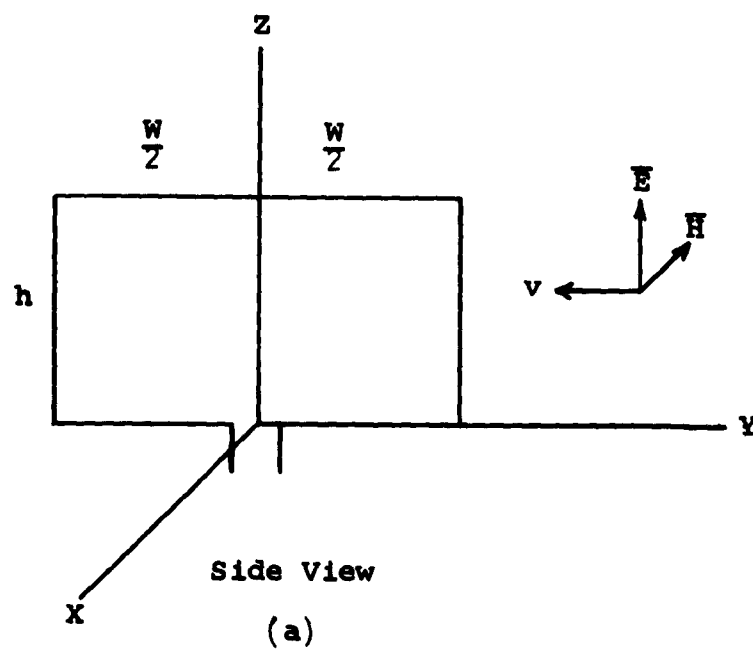
Figure D1   Loop antenna configuration

and $k = \frac{2\pi}{\lambda} = 2\pi f\sqrt{\mu\epsilon} = \omega\sqrt{\mu\epsilon}$,
$\qquad$ (D-5)

$$e = j\, A\, \omega\sqrt{\mu\epsilon}\, E_z\, e^{-jkr} \qquad (D-6)$$

For "N" turns, then

$$e = j\, NA\, \omega\sqrt{\mu\epsilon}\, E_z e^{-jkr} , \qquad (D-7)$$

By Faraday's Law and with $\theta = 0$,

$$e = -NA\, \frac{\partial \overline{B}}{\partial t} = -NA\mu\, \frac{\partial \overline{H}}{\partial t} \quad . \qquad (D-8)$$

In free space,

$$\eta = \frac{E_v}{H_H} \qquad (D-9)$$

and upon substitution

$$e = -\frac{NA\mu}{\eta}\frac{\partial E_z}{\partial t} = \frac{NA\mu}{\eta}\, j\omega\, E_z e^{-jkr} \quad . \qquad (D-10)$$

Since the relation

$$\eta = \sqrt{\frac{\mu}{\epsilon}} \qquad (D-11)$$

holds,

$$e = jNA\, \omega\sqrt{\mu\epsilon}\, E_z e^{-jkr} \quad . \qquad (D-12)$$

Using either (D-7) or (D-12),

$$|e| = \frac{2\pi}{\lambda}\, E_z\, AN \qquad (D-13)$$

with $\theta = 0$ and with $W \ll \lambda$. The AN-product becomes

$$AN = \frac{\lambda}{2\pi}\, \frac{|e|}{E_z} \quad . \qquad (D-14)$$

Considering $\lambda = 3 \times 10^7$m, $E_z = 1\mu v/m$, and $e' = 1\mu v$, equation (D-14) becomes

$$AN \approx 5 \times 10^6 \left[m^2\right]. \qquad (D-15)$$

This AN-product is obviously too large. For any combination of area and turns, the resultant loop is certainly not portable.

A possible alternative is to restrict the loop area to a size that is portable and consider core material to reduce the required turns. A few calculations show that the weight of the core material is excessive for portability.

In view of this inability to meet the portability requirements, further investigation into the characteristics of the loop antenna was abandoned.

Perhaps the most important aspect of a vertical antenna is the capacity to ground. This capacity is given by[1]

$$C = \frac{7.36 \ m}{\log_{10}\frac{2m}{d} - k}\mu\mu fd \quad . \qquad (D-16)$$

where

    m = length in feet

    d = diameter in feet

    h' = height of lower end above ground

---

[1]Terman, F. E., Radio Engineers' Handbook, McGraw-Hill Book Company, Inc., New York, 1943, p. 116.

and $k = \dfrac{h'}{m}$ or $\dfrac{m}{h'}$, whichever is less than unity, from Table 30.[2]

Table D-1 shows the antenna capacity for various values in equation (D-16). In general, the capacity doubles with doubling the height or with increasing the diameter by a factor of 10. Lowering the height above the ground increases the capacity only slightly.

m (ft)	d (ft)	h' (ft)	k^{*}	C ($\mu\mu$fd)
20	1/12	1	.376	64.
20	1	1	.376	120.
20	1/6	1	.376	73.6
20	1/12	2	.345	60.6
40	1/12	1/2	.418	115.
40	1/12	1	.398	114.
30	1/12	1/2	.403	90.1
30	1/12	1	.3935	89.8

[*]See equation (D-16)

Table D-I Capacity of a vertical antenna with
variations in dimensions

_____

2
Ibid., p. 116.

The last entry in Table D-I shows that a 30-ft antenna, 1 inch in diameter, and mounted 1 ft above the ground has a capacity of approximately 90 $\mu\mu$fd. The reactance of this antenna in the 0-50 cps region is obviously quite large. In fact, the magnitude of the reactance implies that matching to a receiving device is a problem.

Methods such as capacity top-loading and inductive loading which are used to increase antenna capacity are not applicable here because of the portability requirement.

In spite of the high reactance, the vertical antenna has some advantages. Perhaps the foremost is that the reception pattern is omnidirectional. And in addition, it can be made quite portable by using lightweight material and telescoping sections of convenient length.

A Hall device was also considered as an antenna or sensing element. The impedance is resistive; and therefore is relatively independent of frequency.[3] However, in addition to being directional, it also requires much higher signal levels than either a loop or whip antenna for unity signal-to-noise ratio.

---

[3]Monsen, G. J., "Pickup Devices for Very-Low Frequency Reception," Electronics, April 14, 1961, p. 68.

Antenna Capacitance

The vertical antenna finally constructed had the following dimensions:

m(height) = 28.96 ft. = 4.4 meters

h' (height above ground) = 0.375 ft.

d (diameter) = 0.11 ft.

From these dimensions,

$$\frac{h'}{m} = 0.013 \ .$$

The value,

k = 0.413,

was determined by extending the curve, Figure D2, which was drawn from Table 30 referred to previously.

Using relation (D-16), the capacity was found to be 92.33 $\mu\mu$fd. From this, the reactance, as shown in Figure D3, was determined.

Since m $\ll \lambda$ in the 0-50 cps region, the effective height "h_e" can be considered as equal to m/2 or 2.2 meters.
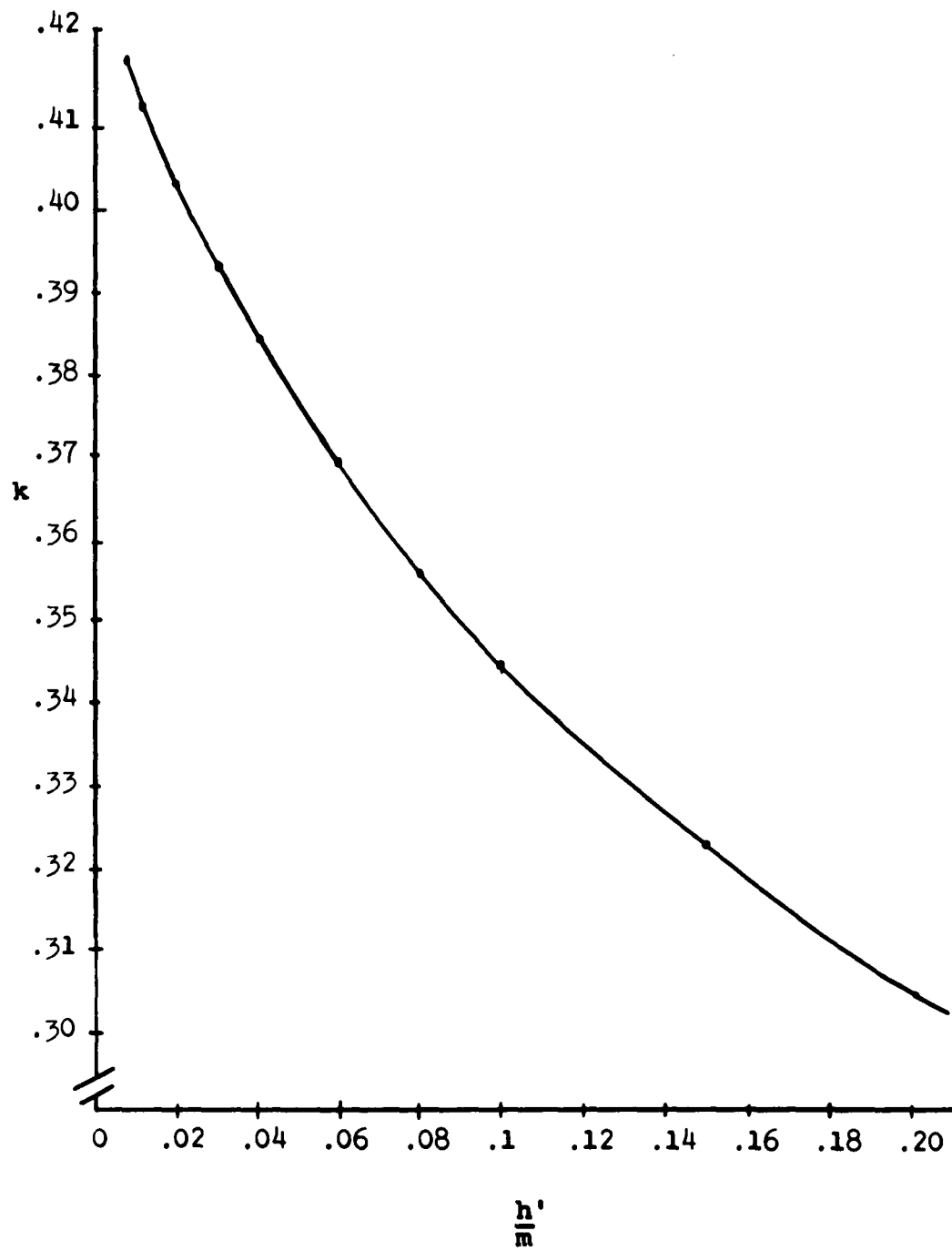
Figure D2 Values of the constant k for $\frac{h'}{m}$
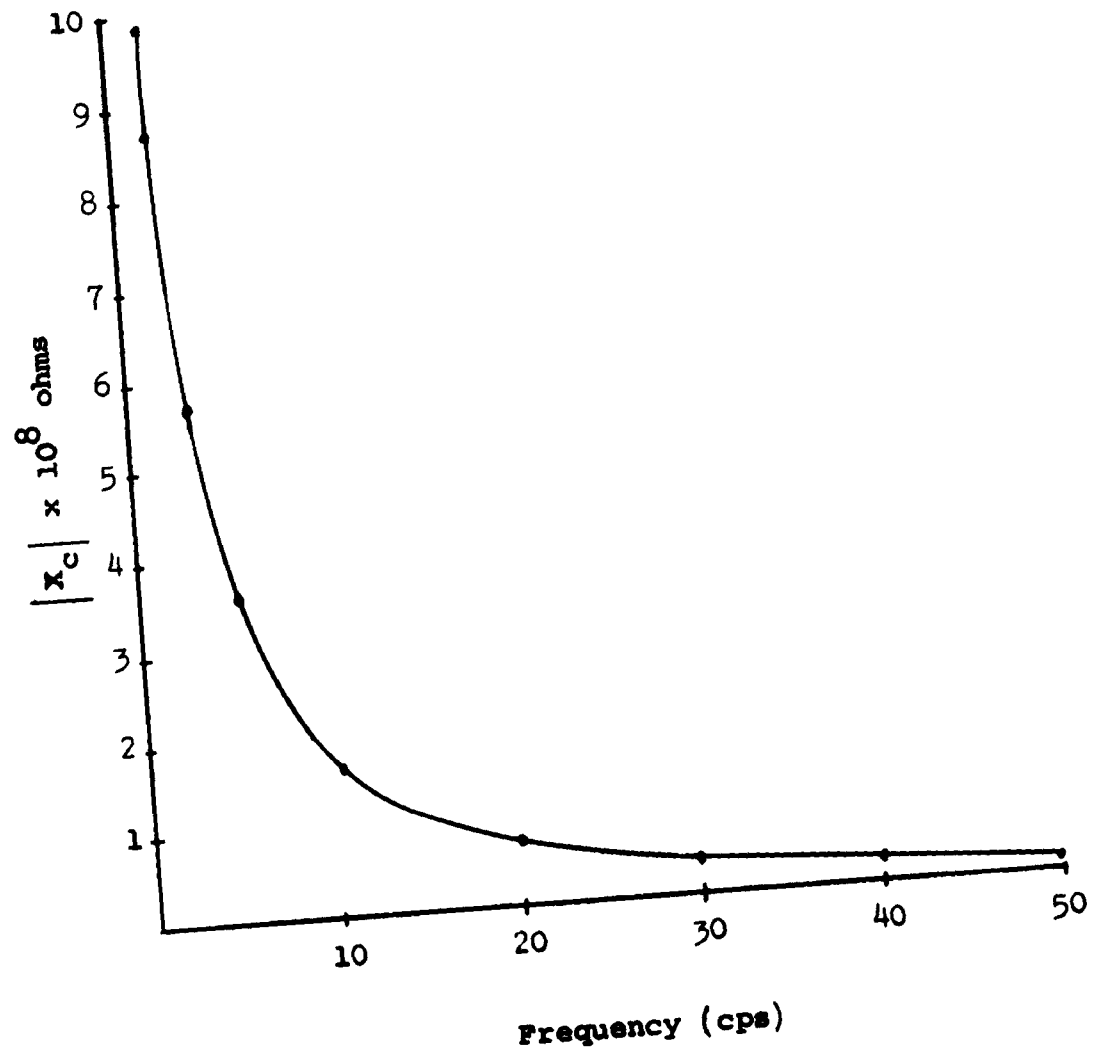
Figure D3   Antenna reactance versus frequency

LIST OF REFERENCES

Aarons, J., "Low Frequency Electromagnetic Radiation 10 to 900 cps," Jour. Geophys. Res., 61, 647 (1956).

Aarons, J., G. Gustafsson, and A. Egeland, "Correlation of Audio-Frequency Electromagnetic Radiation with Auroral Zone Micropulsations," Nature, 185, 148, (1960).

Aarons, J., and M.Henissart, "Low Frequency Noise in the Range 0.5 to 20 cps," Nature 172, part 2, 682 (1953).

Anderson, Wallace L., Doctoral Dissertation, The Fields of Electric Dipoles in Sea Water--The Earth-Air-Ionosphere Problem, University of New Mexico, 1961.

Austin and Cohen, Bulletin of Bureau of Standards 7, 315 (1911).

Appleton, E. V., and F. W. Chapman, "The Nature of Atmospherics," Proc. Roy. Soc. A 158, 1 (1937).

Balser, M., and C. A. Wagner, "Measurements of Spectrum of Radio Noise from 50 to 100 Cycles per Second," Journal of Research NBS, 64D, No. 4 (1960).

Barber, N. F., and D. D. Crombie, "VLF Reflections from the Ionosphere in the Presence of a Transverse Magnetic Field," Jour. Atmos. Terr. Phys., 16, 37 (1959).

Boothe, R. R., B. M. Fannin, and F. X. Bostick, "A Geomagnetic Micropulsation Measuring System Utilizing Air-Core Coils as Detectors," Report Nr. 115, Electrical Engineering Research Laboratory, University of Texas, August 1, 1960.

Campbell, Wallace H., "Studies of Magnetic Field Mircropulsations with Periods of 5 to 30 seconds," Jour. Geophys. Res. 64, 1819 (1959).

Chapman, F. W., and A. G. Edwards, Proc. U.R.S.I. 8, part 2, 351 (1950).

Chapman, F. W., and A. Jolley, Proc. U.R.S.I. 10, part 4, 33 (1954).

Chapman, F. W., and R. C. V. Macario, "Propagation of Audio Frequency Radio Waves to Great Distances," Nature 177, 930 (1956).

Chapman, F. W., and W. D. Mathews, "Audio-frequency Spectrum Atmospherics," Nature 172, 495 (1953).

Chapman, J., and E. T. Pierce, "Relations Between the Character of Atmospherics and Their Place of Origin," *Proc. Inst. Radio Engr.*, 45, 804 (1957).

Cowles, L. G., "Parallel-T Resistance Capacitance Networks," *Proc. IRE*, No. 12, Dec., 1952, p. 1712.

Crary, J. H. and R. A. Helliwell, "Calculations and Interpretation of VLF Field Strengths, Polarizations and Angles of Arrival," U.R.S.I. Conference Georgetown University Abstracts, May 1-4, 1961, p. 40.

Crombie, D. D., "Differences Between the East-West and West-East Propagation of VLF Signals Over Long Distances," *Jour. Atmos. Terrest. Phys.*, 12, 110 (1958).

Davis, Robert C., "The Average Rate of Lightning Flashes to Ground," U.R.S.I. Conference Georgetown University Abstracts, May 1-4, 1961, p. 23.

Duffus, H. J., P. W. Nasmyth, J. A. Shand, and Sir Charles Wright, "Note on Low Frequency Electromagnetic Studies at P.N.L.," P.N.L. (Pacific Naval Laboratory), VLF Symposium, NBS Boulder, Vol. II, paper 19, 1957.

Duffus, H. J., P. W. Nasmyth, J. A. Shand, C. S. Wright, "Sub-audible Geomagnetic Fluctuations," *Nature*, 181, part 2, 1258 (1958).

Fitchen, F., R. Dubois, and C. Polk, "Schumann Resonances of the Earth-Ionosphere Cavity," U.R.S.I. Conference University of Texas, October 1961.

Gallet, Roger M., "Very-low-frequency Emissions Generated in the Earth's Exosphere," *Proc. IRE*, 47, 211 (1959).

Gallet, R. M., and R. A. Helliwell, "A Theory of the Production of VLF Noise (so-called Dawn Chorus) by Traveling Wave Amplification in the Exosphere of the Earth," VLF Symposium Vol. II, paper 20, 1957.

Gallet, R. M., and R. A. Helliwell, "Origin of Very-low-frequency Emissions," *Jour. Res. NBS*, 63D, 21 (1959).

Goldberg, P. A., "Electromagnetic Phenomena of Natural Origin in the 1.0-150 cps Band," *Nature*, 177, 1219 (1956).

Grierson, J. K., "A Technique for Rapid Analysis of Whistlers," *Proc. IRE*, 45, 806 (1957).

Gruentz, O.O., "8000 Cycle Sound Spectrograph," *Bell Lab. Review*, Vol. 29, 256, June 1951.

Gustafsson, G., A. Egeland, and J. Aarons, "Audio-frequency Electromagnetic Radiation in the Auroral Zone," _Jour_. _Geophys_. _Res_. 65, No. 9 (1960).

Hales, A. L., "A Possible Mode of Propagation of the "Slow" or Tail Component in Atmospherics," _Proc_. _Roy_. _Soc_. _A_ 193, 60, (1948).

Helliwell, R. A., "Whistlers and Very Low Frequency Emissions," _Geophysics and the IGY_, Geophysical Monograph No. 2, American Geophysic Union, Washington D. C., July, 1958.

Helliwell, R. A., "Low Frequency Propagation Studies, Part I- Whistlers and Related Phenomena," June, 1953-Sept., 1956, Report, (Revised May, 1958) Final Report, Stanford Electronics Laboratories, Stanford University.

Helliwell, R. A., J. H. Crary, J. H. Pope, and R. L. Smith, "The Nose Whistler-a New High-Latitude Phenomenon," _Jour_. _Geophys_. _Res_. 61, 139 (1956).

Helliwell, R. A., and M. G. Morgan, "Atmospheric Whistlers," _Proc_. _IRE_, 47, No. 2 (1959).

Hepburn, F., "Wave-guide Interpretation of Atmospheric Waveforms," _Jour_. _Atmos_. _Terrest_. _Phys_., 10, 121 (1957a).

Hepburn, F., "Atmospheric Waveforms with Very-low-frequency Components below 1 kcs Known as Slow Tails," _Jour_. _Atmos_. _Terrest_. _Phys_., 10, 266 (1957b).

Hepburn, F., "Classification of Atmospheric Waveforms," _Jour_. _Atmos_. _Terrest_. _Phys_., 12, 1 (1958).

Hepburn, F., and E. T. Pierce, "Atmospherics with Very-low Frequency Components," _Nature_, 171, 837, (1953).

Holzer, R. E., and O. E. Deal, "Low Audio-frequency Electro-magnetic Signals of Natural Origin," _Nature_, 177, 536 (1956).

Hopkins, Geo. H. Jr., "A Survey of Past and Present Investigations of the Natural Earth Currents," Report No. 113, Electrical Engineering Research Laboratory, University of Texas, April 1, 1960.

Large, M. I., Dissertation, _Some Investigations in Atmospheric Electricity_, Cambridge University, 1957.

Large, M. I., and T. W. Wormell, "Fluctuations in the Vertical Electric Field in Frequency Range from 1 cps to 500 cps," _Recent Advance Atmospheric Electricity_, Pergamon Press Ltd., New York, 1958, p. 603.

Liebermann, L. N., "Anomalous Propagation Below 500 c/s," VLF Symposium NBS, Boulder, Vol. III, paper No. 25, 1957.

Liebermann, L. N., "Extremely Low Frequency Electromagnetic Waves, I. Reception From Lightning," Jour. Appl. Phys. 27, 1473 (1956a).

Liebermann, L. N., "Extremely Low Frequency Electromagnetic Waves, II. Propagation Properties," Jour. Appl. Phys. 27, 1477 (1956b).

Lutkins, F. E., "The Nature of Atmospherics," Proc. Roy. Soc. 171A, 285 (1939).

Maple, Elwood, "1 to 50 cps Geomagnetic Fluctuations," U.R.S.I. Conference Abstracts, University of Texas, Oct.20-21, 1961, p. 14.

Martin, L. H., R. A. Helliwell, and K. R. Marks, "Association Between Aurorae and Very Low-frequency Hiss Observed at Byrd Station, Antarctica," Nature, 187, 751 (1960).

Menzel, D. H., and W. W. Salisbury, "Audio-frequency Radio Waves from the Sun," Nature, 161, 91 (1948).

Monsen, G. J., "Pickup Devices for Very-Low Frequency Reception," Electronics, April 14, 1961, p. 68.

Pierce, E. T., "Electrostatic Field-changes due to Lightning Discharge," Quart. Jour. Roy. Met. Soc., 81, 211 (1955).

Pierce, E. T., "The Propagation of Radio Waves at Frequencies Less than 1 kcs," Proc. IRE, 48, 329 (1960a).

Pierce, E. T., "Some ELF Phenomena," Jour. Res. NBS, 64D, No. 4, (1960b).

Pierce, E. T., "Attenuation Coefficients at Very Low Frequencies (VLF) During a Sudden Ionospheric Disturbance (SID)," U.R.S.I. Conference Georgetown University Abstracts, May 1-4, 1961, p. 40.

Potter, R. K., "Visible Patterns of Sound," Science, 102, 463 (1945).

Raemer, H. R., "Extremely Low Frequency Terrestrial Noise as a Propagation Research Tool," U.R.S.I. Conference Georgetown University Abstracts, May 1-4, 1961, p. 39.

Schumann, W. O., "The Propagation of Very Long Radio Waves Around the Earth and Signals from Lightning," Nuovo Cimento, 9, 1116, (1952a).

Schumann, W. O., "Über die strahlungslosen Eigenschwignungen
    einer leitenden Kugel, die von einer Luftschicht und
    einer Ionosphärenhülle umgeben ist," Zeitschrift für
    Naturforschung, 7A, 149 (1952b).

Schumann, W. O., "Über die oberfelder bei der ausbreitung
    langer, elektrischer wellen im system erde-luft-ionosphare
    und z anwendungen (horizontaler und senkrechter dipol),"
    Zeits fur ante, Phys, 6, 34, (1954a).

Schumann, W. O., "On the Radiation of Long Waves from a
    Horizontal Dipole in the Cavity Between the Earth and
    Ionosphere," Zeitz fur ange, Phys, 6, 225 (1954b).

Schwartz, Mischa, Information Transmission, Modulation, and
    Noise, McGraw-Hill Book Company, Inc., 1959.

Seshu, S. and N. Balabanian, Linear Network Analysis, John
    Wiley and Sons, Inc., 1959.

Smith, H. W., L. D. Provazek, and F. X. Bostick, Jr.,
    Directional Properties and Phase Relations of the Magneto-
    telluric Fields at Austin, Texas, Report No. 116, Electrical
    Engineering Research Laboratory, University of Texas,
    October 10, 1960.

Storey, L. R. O., "A Method to Interpret the Dispersion Curves
    of Whistlers," VLF Symposium, NBS, Boulder, Vol. I,
    Paper 9, 1957.

Taylor, W. L., "Radiation Field Characteristics of Lightning
    Discharges in the Band 1 kc to 100 kc," U.R.S.I. Conference
    Georgetown University Abstracts, May 1-4, 1961.

Tepley, L. R., "A Comparison of Sferics as Observed in the VLF
    and ELF Bands," Jour. Geophys. Res. 64, 2315 (1959).

Tepley, L. R., "Sferics from Intracloud Lightning Strokes,"
    Jour. Geophys. Res. 66, No. 1, (1961a).

Tepley, L. R., "Observations of Hydromagnetic Emissions,"
    Jour. Geophys. Res. 66, No. 6 (1961b).

Terman, F. E., Radio Engineers' Handbook, McGraw-Hill Book
    Company, Inc., New York, 1943, p. 116.

Valley, G. E., Jr., and H. Wallman, Vacuum Tube Amplifiers,
    Vol. 18, Radiation Laboratory Series, McGraw-Hill Book
    Company, Inc., 1948.

Wait, J. R., On the Mode Theory of VLF Ionospheric Propagation,
    NBS Report No. 5022, October, 1956.

Wait, J. R., "The Attenuation vs. Frequency Characteristics of VLF Radio Waves," Proc. IRE, 45, 768 (1957).

Wait, J. R., "Terrestrial Propagation of Very-Low Frequency Radio Waves," Jour. Res. NBS, 64D, No. 2, 153 (1960a).

Wait, J. R., A Survey and Bibliography of Recent Research in the Propagation of VLF Radio Waves, NBS Technical Note No. 58, (1960b).

Wait, J. R., "Preface to ELF Papers," Conference on Propagation of Electromagnetic Waves at ELF, NBS, Boulder, Jan. 26, 1960, Jour. Res. NBS, 64D, No. 4, p. 381 (1960c).

Wait, J. R., "Mode Theory of the Propagation of ELF Radio Waves," Jour. Res. NBS, 64D, July-August (1960d).

Wait, J. R., Report of U.S. Commission 4, U.R.S.I. "Radio Noise of Terrestrial Origin," Part 4, A Summary of VLF and ELF Propagation Research. Jour. Res. NBS, 64D, No. 6, (1960e).

Wait, J. R., and N. F. Carter, Field Strength Calculation for ELF Radio Waves, NBS Technical Note No. 52 (1960).

Watson-Watt, R. A., J. F. Herd, and F. E. Lutkin, "On the Nature of Atmospherics," Proc. Roy. Soc. A 162, 267 (1937).

Watt, A. D., "ELF Electric Fields from Thunderstorms," Jour. Res. NBS, 64D, No. 5, (1960).

Watt, A. D., and E. L. Maxwell, "Measurement of Statistical Characteristics of VLF Atmospheric Radio Noise," Proc. IRE, 45, part 1, p. 55 (1957).

Watts, J. M., "An Observation of Audio-frequency Electromagnetic Noise During a Period of Solar Disturbance," Jour. Geophys. Res. 62, 199 (1957a).

Watts, J. M., "Audio-frequency Electromagnetic Hiss Recorded at Boulder in 1956," VLF Symposium, NBS, Boulder, Vol. II, Paper No. 17 (1957b).

White, Gifford, "Design and Use of RC Parallel-T Networks," IRE Transactions on Audio, Vol. AV-8, Jan-Feb, 1960.

Whitson, A. L., Arctic Atmospheric Noise and Propagation Studies Part A: Arctic Sferic Data--August 1958 to March 1959, a final report on Contract AF 19(604)-2409, February, 1960.

Willis, H. F., "Audio-frequency Magnetic Fluctuations," Nature, 161, 887 (1948).

Wilson, C. T. R., Phil. Trans. A, 221, p. 75 (1920).

Distribution List for Unclassified Section of Progress

Report Contract Nonr-2798(01)

Addressee	No. of copies
Director, Armed Services Technical Information Agency Arlington Hall Station Arlington, Virginia	10

Director,
Naval Research Laboratory
Washington 25, D. C.
    Code 5420
    Dode 5360
    Code 2027
	
	1
	1
	3

Chief of Naval Operations
Navy Department
Washington 25, D. C.
    Op 07
    Op 94T
	
	1
	2

Commanding Officer and Director Naval Electronics Lab. San Diego 52, California	1
Director Special Projects (SP204) Bureau of Naval Weapons Washington 25, D. C.	25
Commander, US Naval Ordnance Test Station 3202 East Foothill Blvd. Pasadena 8, California	1
Commanding Officer and Director US Navy Underwater Sound Lab. New London, Conn. Attn: Mr. C. B. Dunn	2

Chief of Bureau of Ships
Navy Department
Washington 25, D. C.
    Code 671C
    Code 679
    Code 686
    Code 687A
    Code 687H
	
	1
	1
	1
	1
	1

Commanding Officer and Director
US Navy Underwater Sound Lab.
Fort Trumbull
New London, Conn.
  Attn: Mr. G. M. Milligan   1

Com. Officer and Director
US Naval Ordnance Lab.
Corona, Calif.
  Attn: Mr. A. W. Walters
      Code 45   1

Technical Director
US Naval Ordnance Test Station
China Lake, California   1

Com. Officer and Director
US Naval Ordnance & Lab.
White Oak, Maryland
  Attn: Mr. Robert Miller
      Code 042   1

Applied Physics Laboratory
Johns Hopkins University
Attn: Cdr. Pollow
8621 Georgia Avenue
Silver Springs, Md.   1

Director
Woods Hole Oceanographic Institution
Woods Hole, Mass. (Attn. Dr. Hersey)   1

Dr. Kenneth A. Norton, Chief
Radio Propagation Engr. Div.
Central Radio Prop. Lab.
National Bureau of Standards
Boulder, Colorado   1

National Research Council
Com. on Undersea Warfare
2101 Constitution Ave., N.W.
Wshington 25, D. C.   1

Dr. J. R. Wait, Consultant
Central Radio Prop. Lab.
NBS
Boulder, Colorado   2

Hoffman Radio
R. A. Schor, Unit Supervisor
Communication Section
P.O. Box 2471
Los Angeles 54, California   1

Chief of Naval Research
Navy Department
Washington 25, D. C.
    Code 466   3
    Code 427   1

Ordnance Research Lab.
Pennsylvania State College
P.O. Box 30
State College, Pa.   1

Director,
Scripps Institution of Oceanography
La Jolla, Calif.   1

Director,
Hudson Labs.
Columbia University
P.O. Box 329
Dobbs Ferry, New York   1

Dr. Cullen Crain
Rand Corporation
Santa Monica, California   1

University of Chicago
Laboratories for Appl. Sci.
Museum of Science
Chicago 37, Ill.
  Attn: Mr. Van Zeelind   1

Commanding Officer
Office of Naval Research
Branch Office
1030 East Green Street
Pasadena 1, Calif.   3

National Science Foundation
Engineering Program
Washington 25, D. C.   1

Director
Research Lab. of Elec.
Mass. Institute of Technology
Cambridge 39, Mass.   1

Dr. R. W. P. King
Cruft Laboratory
Harvard University
Cambridge 38, Mass.   1

Dr. R. H. Duncan
Physical Science Lab.
New Mexico State University
University Park
Las Cruces, New Mexico   1

Dr. B. M. Fannin
Elec. Engr. Research Lab.
University of Texas
Austin 3, Texas   1

Elec. Engr. Research
Document File
School of Electrical Engr.
Cornell University
Ithaca, New York   1

Mr. Albert R. Giddis
Project Engineer
Advance Programs Section
Philco Corp.
Western Development Labs.
3875 Fabian Way
Palo Alto, California   1

Mr. Richard C. Becker
Senior Staff Engineer
Amphenol-Borg Elec. Corp.
25th Avenue at Cermak
Broadview, Ill.   1

Mr. Harold A. Wheeler
Wheeler Laboratories, Inc.
122 Cutter Miller Road
Great Neck, N. Y.   1

Mr. J. Y. Wong
Antenna Group (Microwave Section)
National Research Council of Canada
Ottawa 2, Ontario, Canada   1

Stanford Elec. Laboratories
Stanford University
Stanford, California   1

Development Engineering Co.
Attn: Mr. Don Watt
Boulder, Colorado   1

Development Engineering Co.
Attn: Mr. Lucien Rawls
Leesburg, Virginia   1

Space Electronics Corp.
1200 AirWay
Glendale 1, California
  Attn: Mr. Frank W. Lehan   1

Stromberg-Carlson
Div. of General Dynamics
Rochester, N. Y. Attn: Victor Savchuk   1

P. S. Carter
Radio Corporation of America
Rocky Point, L. I., New York   1

Dr. J. H. Mulligan, Jr.
Chairman, EE Department
New York University
New York 53, New York   1

Mr. Loren S. Bearce
Code 5423
Naval Research Laboratory
Washington 25, D. C.   1

The Mitre Corporation
Middlesex Turnpike
Bedford, Massachusetts
  Attn: Mr. Karl Swartzel   1

Dr. Ronald V. Row
Sylvania Elec. Systems
Div. of Sylvania Elec. Products, Inc.
100 First Avenue
Waltham 54, Massachusetts   1

Mr. E. L. Sanderson
US Naval Mine Detection Laboratory
Panama City, Florida   1

Dr. L. Katz
Applied Physics Laboratory
Johns Hopkins University
Silver Springs, Maryland   1

Program Director
Advanced Science Programs
National Science Foundation
1951 Constitution Avenue
Washington 25, D. C.   1